Western Graduate&PostdoctoralStudies

Electronic Thesis and Dissertation Repository

11-17-2022 10:00 AM

Expanding the Scope of Clickable Azide-Functionalized Nanoclusters to include Au144

Johanna A. de Jong, *The University of Western Ontario*

Supervisor: Workentin, Mark S., *The University of Western Ontario*
A thesis submitted in partial fulfillment of the requirements for the Master of Science degree in Chemistry

Follow this and additional works at: https://ir.lib.uwo.ca/etd

Part of the Materials Chemistry Commons, Organic Chemistry Commons, Other Chemistry Commons, and the Physical Chemistry Commons

Recommended Citation

Abstract

Thiolate-protected Au_{144} nanoclusters (NCs) are an intriguing member of the gold NC family. Their geometric structure, distinct electrochemical features, and susceptibility to structural rearrangement under the duress of ligand exchange have been studied. However, there are currently no established protocols for surface modification or tuning of their ligand shells post synthesis. Here, the direct synthesis of three regioisomers of azide-modified Au_{144} NCs with 60 azide moieties, i.e., $Au_{144}(SC_2H_4C_6H_4-N_3)_{60}$, is reported, in which the azide functionality is located at the *ortho-*, *meta-*, or *para* position of the ligand's phenyl ring. The regioisomeric effect of the azide group on $Au_{144}(SC_2H_4C_6H_4-N_3)_{60}$ synthesis and physical properties are described. A proof-of-concept cluster surface strain promoted alkyne-azide cycloaddition (CS-SPAAC) reaction is also demonstrated, revealing all 60 azides can be accessible in the para derivative. The CS-SPAAC chemistry was further extended to append a functional TEMPO group, which can be utilized towards an alcohol electro-oxidation application.

Keywords

Summary for Lay Audience

At the macro scale, bulk gold is known to be an excellent material for making lustrous jewelry and coinage. However, at the nanoscale, a scale too small for the naked eye to perceive, gold materials acquire new size and structure-dependent properties that suit various technological and medical applications. Among these ultrasmall materials are gold (Au) nanoclusters (NCs), a class of nano-sized compounds. Au NCs have a core-shell configuration that can be tuned to target different optical or chemical properties. Their cores contain a geometric framework of a precise number of Au atoms, and the shell is made up of ligands (organic small molecules). Existing knowledge of tunable NC features focuses mainly on their gold cores. However, it has recently been demonstrated that NC ligand shells can be modified following NC synthesis via "click chemistry"; a means of connecting molecules together using rapid, high-yielding and highly selective reactions. By incorporating a robust functional group amenable to click chemistry into the ligand structure of NCs, i.e. an azide (N_3) group, new molecules can be tethered to the surface of NCs following their synthesis. This thesis focuses on the development of a NC containing 144 gold atoms in its core and 60 azide-containing ligands in its shell. The 60 ligands are each capable of undergoing a click reaction, specifically the cluster surface strain-promoted alkyne-azide cycloaddition (CS-SPAAC) reaction, to attach new functionality to the NC at 60 different sites within its ligand shell. This azide-functionalized Au_{144} NC can be used as a template to introduce new properties to NCs and therefore expand the scope of their applications.

Co-Authorship Statement

The work described in this thesis contains contribution from the author, under supervision of Prof. Mark S. Workentin.

Chapter 1 was written by the author and edited by Prof. Mark S. Workentin and Dr. Mahdi Hesari.

Chapter 2 describes the synthesis and characterization of three azide-modified Au_{144} NCs. Mass spectrometry was conducted by Hirunika Eshangi Wijesinghe, a member of the Dass group at the University of Mississippi. Excitation data was collected with the assistance of Adyn Melenbacher using instrumentation in the Stillman group at Western University. Photoluminescence spectra were collected by the author with the assistance of Kenneth Chu and Dr. Mahdi Hesari using instrumentation provided by the Ding group at Western University. DFT calculations and electrochemical experiments were conducted by Mahdi Hesari. All other experiments were performed by the author. Details of the electrochemistry experiments were partially written by Dr. Mahdi Hesari. The rest of this chapter was written by the author and edited by Prof. Mark S. Workentin and Dr. Mahdi Hesari.

Chapter 3 describes the click reaction and subsequent electrochemistry and electrocatalysis of Au_{144} NCs with functionalized derivatives containing Ferrocene and TEMPO. Electrocatalytic experiments, including the embedding of the NCs in a Nafion polymer, were performed by Dr. Mahdi Hesari. Details of electrochemical and electrocatalytic experiments were partially written by Dr. Mahdi Hesari. The rest of this chapter was written by the author and edited by Prof. Mark S. Workentin and Dr. Mahdi Hesari.

Chapter 4 was written by the author and edited by Prof. Mark S. Workentin and Dr. Mahdi Hesari.

Acknowledgments

First, I would like to thank my family, for their unconditional, and, at times, seemingly blind faith in my abilities.

I would also like to thank my friends, Paul, Mohammed, Tony, and Maria, Jack and Alex for brightening up my workday and not only providing comic relief, but also empathy on the days reactions weren't going as planned.

Thank you to the experts who contributed directly and indirectly to my work: Haidy Metwally, Kristina Jurcic, Mathew Willans, Aneta Borecki, and Paul Boyle. Thank you to Prof. Joe Gilroy, Michael Anghel, Jasveer Dhindsa, Francis Buguis, Daniela Cappello and Alexander Watson, for allowing me to use the Gilroy group instrument room and training me to conduct thermogravimetric analysis and electrochemical experiments. Thank you Prof. Zhifeng Ding for allowing me to use your electrochemical and spectroscopic instrumentation. Thank you to Olivia Aviles and Prof. Francois Lagugne-Labarthet for taking the time to analyze my samples with Surfaced-Enhanced Raman Spectroscopy (SERS). Thank you to the ChemBioStores staff, Monica Chirigel, Yuhua Chen, and Robin Martin, for supplying and shipping materials for my research. Thank you to Warren Lindsay and John Vanstone for keeping our lab running properly. Thank you to Yves Rambour, who provided glassblowing services to our chemistry department for more than 15 years, including the custom-built Schlenk lines in our lab, and sadly passed away in 2021.

Thank you to the experts who collaborated with me to obtain data in this work: Adyn Melenbacher and Prof. Martin Stillman, Hirunika Eshangi Wijesinghe and Prof. Amala Dass, and Kenneth Chu, Mahdi Hesari and Prof. Zhifeng Ding.

Thank you to the talented chemists who guided and advised me in the lab over the course of my research experiences at Western: David Tong, Praveen Gunawardene and Nils Vogeler.

Thank you to Prof. John Corrigan, my co-supervisor during my 4491 thesis, and an invaluable source of expertise during my MSc.

Thank you to my committee members, Prof. James Wisner and Prof. Robert Hudson, for the knowledge and experience that you shared with me over the course of my research.

Last, but certainly not least, thank you to my kind and supportive supervisor, Prof. Mark S. Workentin, and my friend and mentor, Dr. Mahdi Hesari.

Table of Contents

List of Figures

List of Appendices

List of Abbreviations

~	approximately
AIE	aggregation-induced emission
Au_{144}	$Au_{144}(SC_2H_4Ph)_{60}$
Au_{144}-N_3	$Au_{144}(SC_2H_4\text{-}C_6H_4\text{-}N_3)_{60}$
BCN	exo-9-hydroxymethylbicyclo[6.1.0]non-4-yne
CA	chronoamperometry
CS-SPAAC	Cluster-Surface Strain-Promoted Alkyne-Azide Cycloaddition
CuAAC	Copper-catalyzed Alkyne-Azide Cycloaddition
CV	cyclic voltammetry
Da	daltons
DBCO-OH	5-hydroxy-1,2:5,6-dibenzocyclooct-7-yne
DCC	N,N'-dicyclohexylcarbodiimide
DCM	dichloromethane, methylene chloride
DMAP	4-dimethylaminopyridine
DPV	differential pulse voltammetry
eq.	equivalents

ESI-MS	electrospray-ionization mass spectrometry
ET	electron transfer
EtOAc	ethyl acetate
EtOH	ethanol
GC	glassy carbon
Hex	hexanes
HOMO	highest-occupied molecular orbital
Hz	hertz
kDa	kilodaltons
LSPR	localized surface plasmon resonance
LUMO	lowest unoccupied molecular orbital
m	meta-
m	milli
M	molar
m/z	mass/charge
MALD-MS	matrix-assisted laser desorption ionization mass spectrometry
MBA	methylbenzene thiol
MBT	mercaptobenzoic acid
MeOH	methanol

NCs	nanoclusters
NHC	N-heterocyclic carbene
nm	nanometer
NMR	nuclear magnetic resonance
NPs	nanoparticles
o	*ortho-*
p	*para-*
PBIS	p-band intermediate state
pH	potential of hydrogen
Ph	phenyl
PL	photoluminescence
ppm	parts per million
RIM	restriction of intramolecular motion
SCE	saturated calomel electrode
SG	glutatathionate
TBAPF$_6$	tetrabutylammonium hexafluorophosphate
^{t}Bu	tert-butyl
TEMPO	2,2,6,6-tetramethylpiperidine -1oxyl
TOA$^+$	tetraoctylammonium

V   volts

μ   micro

Chapter 1

1   Introduction

1.1   Gold Nanoclusters: A Unique Size Regime

The study and obsession over gold materials predates modern science,[1] and yet thousands of years later we find ourselves studying them for the same reasons humanity began to obsess over gold so long ago: flexibility and resistance to oxidation. Of course, today flexibility refers not only to gold's malleability. It also refers to the diversity of materials that can be synthesized with gold (Au) from the atomic to the macro scale, including Au ions, Au(I) complexes, nanoclusters (Au NCs), nanoparticles (Au NPs), nanocrystals, nanorods, nanocages, and self-assembled monolayers on gold, in addition to bulk gold metal.

At different size regimes, gold has vastly different features. Bulk gold is known to be extremely ductile and conductive, while gold particles (1-100 nm size regime) are known to exhibit tunable localized surface plasmon resonance (LSPR) based on their size and shape. LSPR is a process in which conduction electrons are collectively excited in response to incident light and is responsible for their bright red colour, observed in things like glazes, paints, and stained-glass windows. Scaling down from 3.3 nm to 1.8 nm, LSPR diminishes, and the metallic band structure of gold disperses into quantized energy levels. Atomically precise Au particles (<2 nm) that exhibit quantized energy levels are referred to as nanoclusters (Au NCs). Their atomic precision allows for the establishment of useful structure-function relationships. These relationships are exploited to optimize catalytic and electrocatalytic reactions, tune excitation and emission energies for imaging and photonic devices, as well target specific biological functions for medical applications. In recent decades, researchers have unearthed a complex library of Au NCs, with each individual Au NC exhibiting unique electronic and structural features.

1.2   The Synthesis and Design of Au NCs

This library of Au NCs is astonishing when one considers the magnitude of tuning required, kinetically and thermodynamically,[2-4] to access a single atomically-precise NC. To begin with, NC synthesis does not start on the nanoscale, but is approached either from the bulk regime through etching processes, or bottom-up from the atomic regime (**Figure 1**). The existing body of known NCs are predominantly synthesized using bottom-up techniques that require careful consideration of every element; reaction solvent,[5] pH,[6, 7] equivalencies,[8] temperature,[9] stir rate,[10] amount of dissolved oxygen,[11] as well as reaction duration.
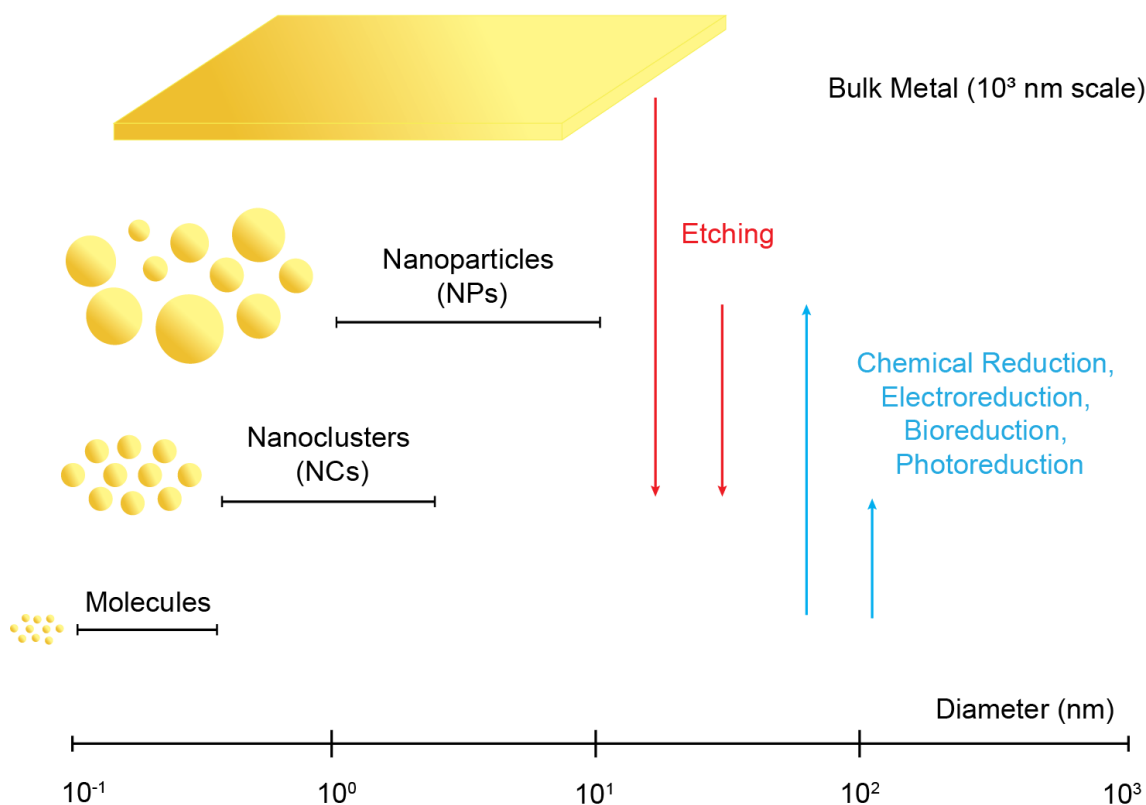
Figure 1. Synthetic approaches to synthesizing NCs.

Additionally, tuning the size and amount of gold present in a given nanocluster is merely part of the equation. The syntheses of Au NCs also require an outer shell of electron rich donor ligands that protect the NCs against aggregation and influence the resulting NC core size and structural features. While their overarching features are ascribed to their

size, NCs physical and chemical properties are strongly influenced by the protecting ligand(s) structure.[12-21] Various types of ligands have been used to synthesize nanoclusters, the most common being phosphines, thiolates, alkynes and N-heterocyclic carbenes (NHCs) (**Figure 2**). Phosphines were the very first ligand to ever be used in NCs, originating with $Au_{11}(PPh_3)_7(SCN)_3$ in 1969.[22] However, they exhibit the weakest bonding strength relative to thiolates and NHCs.[23] While much headway has been made recently in the development of NHC-protected NCs,[24] and alkyne-protected NCs,[25] thiolates are by far the most well-understood and established ligands used to make NCs due to the stability afforded to them by robust Au-S bonding[26].
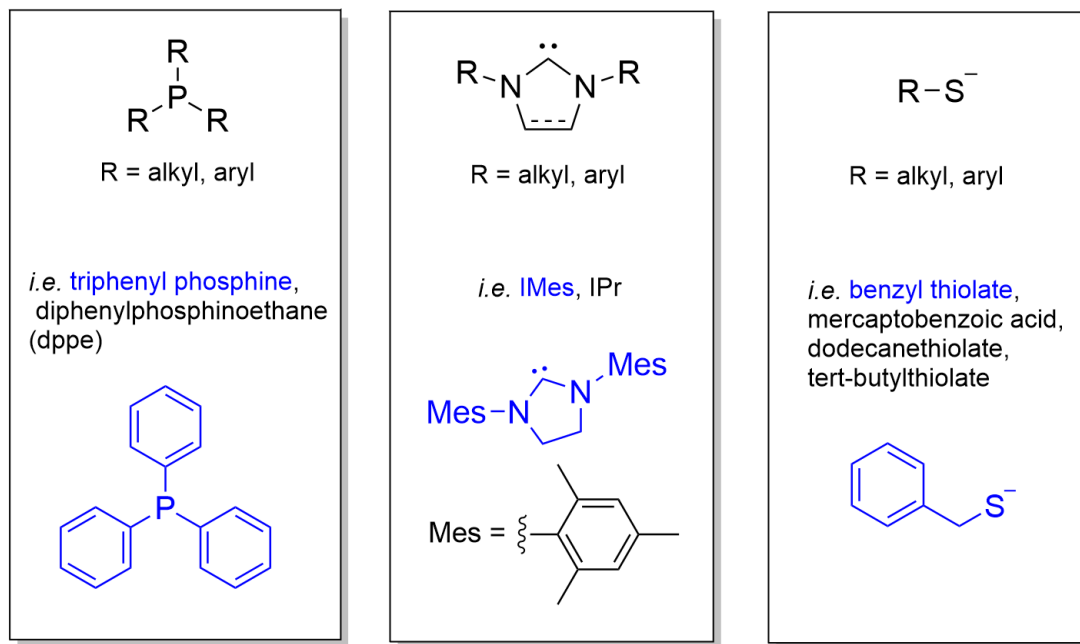
Figure 2. Representative examples of ligands used to make NCs.

The popularity of thiolate-protected Au NCs can arguably be attributed to the development of the Brust-Schiffrin[27] and modified Brust-Schiffrin[28] syntheses, which provided a foundation from which the most widely-studied NCs were discovered.[29, 30] The basic premise of both methods is that Au(III) is partially reduced by an excess of thiol to form Au(I) polymeric intermediate species.[31] The Au(I) intermediate species are then reduced using aqueous sodium borohydride to achieve thiolate-protected Au particles (NPs or NCs) (**Scheme 1**). When synthesizing NCs, the sodium borohydride

reduction process is frequently referred to as "*size-focusing*", as many different clusters are formed, but only one is stable enough to survive.[2, 32]
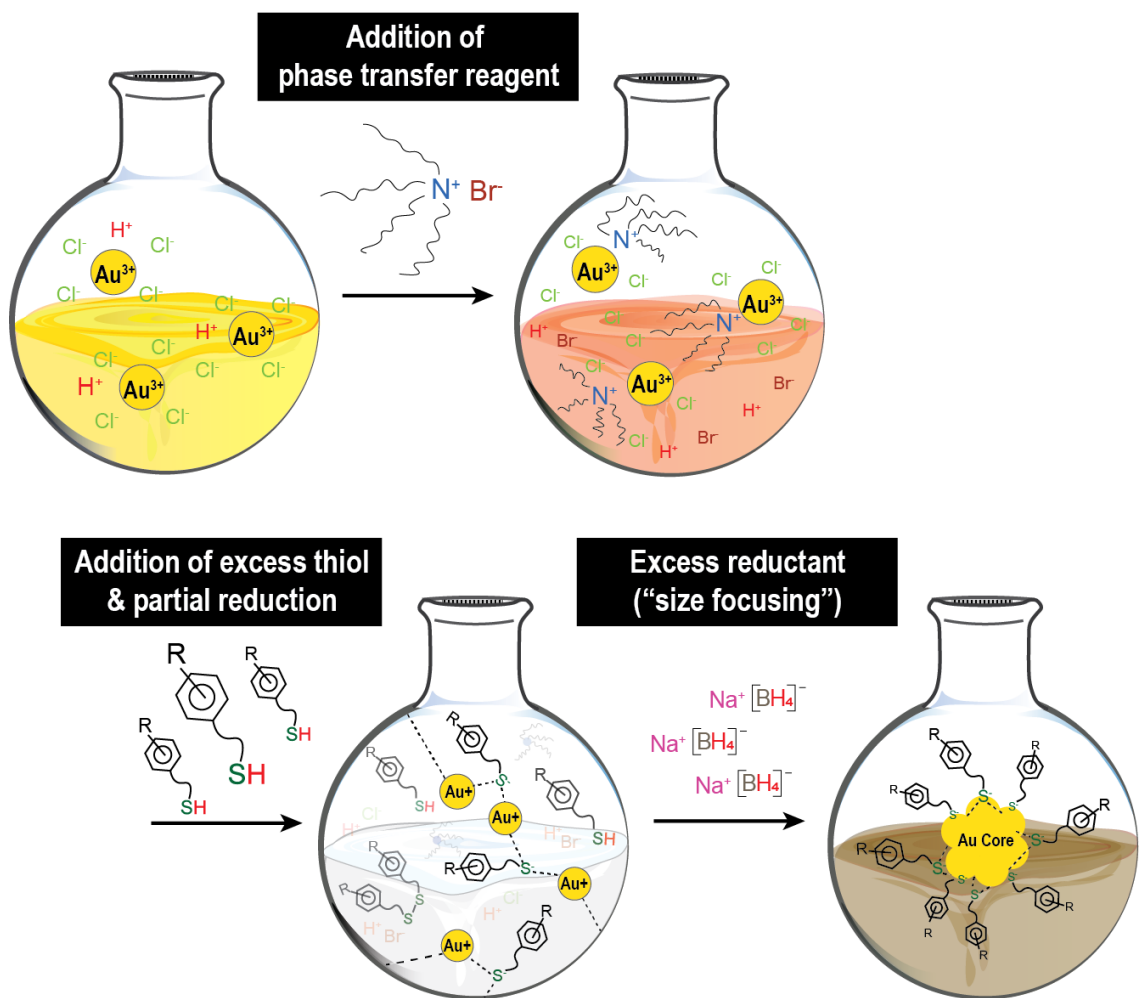
Scheme 1. Brust-Schiffrin approach to NC synthesis.

By either exploiting the sensitivity of the size-focusing process directly, or further focusing its products with heat or ligand exchange-driven processes, a handful of thiols have been used to access Au NCs of various sizes capped by the same ligand. For instance, phenylethane thiol (PhC$_2$H$_4$SH) has been used to access Au$_{19}$(SR)$_{13}$,[3] Au$_{24}$(SR)$_{20}$,[33] Au$_{25}$(SR)$_{18}$,[34] Au$_{38}$(SR)$_{24}$,[35] Au$_{40}$(SR)$_{24}$,[36] Au$_{67}$(SR)$_{35}$,[37] Au$_{137}$(SR)$_{56}$,[38] Au$_{144}$(SR)$_{60}$,[39-41] and Au$_{333}$(SR)$_{79}$,[42] where SR=PhC$_2$H$_4$S$^-$. The breadth of NCs that can be accessed using just one ligand emphasizes the utility of the methods originating from the Brust-Schiffrin synthesis. Sensitivity in the case of these syntheses gives rise to a wealth

of accessible size regimes, provided one has the correct starting materials. The variance in core size irrespective of ligand structure in these examples also incites a different question: how can one introduce flexibility and function to both Au NC cores and their corresponding ligand shells?

1.3　　Functionalizing the Ligand Shell of NCs

Incorporating functionality into the protecting ligand structure presents an opportunity to modify or introduce new properties to NCs. For instance, the incorporation of carboxyl groups into the structure of NCs has been very successful, using ligands such as mercaptobenzoic acid[43, 44] and mercaptoundecanoic acid[45]. Carboxyl groups not only impart water-solubility and pH-responsive features to NCs, but allow for their luminescence to be modified through aggregation-induced emission[46, 47] (AIE) and restriction of intramolecular motion[48] (RIM). Glutathione, a peptide containing both an amino and two carboxyl functional groups, when used to synthesize $Au_{25}(SR)_{18}$, has demonstrated stronger luminescence relative to other ligand-protected $Au_{25}(SR)_{18}$ NCs.[49] Glutathione-protected NCs have also exhibited exceptional renal clearance[50] and great promise as photosensitizers,[51] radiosensitizers,[52] and nanosensors[53]. Amino groups are also a handle for introducing greater utility to the ligand shell of NCs. For example, the amino group of glutathione has also been exploited in a post-synthesis amide coupling reaction to couple a chromophore directly to NCs for light-harvesting applications.[54] Other examples of how functional groups may be used to improve/modify the properties of NCs include the use of sulfonic thiolate ligands to impart greater stability to NCs in solution,[55] fluorinated ligands to improve their hydrophobicity and self-assembly,[56] and pyridyl ligands to impart tunable surface protonation-dependent solubility to NCs[57].

Unfortunately, an obstacle to adding functionality onto the surface of NCs is that functional groups that are susceptible to $NaBH_4$ reduction or interfere with the size evolution of NC syntheses must be incorporated following NC synthesis. The most common method used to impart changes to the functionality of NCs following their synthesis is "*ligand exchange*", whereby ligands of pre-existing NCs are replaced, often using an external driving force such as excess replacement ligand, heat, etc., to assist and accelerate exchanges to completion (**Scheme 2**).[58-62] The ligand exchange process

requires consideration of: (i) the affinity of the new ligand to the metal core compared to the original one, (ii) the change in solubility that the new ligand will impart to the NC, and (iii) whether the new ligand will preserve the original NC size or core structure.[18] Additionally, controlling the extent of exchange or ensuring complete exchange is challenging when using ligand exchange methods.[63-65] Ultimately, ligand exchange when it pertains to NCs is an invasive surgical procedure. Due to the disturbance of the ligand-gold interface, NCs may lose their structure and atomic precision altogether, or they may be transformed into NCs of a different size.
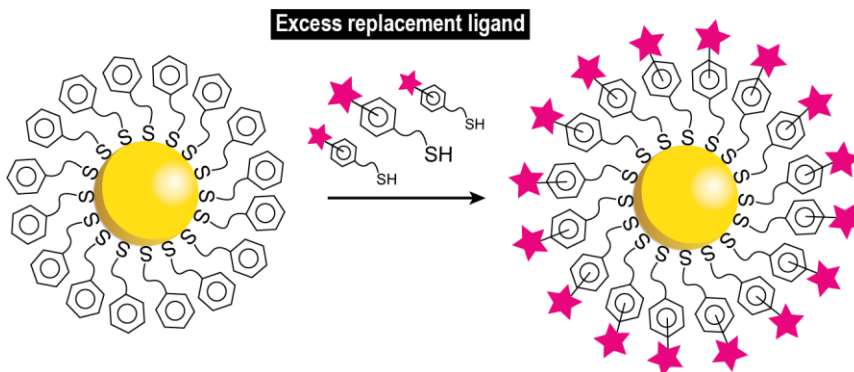
Scheme 2. Post-synthesis introduction of function to NCs via ligand exchange.

In pursuit of a less invasive approach, our group has addressed challenges with ligand exchange by expanding the synthetic toolbox of NP and NC surface modification to include, among other reactive groups, azides as a vehicle for interfacial click chemistry (**Scheme 3**).[66-68] "Click" chemistry, a term that was coined by K. Barry Sharpless, refers to chemoselective, solvent-tolerant, and high-yielding reactions that produce little to no byproducts.[69] A subclass of these reactions is bioorthogonal click chemistry; click reactions that do not interfere with biological processes.[70]
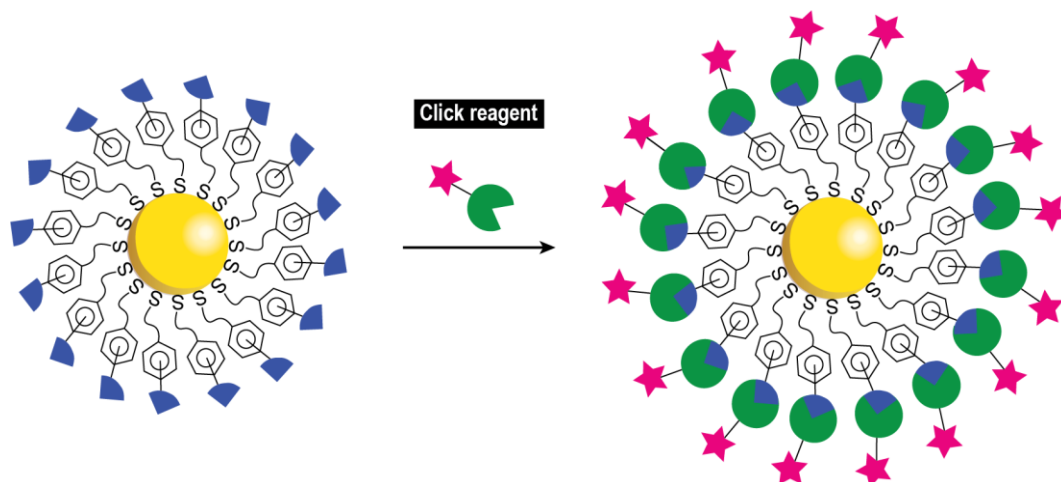
Scheme 3. Post-synthesis introduction of function to NC via click chemistry.

The use of interfacial click chemistry is advantageous because it avoids the alteration of regions of ligand structure directly bound to NC cores, lessening the risk of core modification. We have previously demonstrated interfacial click chemistry on the surface of an azide-functionalized $Au_{25}(SR)_{18}^-$ NC, where $SR=N_3C_6H_4C_2H_4S^-$.[66] This azide-functionalized NC was amenable to a cluster surface strain-promoted alkyne-azide cycloaddition (CS-SPAAC) reaction with a model strained alkyne, (Z)-cyclooct-1-ene-5-yne. The SPAAC reaction is a bioorthogonal click reaction in which an azide undergoes a [3 + 2] cycloaddition with a strained alkyne to form a triazole cycloadduct without the need for any catalyst.[71] The Zhang group has demonstrated that $Au_{25}(PPh_3)_{10}(SC_6H_4N_3)_5Cl_2$, $Au_{28}(SC_6H_4N_3)_{20}$ and $Au_{36}(SC_6H_4N_3)_{24}$ can be synthesized using ligand exchange and also undergo a CS-SPAAC reaction with a different strained alkyne, 5-hydroxy-1,2:5,6-dibenzocyclooct-7-yne (abbreviated as DBCO-OH).[72] While azides are only emerging as a means of NC surface modification, these examples demonstrate their potential as both an alternate and complementary approach to ligand exchange.

Furthermore, the presence and structural impact of the azide group on NCs provides insight into the fundamental structure-property relationships of NCs and can inform future ligand design. We recently reported the regioisomeric effect of the azide functionality at the *ortho-* (*o-*)*, meta-* (*m-*)*, and *para-* (*p-*) positions of the Au_{25}

phenylethane thiolate ligand.[73] The position of the azide group was not observed to affect the size of the $Au_{25}(SR)_{18}$ NC. However, it had a significant influence on the reactivity of the NCs toward the CS-SPAAC reaction, the most reactive being the *p-* derivative. A related study using *o-, m-,* and *p*-mercaptobenzoic acid revealed the position of carboxyl groups, when utilizing a thiophenolic ligand, also have a minimal structural impact on $Au_{25}(SR)_{18}$ NCs.[74] In contrast, a study using *o-, m-,* and *p*-methylbenzene thiol resulted in the synthesis of three different clusters; $Au_{40}(o\text{-}MBT)_{24}$, $Au_{104}(m\text{-}MBT)_{41}$, and $Au_{130}(p\text{-}MBT)_{50}$, respectively.[75] While discrepancies between their experimental protocols cannot be discounted, these studies highlight the interplay between function and size direction in ligand design.

1.4   Properties and Applications of $Au_{144}(SR)_{60}$ NCs

Given the flexibility that direct syntheses of azide-functionalized NCs offer and the biorthogonal nature of the azide, it is desirable to extend the click chemistry methodology to other stoichiometries of Au NCs. $Au_{144}(SR)_{60}$ NCs are an ideal candidate because their size-dependent properties are distinctly different from $Au_{25}(SR)_{18}$ NCs. For instance, based on their optical features, $Au_{25}(SR)_{60}$ NCs are considered ultrasmall NCs (<50 Au atoms) with more structure-dependent features, whereas $Au_{144}(SR)_{60}$ NCs are considered large-sized Au NCs (> 100 Au atoms), with more size-dependent features.[76] Additionally, like $Au_{25}(SR)_{18}$ NCs, $Au_{144}(SR)_{60}$ NCs can be synthesized in appreciable yields under ambient conditions.[39]

$Au_{144}(SR)_{60}$ NCs and $Au_{25}(SR)_{18}$ NCs were first synthesized by the Whetten group within the same time period, reporting high yields of a 28 kDa species with a 1.7 nm Au core diameter and ~146 Au atoms in 1997,[77] and the isolation of a 10.4 kDa species with a ~0.9 nm Au core diameter, misidentified as $Au_{28}(SG)_{16}$ (HSG=glutathione), in 1998.[78] While it took ten years for the first crystal structure of $Au_{25}(SR)_{18}$ to be elucidated,[79, 80] it took 21 years for $Au_{144}(SR)_{60}$.[81] In fact, not a single $Au_n(SR)_n$ NC was analyzed via single-crystal X-ray diffractometry prior to 2007.[82] However, atomic precision is so integral to the study of NCs that the onset of their crystallographic elucidation resulted in

a paradigm shift in NC research towards preferentially utilizing NCs with solved crystal structures.

$Au_{144}(SR)_{60}$ NCs are perhaps historically the most sought-after gold nanocluster size regime despite their elusive crystal structures. Prior to their exact molecular formula being determined, the Murray group observed that they exhibited quantized capacitance charging,[83] and the Whetten group analyzed their spectroscopic features[84]. In 2009, Lopez-Acevedo *et al.* used density functional theory to accurately compute their molecular formula.[85] This formula was later confirmed in the same year using electrospray ionization mass spectrometry (ESI-MS).[41, 86] The structure of $Au_{144}(SR)_{60}$ NCs comprises of a hollow icosahedral grand core of 114 Au atoms and 60 surface-bound ligands arranged in rigid SR-Au(I)-SR staple motifs.[81, 87] In the last decade, the $Au_{144}(SR)_{60}$ size regime has been accessed using benzyl thiolate,[81, 87] phenylethane thiolate,[39, 40] hexyl thiolate,[88, 89] mercaptobenzoic acid,[90] phenylacetylene,[91] and 2-fluorophenylacetylene[92] ligands.

Due to their elucidated structure, $Au_{144}(SR)_{60}$ has become model system for better understanding quantum confinement effects.[89, 93, 94] Notably, Au_{144} still occupies a molecular rather than metallic state.[41, 93, 95] Consequently, it exhibits physical, chemical and electrochemical properties that differ from its ultrasmall counterparts, including a much smaller HOMO-LUMO gap,[96] single-electron charging behavior,[39, 97-99] and a lower surface-to-volume ratio. These unique features make $Au_{144}(SR)_{60}$ the subject of research for the development of nanoelectronic devices[99-101] and electrocatalysis.[87, 102-104] Furthermore, $Au_{144}(SR)_{60}$'s thermodynamic stability and small size relative to nanoparticles also indicate it has potential use in theranostic applications.[105-109]

A variety of ligands have been used to synthesize $Au_{144}(SR)_{60}$ NCs, yet none have exhibited interfacial reactivity. Moreover, the implications of developing an azide-functionalized $Au_{144}(SR)_{60}$ NC extend beyond post-synthesis functionalization. Owing to lower surface-to-volume ratios and fewer points of contact between their core and ligand shell, the structure of $Au_{144}(SR)_{60}$ alludes that they may be less sensitive to ligand modification when compared to $Au_{25}(SR)_{18}^-$. However, empirical evidence suggests the

opposite is true: ligand structure has a strong influence on the optoelectronic properties of $Au_{144}(SR)_{60}$ NCs.[91, 110, 111] Ligand exchange on $Au_{144}(SR)_{60}$ NCs, for example, has resulted in size transformations from $Au_{144}(SC_2H_4Ph)_{60}$ to $Au_{99}(SPh)_{42}$[112], $Au_{133}(S\text{-}p\text{-}C_6H_4\text{-}^tBu)_{52}$[113], and $Au_{279}(SC_6H_4\text{-}^tBu)_{84}$[114]. Therefore, while from an organic chemistry perspective, organic azides are small and non-toxic moieties that can be easily incorporated into substrates with minimal structural effects,[115] it has yet to be established that the electronic properties of $Au_{144}(SR)_{60}$ NCs are negligibly impacted by ligand modification.

1.5   Scope of Thesis

This thesis describes the synthesis and characterization of the azide-functionalized $Au_{144}(SR)_{60}$ NC platform for post-synthesis interfacial surface modification, $Au_{144}(SC_2H_4C_6H_4\text{-}N_3)_{60}$ (abbreviated as Au_{144}–N_3), containing 60 surface azides amenable to click chemistry. Further, it examines the regioisomeric effect of the *ortho-*, *meta-* and *para-* ligands on the Au_{144}–N_3 NC synthesis. Chapter 2 describes the synthesis and characterization of the Au_{144}-N_3 NCs. In Chapter 3, a proof-of-concept CS-SPAAC reaction is performed on the *p*-Au_{144}-N_3 NCs with a model strained alkyne, *exo*-9-hydroxymethylbicyclo[6.1.0]non-4-yne (BCN). This proof-of-concept reaction is followed by the post-synthesis modification of the *p*-Au_{144}-N_3 NCs with two functionalized strained-alkyne derivatives. The first BCN-derivative examined contains 2,2,6,6-tetramethylpiperidine-1-oxyl (TEMPO), a stable radical. The electrocatalytic capability of the Au_{144}–TEMPO NCs towards oxidation of alcohols to aldehydes is demonstrated using n-butanol as a model reaction. The second derivative reported contains ferrocene, a redox-active material. The amenability of the Au_{144}-N_3 NCs to modification with ferrocene is briefly examined and compared to previous research in which the same ferrocene-modified strained alkyne was reacted with azide-modified Au_{25} NCs. Lastly, Chapter 4 summarizes the findings described in Chapters 2 and 3 and briefly presents future work towards the development of surface- reactive NCs.

Chapter 2

2 Synthesis and Characterization of Azide-Modified Au$_{144}$(SR)$_{60}$ NCs

2.1 Ligand Synthesis

The ligands used for the design and synthesis of the Au$_{144}$-N$_3$ derivatives were *o-, m-,* and *p*-azidophenylethanethiol, prepared according to Gunawardene *et al.*[73] (**Scheme 4**). First, an S$_N$2 reaction was conducted on nitrophenethyl bromide to substitute its bromide substituent for an acetyl-protected thiol using potassium thioacetate. A zinc reduction was then used to reduce the aromatic nitro group of the product to an amine. The resulting aminophenethyl thioacetate was immediately filtered into a new reaction flask, acidified, and converted to azidophenethyl thioacetate using sodium nitrite followed by sodium azide. Lastly, the thioacetyl group was deprotected using aqueous base.
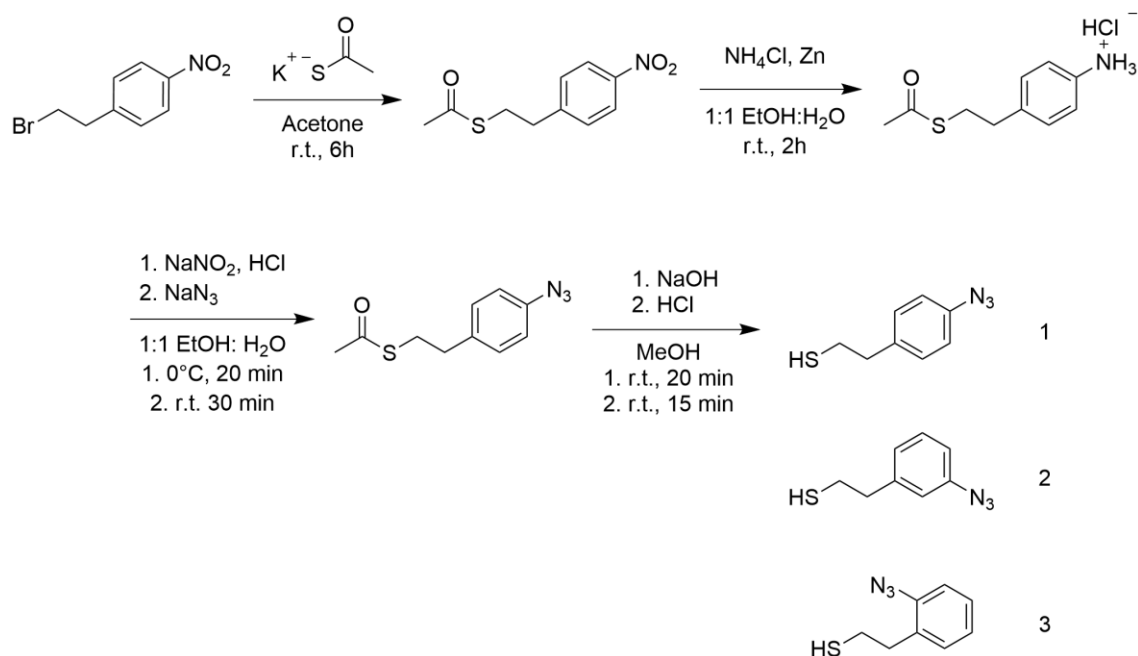
Scheme 4. Synthesis of azidophenylethane thiol ligands (1-3) from nitrophenethyl bromide.

2.2   Synthesis of Au$_{144}$(SR)$_{60}$ NCs

Despite the structural similarity of the ligands, it was observed that the inclusion of the azide within the ligand structure had a non-negligible effect on the Au$_{144}$(SR)$_{60}$ NC synthesis progressions and yields. The azide-functionalized Au$_{144}$(SR)$_{60}$ NCs were synthesized in acetonitrile according to Hesari *et al.*[39] (**Scheme 5**). Briefly, chloroauric acid was combined with a slight excess (1.2 eq.) of tetraoctylammonium bromide. The mixture was cooled in an ice bath and a great excess (6.0 eq.) of azidophenylethane thiol was added dropwise at a slow stir rate. The addition of the thiol resulted in the formation of a white polymeric mixture that could then be reduced with sodium borohydride solution to yield the crude product (further details provided in experimental section).
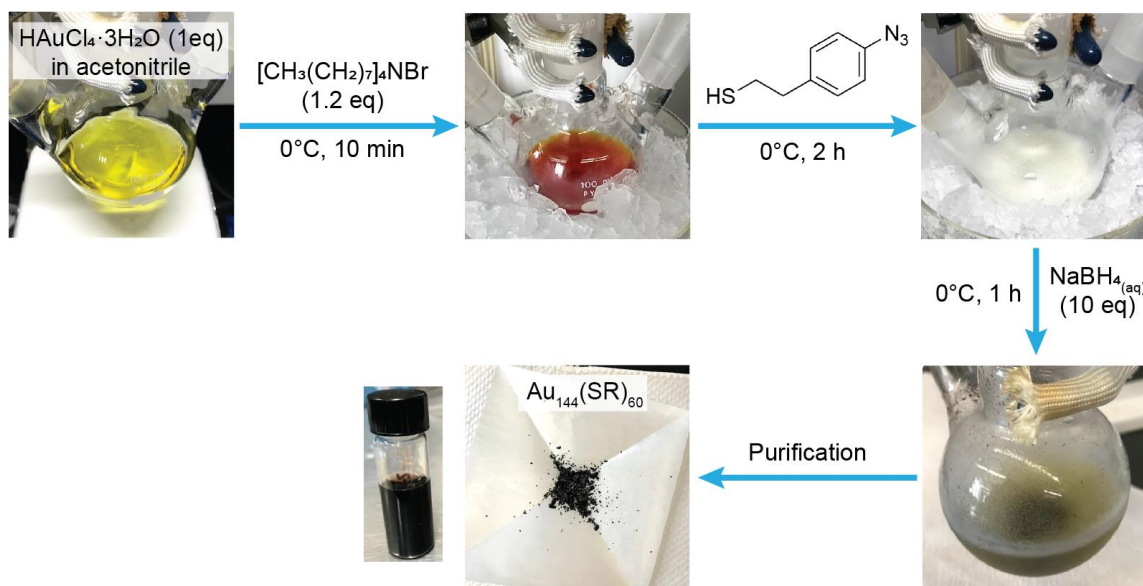
Scheme 5. Synthesis of Au$_{144}$(SC$_2$H$_4$-*p*-C$_6$H$_4$-N$_3$)$_{60}$ (*p*-Au$_{144}$-N$_3$) NCs.

The UV-Visible (UV-Vis) spectroscopic features of the Au$_{144}$(SC$_2$H$_4$-*p*-C$_6$H$_4$-N$_3$)$_{60}$ NCs (abbreviated as *p*-Au$_{144}$-N$_3$) emerged after one hour following the addition of sodium borohydride, whereas for the parent Au$_{144}$(SC$_2$H$_4$-Ph)$_{60}$ NC (abbreviated as Au$_{144}$), spectroscopic features emerged within a 20-minute timeframe. The slower size evolution was accompanied visually by a slower rate of precipitation of the Au$_{144}$-N$_3$ NCs. The length of the size evolution process was also observed to be critical to the monodispersity of the product, as a greater reduction period led to the formation of Au$_{25}$(SR)$_{18}$ as a side

product, which was extracted into acetonitrile during the purification process and observed using UV-Vis spectroscopy. Notably, if the reaction was stopped at 1h, appreciable amounts of $Au_{25}(SR)_{18}$ NCs were not obtained, though small amounts were later visible during mass spectrometry analyses. Density functional theory (DFT) was used to analyze the *o-*, *m-*, and *p-* ligands and revealed that the presence of the azide group shifts electron density in the highest occupied molecular orbitals (HOMOs) away from the thiol. The lowest unoccupied molecular orbital (LUMO) of *p-*azidophenylethanethiol was most like the parent phenylethanethiolate ligand, however the LUMOs of *o-* and *m-* ligands exhibited much less sulfur character (**Figure S1**). Therefore, the effect of the azide group on the electronic structure of the ligands may have played a role in the rate of size evolution of the NCs, although steric factors are also likely a contributing factor.

The Au_{144}-N_3 derivatives exhibited UV-Vis (**Figure 3a**) and ^{1}H NMR spectroscopic data (**Figures S2-S5**) that matched the characteristic broad absorbance centered at 532 nm and broadened chemical shifts, respectively, of Au_{144}. The yield of the *o-*Au_{144}-N_3 NCs was lower (9-12% yield based on the mass of gold used), likely owing to the sterics of the azide moiety located at the ortho position. Importantly, the azide functionality was incorporated on the surface of the Au_{144} NCs and its asymmetric and symmetric IR stretches could be easily identified within the IR spectrum of the products at 2113 cm $^{-1}$ and 1289 cm $^{-1}$, respectively (**Figure 3b**).
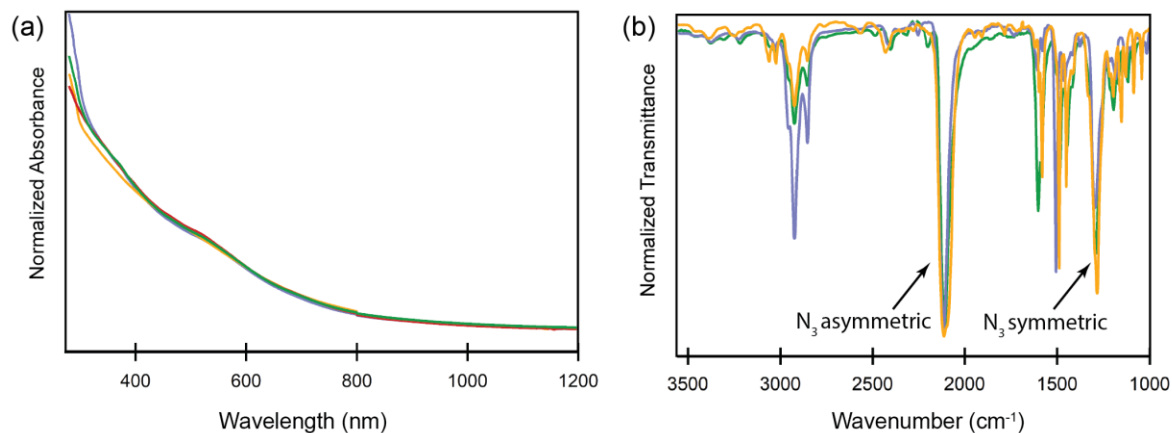
Figure 3. Spectroscopy of Au$_{144}$–N$_3$ NCs. (**a**) UV-visible and (**b**) infrared spectra of Au$_{144}$ (red), o-Au$_{144}$–N$_3$ (yellow), m-Au$_{144}$–N$_3$ (green), p-Au$_{144}$–N$_3$ (purple)

2.3   Mass spectrometry and thermogravimetric analysis of Au$_{144}$(SR)$_{60}$ NCs

The mass spectrometry data of Au$_{144}$ and the Au$_{144}$-N$_3$ NCs were obtained using matrix-assisted laser desorption ionization mass spectrometry (MALDI-MS) with trans-2-[3-(4-*tert*-Butylphenyl)-2-methyl-2-propenylidene]malononitrile (DCTB) as the matrix (**Figure 4a**). High laser intensities were required to ionize the NC samples. Au$_{144}$ ionized more readily when compared to the Au$_{144}$-N$_3$ NCs and exhibited a single broad signal that began at ~36125 Da and extended to ~27432 Da, with a maximum at ~33375 Da. The mass signal of Au$_{144}$ was consistent with previously reported MALDI-MS data and indicative of the loss of ligand (SR=SC$_2$H$_4$-Ph) fragments, and staple motifs (n[SR-Au(I)-SR], 0<n<30) during the ionization process.[38, 87, 116, 117] Sharp signals from Au$_{25}$(SC$_2$H$_4$-Ph)$_{18}$ were also observed as a minor impurity in the sample. Electrospray-ionization mass spectrometry (ESI-MS) of the sample corroborated Au$_{144}$(SR)$_{60}$ was present as the major species, observed in both its +4, +3 and +2 charge states. The +4, +3 and +2 charge states of Au$_{137}$(SC$_2$H$_4$-Ph)$_{56}$ and the +1 and -1 charge states of Au$_{25}$(SC$_2$H$_4$-Ph)$_{18}$ were present in the sample as minor impurities.
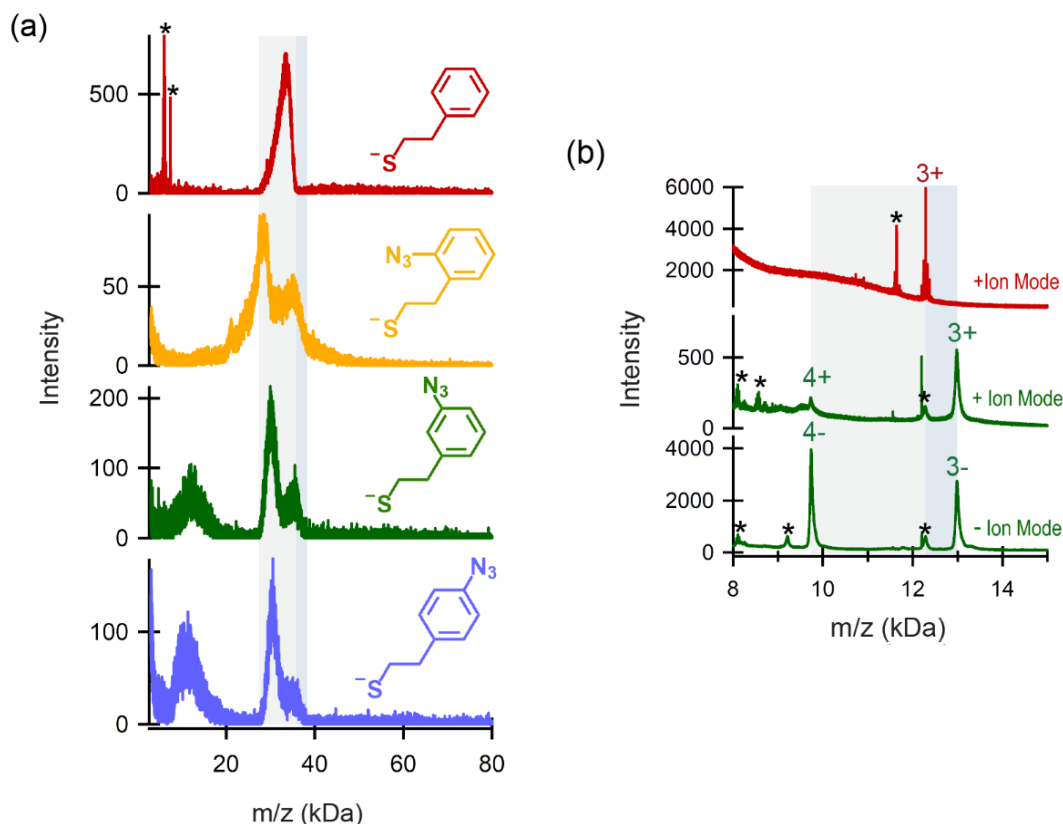
Figure 4. Mass spectrometry of Au$_{144}$(SR)$_{60}$ NCs. (**a**) MALDI-MS of Au$_{144}$ (red), o-Au$_{144}$–N$_3$ (yellow), m-Au$_{144}$–N$_3$ (green), p-Au$_{144}$–N$_3$ (purple) (**b**) ESI-MS of Au$_{144}$ (red) in positive ion mode and m-Au$_{144}$–N$_3$ (green) in both positive and negative ion modes. Asterisks indicate other NC impurities.

The three Au$_{144}$-N$_3$ NCs exhibited fragmentation ranges similar to Au$_{144}$ (**Figure 4a**). The o-Au$_{144}$-N$_3$ NCs had the broadest mass fragment distribution, with a greater fragment intensity below 30,000 Da than that of the p- and m-Au$_{144}$–N$_3$ NCs. Additionally, the o-Au$_{144}$-N$_3$ NCs contained a mass signal at ~21,075 Da, matching the mass of Au$_{107}$, a fragment that potentially originates from the Au$_{114}$ grand core following the stripping of all its surface motifs. In contrast, the MALDI-MS of the m- and p- ligands were virtually identical, with a smaller maxima and larger maxima consistent with Au$_{137}$(SC$_2$H$_4$-C$_6$H$_4$-N$_3$)$_{48}$ (n=7) and ~Au$_{128}$(SC$_2$H$_4$-C$_6$H$_4$-N$_3$)$_{28}$ (n=16), respectively. The greater fragmentation of the o-Au$_{144}$-N$_3$ NCs is likely due to the interference of the azide motif at the ortho position with the thiolate-Au bonding.

ESI-MS spectroscopy was successfully used to analyze the m-Au$_{144}$–N$_3$ NCs, in which its +3/-3 and +4/-4 charged fragments were observed, however the o- and p-Au$_{144}$ NCs could not be ionized via ESI methods (**Figure 4b**). Other minor fragments in the ESI-MS spectrum of m-Au$_{144}$–N$_3$ included the +2, +3/-3, and +4/-4 charge states of Au$_{137}$, and +2 and +1 charge states of Au$_{25}$. While the pattern of fragmentation in the MALDI-MS analysis emphasized the similarity between the Au$_{144}$-N$_3$ NCs, the effect of the position of the azide on the ability of the samples to ionize indicates that small changes to ligand structure influence the Au$_{144}$(SR)$_{60}$ NC regime.

The differences in the ligand features between Au$_{144}$ and p-Au$_{144}$-N$_3$ were also observed via thermogravimetric analysis (TGA). Thermogravimetric analysis can be used to measure the thermal stability and percentage of volatile components in materials. During TGA, the Au$_{144}$(SR)$_{60}$ ligands volatilize, leaving residual gold from the core component of the NCs. The percentage of remaining material can therefore be used to give an indication of the purity and thermostability of the NC samples and verify their stoichiometry. The Au$_{144}$ NCs in non-zero oxidation states contain counterions that contribute to their mass and alter their residual mass percentages. Therefore, as Au$_{144}^{-1}$ contains a tetraoctylammonium (TOA$^+$) counterion, its residual mass was calculated to be lower than Au$_{144}^{0}$. The theoretical residual mass percentage of Au$_{144}$ in its 0 and -1 oxidation states correspond to 77.5 and 76.5%, respectively. The observed residual mass percentage of Au$_{144}$ was 76.8%. The theoretical residual mass percentage of Au$_{144}$-N$_3$ NCs correspond to 72.6% in an oxidation state of 0 and 71.8% in an oxidation state of -1. The observed residual mass of the Au$_{144}$-N$_3$ NCs was 72.7%. Therefore, the percentage of mass remaining in TGA of the Au$_{144}$ and p-Au$_{144}$-N$_3$ matched the metal to ligand ratio of Au$_{144}$(SR)$_{60}$ NCs and indicated the samples were comprised of almost exclusively Au$_{144}$(SR)$_{60}$ (**Figure 5, Table 1**). Additionally, the TGA of the Au$_{144}$ NCs exhibited a much sharper trend in mass depletion, while the p-Au$_{144}$-N$_3$ NCs exhibited a more gradual mass loss, with a notable initial drop between 150°C and 200°C, indicative of N$_2$ loss and the decomposition of the azide fragment. Overall, the TGA data complemented mass spectrometric data supporting the synthesis of Au$_{144}$(SR)$_{60}$ NCs.
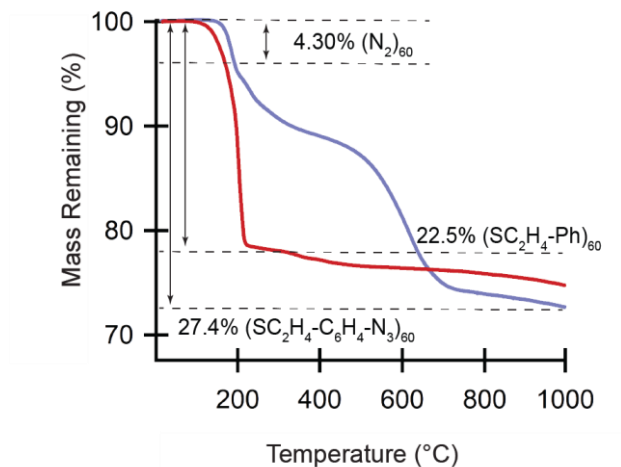
Figure 5. TGA of Au_{144} (red) and p-Au_{144}-N_3 NCs (purple). Dotted lines indicate theoretical mass percentages.

Table 1. Theoretical and Experimental TGA Mass Percentages.

Sample	Ligand Molecular Weight (g/mol)	Theoretical Residual Mass Percentage for $Au_{144}(SR)_{60}^0$ NC	Theoretical Residual Mass Percentage for $[Au_{144}(SR)_{60}^{-1}][TOA^+]$ NC	Experimental Residual Mass Percentage
Au_{144}	137.22	77.50	76.53	76.82
p-Au_{144}-N_3	178.23	72.62	71.76	72.68

2.4   Excitation and photoluminescence spectroscopy of $Au_{144}(SR)_{60}$ NCs

The photoluminescence (PL) spectra of the Au_{144} and the Au_{144}-N_3 NCs were obtained in dichloromethane at concentrations of 5 μM. The excitation wavelength was 532 nm, at a laser intensity of 10 mW (**Figure 6a**). The Au_{144}-N_3 NCs' emissions were similar to that of the Au_{144} NCs, owing to the similarity of their Au core structural features. The

17

maximum emission of Au_{144} was located at 933 nm. Slight shifts in maximum emission were observed for the *m*-azido and *p*-azido NCs, at 935 nm and 916 nm, respectively, while the greatest shift in peak maxima was observed for the *o*-azido NCs at 906 nm, a hypsochromic shift of 27 nm. The excitation spectra of the NCs were also collected (**Figure 6b**), measuring the edge of their emission at 850 nm. The excitation spectra of the NCs revealed greater optical fine structure than is observable in the UV-Vis spectra. These features are consistent with preexisting computational and experimental data pertaining to the optical features of $Au_{144}(SR)_{60}$ NCs and emphasized the structural similarity of their gold cores.[76, 89, 95, 118, 119]
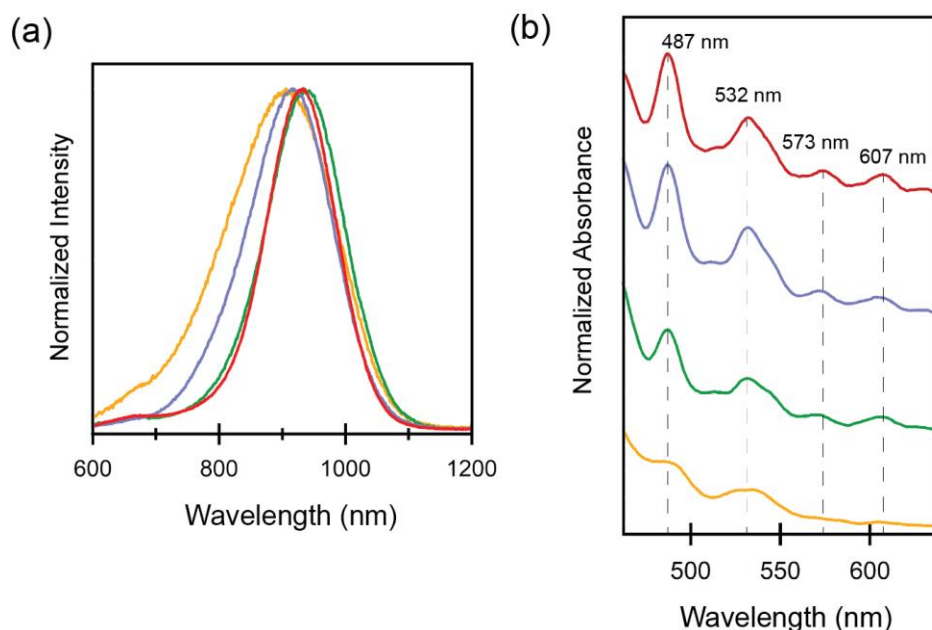
Figure 6. Spectroscopy of $Au_{144}(SR)_{60}$ NCs. (a) PL emission spectra of NCs, excited at 532 nm, and (**b**) excitation spectra of NCs, measuring at 850 nm, Au_{144} (red), *p*-Au_{144}-N_3 (purple), *m*-Au_{144}-N_3 (green), *o*-Au_{144}-N_3 (yellow).

2.5   Electrochemistry of *p*-Au_{144}-N_3 and *m*-Au_{144}-N_3 NCs

Figure 7a displays differential pulse voltammograms (DPVs) of 0.75 mM Au_{144} in dichloromethane containing 0.1 M tetra-*n*-butylammonium hexafluorophosphate ($TBAPF_6$) as the supporting electrolyte. The working electrode (WE) potential was

scanned from –1.9 to +1.8 V vs. SCE in both oxidation and reduction directions (indicated with red arrows). The DPV of Au_{144} displays 15 distinct redox pairs corresponding to consecutive electron transfers (ETs). These obtained electrochemical features of Au_{144} are similar to the previously reported DPVs.[39, 120]
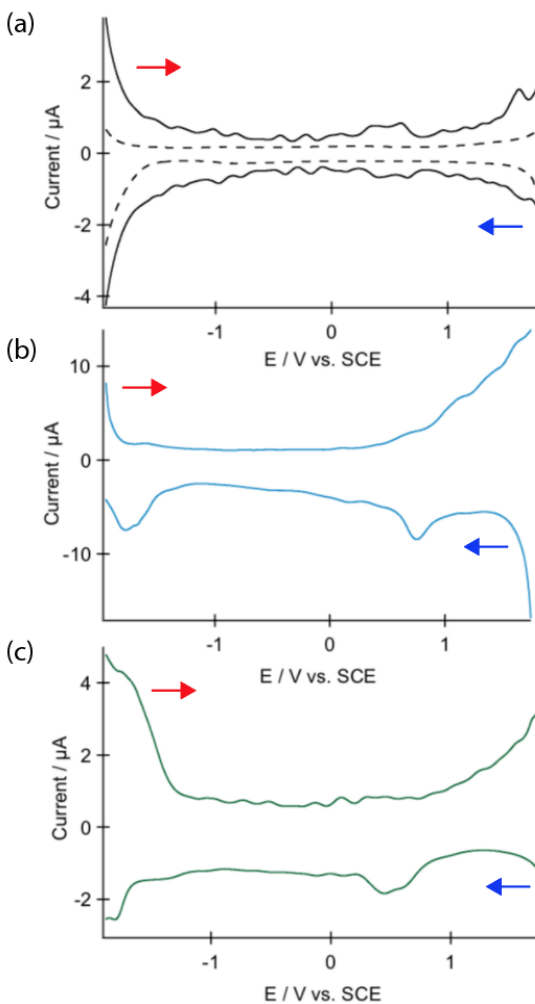
Figure 7. Electrochemistry of Au₁₄₄ NCs derivatives. DPVs of (**a**) 0.75 mM Au_{144}, (**b**) 0.75 mM *p*-Au_{144}-N_3, and (**c**) 0.5 mM *m*-Au_{144}-N_3 in dichloromethane containing 0.1 M tetra-n-butylammonium hexafluorophosphate (TBAPF₆) using a 2-mm Pt disk electrode. DPVs collected at peak amplitude of 50 mV, a pulse width of 0.05 s, 4 mV increment per cycle, and a pulse period of 0.2 s were applied to obtain DPVs. The arrows indicate potential scan directions. The dotted lines indicate background scan prior to addition of analyte.

DPVs of 0.75 mM of the p-Au$_{144}$-N$_3$ NCs in DCM/0.1 M TBAPF$_6$ are shown in **Figure 7b**. The following changes were observed in the electrochemical features of the p-Au$_{144}$ NCs in comparison with those observed for the Au$_{144}$; (*i*) the redox couples are less pronounced in the oxidation and reduction direction scans, though some features can be seen at potential larger than 0.51 V. (*ii*) in the reverse scan (indicated with blue arrow) peaks at +0.76 V and –1.77 V vs. SCE. It appears that the presence of the azide influenced the electrochemical behavior of the p-Au$_{144}$-N$_3$ NCs. More importantly, owing to the position of the azide group, i.e., *para-*, it is highly plausible that the NCs form a film on the electrode surface and, somehow, influence the ET process between the WE and the NCs by generating a semiconductive organometallic layer. To evaluate the effect of to the azide position on the electrochemistry of Au$_{144}$(SR)$_{60}$ NCs, the m-Au$_{144}$-N$_3$ NCs were also investigated in DCM/0.1 M TBAPF$_6$. The electrochemistry of the m-Au$_{144}$-N$_3$ NCs is shown in **Figure 7c**. Interestingly, the DPVs of the m-Au$_{144}$-N$_3$ NCs reveal more features, i.e., redox peaks, in comparison with the p-Au$_{144}$-N$_3$. This observation supports the influence of the azide position on the electrochemical behavior of Au$_{144}$ NCs and their assembly on the electrode surface to create a sluggish ET. Additionally, both derivatives show a peak at –1.7 V. To further understanding its plausible origin, the electrochemistry of p-azidophenylethanethioacetate was investigated in DCM/TBAPF$_6$ (**Figure S6**). The DPVs show a peak at –1.5 V that is corresponding to electroreduction of azide to initially its radical anion (-PhN$_3^{\bullet-}$) and subsequent reaction, according to Hawley and co-workers (more details are provided in supporting information).[121] The electrochemistry of the o-Au$_{144}$-N$_3$ NCs is shown in **Figure S7**, in which much fewer electrochemical features are observed.

To conclude, o-, m-, and p-Au$_{144}$-N$_3$ were successfully prepared and characterized in this chapter. While the incorporation of the azide groups was observed to noticeably interfere with the electron transfer processes during electrochemical analysis, the azides had little to no impact on the UV-Visible and photoluminescent features of the Au$_{144}$ NCs. Overall, characterization of the NCs indicated both the azide groups as well as the Au$_{144}$ core structure remained intact in all three of the NCs. Equipped with the knowledge that 60

azido- ligands were present on the surface of the NCs, proof-of-concept CS-SPAAC chemistry could now be conducted on the surface of the Au_{144}-N_3 NCs to establish their degree of reactivity towards post-synthesis interfacial modification.

2.5.1 Reagents.

Ammonium chloride (≥99.5%, fisher chemical), anhydrous magnesium sulfate (fisher chemical), Hydrogen tetrachloroaurate trihydrate (≥99.9%, Aldrich), zinc dust (≥98%, Aldrich), sodium borohydride (>98%, Acros Organics), 4-nitrophenethyl bromide (98%, Oakwood), potassium thioacetate (98% purity, Oakwood), celite 545 filter aid (Fisher Chemical), sodium thiosulfate pentahydrate solution (0.1N, Fisher Chemical), anhydrous sodium sulfate (99%, Acros Organics), tetraoctylammonium bromide (98%, Aldrich), phenylethane thiol(≥99%, Aldrich), sodium nitrite(≥97%, Caledon), sodium azide (≥97%, Aldrich), ethyl diazoacetate (13% wt dichloromethane, Aldrich), dichloromethane-d2 (99.9%, Aldrich), chloroform-d (99.8%, Cambridge Isotope Laboratories), hydrochloric acid(37%, Aldrich), triethylamine (≥99.5%, Millipore), tetra-n-butylammonium hexafluorophosphate (98%, Aldrich). Solvents were obtained from fisher chemical or Aldrich and used without further purification.

2.5.2 Instrumentation

Measurements were conducted at room temperature (25 °C) unless otherwise specified.

^{1}H, and ^{13}C{^{1}H} spectra were recorded on a Bruker AvIII HD 400. ^{1}H NMR spectra are reported as δ in units of parts per million (ppm) and referenced against residual protonated chloroform (δ 7.26 ppm, s), or dichloromethane (δ 5.32, t), as indicated. Multiplicities are reported as follows: s (singlet), d (doublet), t (triplet), q (quartet), quin (quintuplet), and m (multiplet). Second order splitting patterns, such as the AA'XX' para-substituted aromatic protons in *p*-azidophenylethane thiol, and for the ethyl substituents in the ligands are reported according to the latter multiplicity values based on their appearance. Coupling constants are reported as a J value in Hertz (Hz). The number of protons (n) for a given resonance is indicated as nH, based on spectral integration values.

$^{13}C\{^1H\}$ NMR spectra are reported as δ in units of parts per million (ppm) or referenced against residual protonated chloroform (δ 77.0 ppm, t).

Thermogravimetric analysis was performed using a TA Instruments Q50 TGA. Each sample was added as a fine powder to a platinum pan and heated at a rate of 10 °C/min from 25 °C to 1000°C under a flow of nitrogen (100 mL/min).

A Voyager DE mass spectrometer operated with an N_2 laser at 337 nm in the positive mode was used to obtain the MALDI-MS data. *trans*-2-[3-(4-*tert*-Butylphenyl)-2-methyl-2-propenylidene]malononitrile (DCTB) was used as the MALDI matrix (100 mg/mL).

ESI-MS was recorded using a Waters Synapt XS instrument. Sample solutions were prepared by dissolution in dichloromethane at a concentration of ~1-2 mg/mL and diluted as needed. The sample solution was then mixed with cesium acetate to facilitate the ionization of (neutral) AuNMs via cesium adduct formation. Typically, cesium acetate (10-20 μL, 50 mg/mL) was added to the sample (150 μL) and mixed prior to introducing the sample via the ESI source. UV-Visible (UV-Vis) spectra were recorded using an Agilent technologies Cary 5000 UV-Vis-NIR spectrophotometer using standard quartz cells (1 cm path length) with a scan range of 200-1200nm.

Photoluminescence measurements were conducted in dichloromethane using Acton 2300i spectrograph equipped with an iDus BRDD CCD camera. A 532 nm COHERENT laser (model 1037860, VERDI 5W) attached to a cooler (model: T255p) was utilized to excite the NC solutions.

Excitation spectra were measured using a Photon Technology International Quanta Master (QM4) scanning spectrophotometer (PTI, London, Canada) equipped with a Xenon flash lamp, emission monochromator with a grating blazed at 750 nm, and a red sensitive GaAs photomultiplier tube. For emission spectra of the Au_{144}, *m*-Au_{144}-N_3, and *p*-Au_{144}-N_3 NCs, the emission slits were set to 10 nm and the excitation slits were set to 20 nm. For excitation spectra of the Au_{144} and *p*-Au_{144}-N_3 the excitation slits were set to 10 nm and the emission slits were opened to 20 nm. For excitation spectra of the *m*-

Au_{144}-N_3, the excitation slits were 10 nm and the emission slits were 30 nm. Spectra were smoothed using Fourier Transform smoothing.

Attenuated total reflectance IR (ATR-IR) spectra were recorded using a PerkinElmer Spectrum Two FT-IR spectrometer.

The electrochemistry of the $Au_{144}(SR)_{60}$ NCs were investigated using a CH instrument (model 760E), and a three-electrode system including a 2 mm Pt disk, Pt coil and $Ag/Ag^+/TPAPF_6$ which served as working, counter, and reference electrodes. The solution was purged with argon prior to the electrochemical studies.

2.5.3 Preparation and Characterization of Compounds

p-azidophenylethanethiol (1)
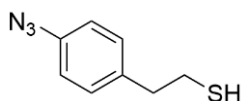
Prepared according to Gunawardene *et al.*[66]

^{1}H NMR (CDCl$_3$, 400 MHz): δ (ppm) 7.18 (d, 2H, *J*=8.4 Hz), 6.98 (d, 2H, *J*=8.4 Hz), 2.90 (q, 2H, *J*=7.2 Hz), 2.77 (q, 2H, *J*=7.2 Hz), 1.36 (t, 1H, *J*=8.0 Hz).

m-azidophenylethanethiol (2)
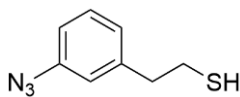
Prepared according to Gunawardene *et al.*[73]

^{1}H NMR (CDCl$_3$, 400 MHz): δ (ppm) 7.29 (t, 1H, *J*=7.6 Hz), 6.98 (d, 1H, *J*=7.6 Hz), 6.91 (dd, 1H, *J$_1$*=7.6 Hz, *J$_2$*=2.0 Hz), 6.85 (s, 1H), 2.92 (t, 2H, *J*=7.6 Hz), 2.79 (q, 2H, *J*=7.6 Hz), 1.38 (t, 1H, *J*=8.0 Hz).

o-azidophenylethanethiol (3)
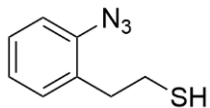
Prepared according to Gunawardene *et al.*[73]

^{1}H NMR (CDCl$_3$, 400 MHz): δ (ppm) 7.29 (dt, 1H, *J$_1$*=7.6 Hz, *J$_2$*=1.0 Hz), 7.17 (m, 2H), 7.08 (dt, 1H, *J$_1$*=7.6 Hz, *J$_2$*=1.0 Hz), 2.89 (t, 2H, *J*=7.6 Hz), 2.75 (q, 2H, *J*=7.6 Hz), 1.38 (t, 1H, *J*=8.0 Hz).

Au₁₄₄(SC₂H₄-C₆H₄-N₃)₆₀ NCs (o-Au₁₄₄-N₃ (4), m-Au₁₄₄-N₃(5), p-Au₁₄₄-N₃(6))

The protocol for the synthesis of $Au_{144}(SC_2H_4-C_6H_4-N_3)_{60}$ NCs was adapted from a one-pot monodispersed Au_{144} synthesis developed by Hesari *et al*[39]. Briefly, gold (III) chloride trihydrate (250 mg, 635 mmol, 1.0 eq.) was added to a 100 mL multi-neck flask fitted with a stir bar and dissolved in 25 mL of acetonitrile. This was followed by the addition of tetraoctylammonium bromide (417 mg, 763 mmol, 1.2 eq.). The mixture was cooled to 0°C in an ice bath over 10 minutes. Next, azidophenylethanethiol (683 mg, 3.81 mol, 6.0 eq.) was added dropwise over 5 minutes while stirring at 80 rpm. The reaction was stoppered and stirred for 2 hours, or enough time for the reaction mixture to form a colourless white suspension. Sodium borohydride (240 mg, 6.34 mol, 10 eq.) was dissolved in 5 mL of ice-cold milli-Q water and added in one portion at the highest possible controlled stir rate (generally 540 rpm). The reaction rapidly formed a black/brown solution. It was allowed to stir for 1 hour during which the black crude precipitated out. The crude NCs were isolated by gravity filtration and rinsed with a small amount of ice-cold acetonitrile (3 x ~2-3 mL) to wash away any potential $Au_{25}(SR)_{18}$. Reactions stopped at 1h were not observed to contain appreciable amounts of $Au_{25}(SR)_{18}$, however small amounts of $Au_{25}(SR)_{18}$ NCs could be detected during mass spectrometric analysis. The NCs were dried using rotary evaporation and purified by washing repeatedly with a methanol/water mixture, gradually increasing the percentage of methanol in the washing solution from 50% to 95% to remove excess thiol and borohydride salt and obtain the product as a shiny black powder. The typical yield of the reaction was 90-100 mg (26-29% yield based on mass of gold) for the *para-* and *meta-*regioisomers and 30-40 mg (9-12% yield based on the mass of gold used) for the *ortho-*regioisomer.

Au₁₄₄(S-C₂H₄-Ph)₆₀ NCs (7)

Prepared according to Hesari *et al.*[39] Crystals of **7** were obtained by dissolving 20 mg in 2 mL of DCM in an NMR tube and filling the tube to the brim with petroleum ether (~6 mL). After placing in a dark cabinet at room temperature for 1 month, the solution in the NMR tube had become colourless and small black crystals were observed on the walls of

the tube (**Figure 8**). The crystals were submitted to the X-ray Diffraction Facility in the Western Chemistry Department. They were then analyzed and an amorphous scattering during survey scans of the crystals was observed. This indicated the crystals were not of high enough quality for structural determination using single crystal X-ray diffractometry. Further attempts to grow high quality crystals by changing critical conditions such as solvent, and concentration were considered.
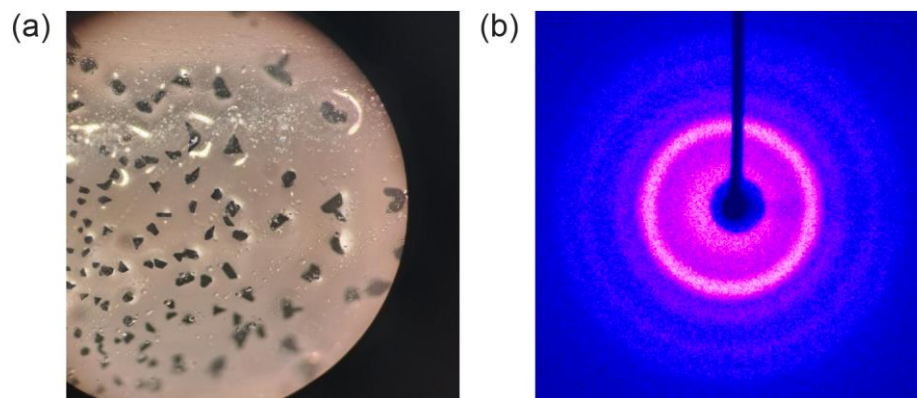
Figure 8. Single crystals of Au$_{144}$. (**a**) Optical image of obtained amorphous crystals grown on walls of NMR tube, (**b**) the observed amorphous scattering during survey scans of crystals.

Chapter 3

3 Post-Synthesis Modifications of *p*-Au$_{144}$–N$_3$ NCs via the CS-SPAAC Reaction

Azide-functionalized Au$_{144}$(SR)$_{60}$ NCs present an intriguing opportunity to examine the reactivity of their 60 surface azide groups towards click chemistry, the effect of modifying their ligand structure on their features, and the breadth of function that can be bestowed to Au$_{144}$(SR)$_{60}$ NCs post-synthesis (**Scheme 6**). In addition, having previously studied click chemistry on the surface of Au$_{25}$(SR)$_{18}$ NCs, click chemistry on Au$_{144}$(SR)$_{60}$ NCs enables one to compare interfacial reactivity at different size regimes. A quick calculation reveals that when scaling from Au$_{25}$(SR)$_{18}$ to Au$_{144}$(SR)$_{60}$, the rate of increase in the number of gold atoms is almost double that of the number of ligands (and their corresponding reactive surface groups). Among other contributing factors, like their structural features, this indicates that the interaction of the ligands with the Au NC core is unique at each size regime. The 60 ligands of the Au$_{144}$-N$_3$ are bound in 30 identical SR-Au-SR staple motifs and should therefore all exhibit the same reactivity towards the CS-SPAAC reaction. However, for any one superatomic molecule to undergo 60 independent surface reactions is a non-trivial process when one considers the new steric hindrance incurred by each CS-SPAAC reaction, and the difficulty that added sterics pose to succeeding CS-SPAAC reactions.
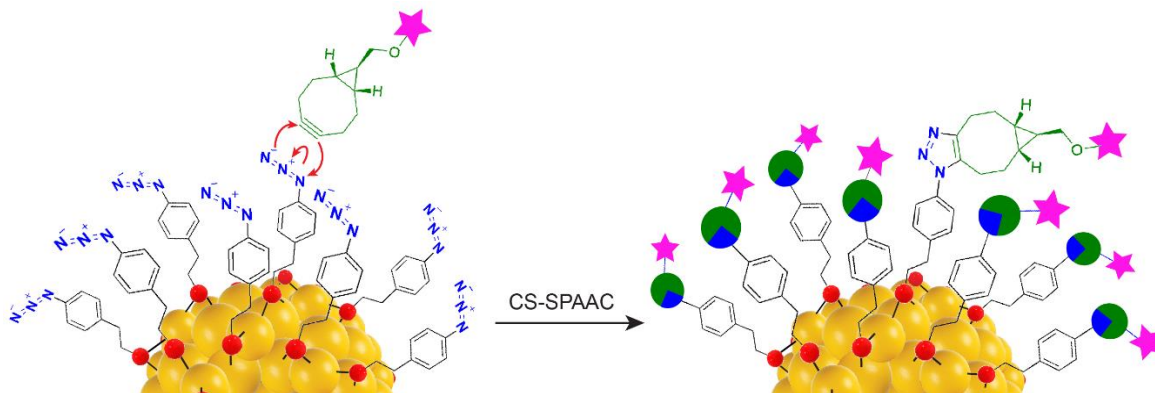
Scheme 6. CS-SPAAC reaction of Au$_{144}$-N$_3$ NCs. Introduction of function (pink star) to the surface of *p*-Au$_{144}$-N$_3$ NCs via the CS-SPAAC reaction, azide (blue), strained alkyne (green)

In order to optimize the investigation of proof-of-concept click chemistry of Au$_{144}$-N$_3$ NCs, we chose to select only one of the three Au$_{144}$-N$_3$ isomers based on our group's previous findings. Our recent study of the azido regioisomers of Au$_{25}$(SR)$_{18}$ NCs revealed *p*-azidophenylethanethiolate ligands exhibited superior reactivity towards the CS-SPAAC reaction.[73] While it had been previously established that electron donating groups decreased the reactivity of aromatic azides towards the CS-SPAAC reaction,[122] it was additionally observed that the position of the azide group within the azidophenylethanethiolate ligands of the Au$_{25}$-N$_3$ NCs also heavily influenced their rate of reactivity. The azide groups in the *m*- and *o*-Au$_{25}$-N$_3$ NCs are oriented more inwards towards the NC core relative to *p*-Au$_{25}$-N$_3$. This prevents the *o*-Au$_{25}$-N$_3$ NCs from stably undergoing the CS-SPAAC reaction altogether, and significantly decreases the reactivity of the *m*-Au$_{25}$-N$_3$ NCs, by a factor of 8 when compared to the *p*-Au$_{25}$-N$_3$ NCs. Therefore, reasoning that the performance of the Au$_{144}$-N$_3$ NC isomers likely mirrored that of the Au$_{25}$-N$_3$ NCs, the *p*-Au$_{144}$-N$_3$ NCs were used as the subject for examining proof-of-concept Au$_{144}$(SR)$_{60}$ CS-SPAAC click chemistry.

3.1 Proof-of-concept CS-SPAAC reaction with *exo*-9-hydroxymethylbicyclo[6.1.0]non-4-yne (BCN)

The amenability of the NCs to the SPAAC reaction was tested first using a readily accessible strained alkyne, *exo*-9-hydroxymethylbicyclo[6.1.0]non-4-yne (BCN),

synthesized according to previously reported literature procedures[123, 124] and added in slight excess (1.1 equivalents) to a stirring solution of the p-Au$_{144}$-N$_3$ NCs in dichloromethane (**Scheme 7**).
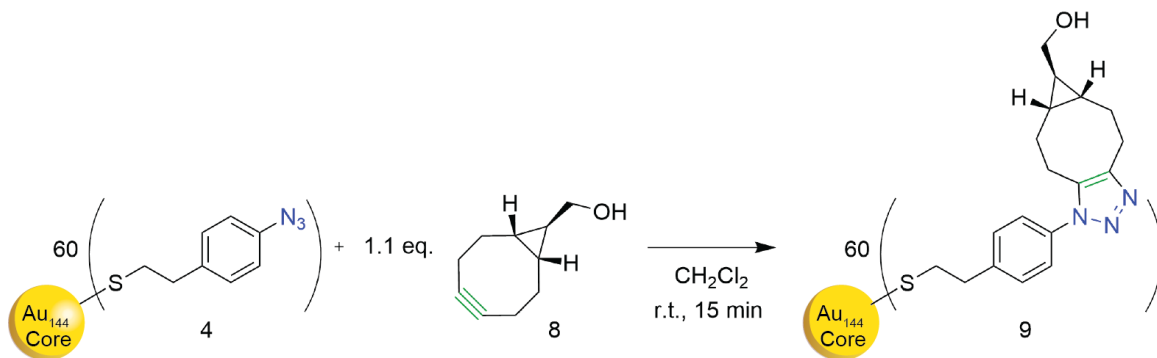
Scheme 7. CS-SPAAC reaction of p-Au$_{144}$-N$_3$ NCs with BCN (8) to produce p-Au$_{144}$-BCN NCs (9)

The NCs were observed to rapidly undergo the CS-SPAAC reaction with BCN and precipitated out of the reaction to produce a fine black suspension. The reaction mixture was dried by rotary evaporation and washed several times with dichloromethane to remove excess BCN. The apparent complete disappearance of the azide stretches and the appearance of a broad O-H stretch at 3358 cm^{-1} due to the hydroxyl group of BCN in the product's IR spectrum revealed all the azide ligands on the surface of the NCs underwent the CS-SPAAC reaction (**Figure 9b**). The UV-Vis spectra (**Figure 9a**) of the product, obtained in methanol, indicated that the structure of the Au$_{144}$(SR)$_{60}$ framework remained intact. TGA further corroborated that all the surface azides had reacted based on the sample's residual mass percentage, with a theoretical residual mass of 72.6% and an experimental mass percentage of 72.7% (**Figure S8**). Unlike the p-Au$_{144}$-N$_3$ NCs, the product of the click reaction was alcohol-soluble, owing to the 60 hydroxyl groups of BCN incorporated onto the NC surface. While the marked change in solubility was not the primary ambition of modifying the NCs with BCN, it highlighted how dependent the NC solubility is on the groups positioned at the NC-solvent interface and indicated the solubility of the NCs was tunable. This could be a valuable tool in the design of NCs for potential targeted properties like cell membrane permeability.
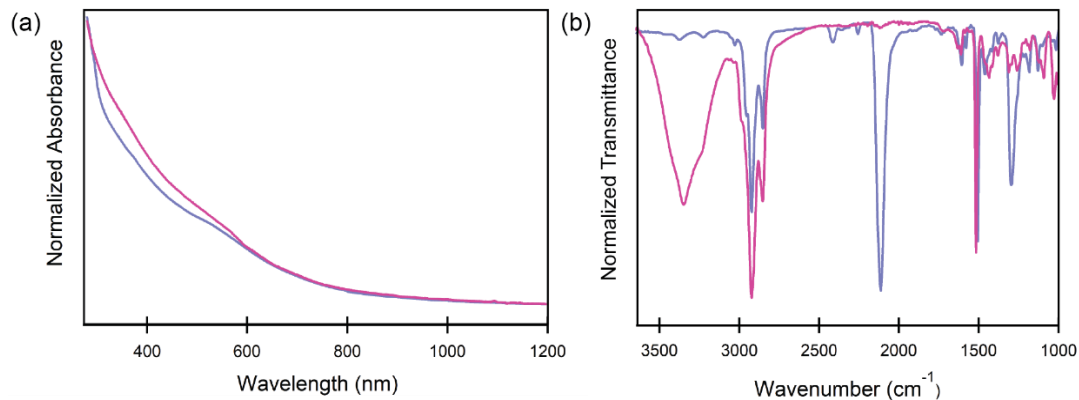
Figure 8. Spectroscopy of *p*-Au$_{144}$-BCN. (**a**) UV-Vis and (**b**) IR spectra of *p*-Au$_{144}$-N$_3$ NCs before (purple) and after (pink) click reaction with BCN

Upon clicking the *p*-Au$_{144}$-N$_3$ NCs with BCN, a PL spectrum was also obtained in methanol using the same concentration and parameters as the other samples (**Figure 10a**). The PL peak of the NCs were observed to broaden, and the peak maxima was shifted to a shorter wavelength at 892 nm. The broadening in the PL emission maxima of the click product may be attributed to the ligand density surrounding the NC core, where more sterically demanding thiolate ligands influence ligand to metal/ligand to metal-metal charge donation processes.[49] Due to the broader emission peak, its excitation spectra could be collected by measuring the edge of its emission at 756 nm, which allowed for the region of 410-460 nm to be probed within the excitation spectrum, avoiding the harmonic of the emission wavelength and revealing two additional excitation maxima at 423 nm and 445 nm (**Figure 10b**).
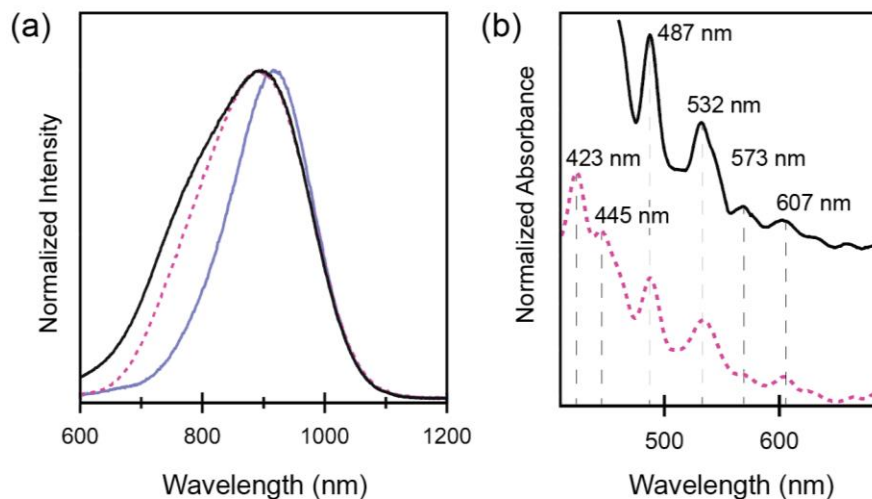
Figure 9. PL and excitation spectra of click products. (**a**) PL spectra with excitation at 532 nm, p-Au$_{144}$-N$_3$ (purple), click reaction product of p-Au$_{144}$-N$_3$ with BCN (pink, dotted), and click reaction product of p-Au$_{144}$-N$_3$ with BCN-TEMPO (black). (**b**) excitation spectra, measuring emission at 850 nm for p-Au$_{144}$-TEMPO (black) and 756 nm for p-Au$_{144}$-BCN (pink, dotted).

3.2   Functionalization of p-Au$_{144}$-N$_3$ NCs with TEMPO and their Catalytic Application

The compound 2,2,6,6-Tetramethylpiperidine-1-oxyl (TEMPO) is a stable nitroxyl radical that is used as a catalyst in oxidation reactions[125-127], a mediator in radical polymerization[128] and a probe for chemical sensing/imaging applications.[129-131] Its stability and range of applications have made it the subject of the development of nanomaterials and surface-modification studies.[132-134] TEMPO has been used previously in combination with Au nanoparticles (AuNPs) in the electrochemical detection of hydrogen peroxide.[135] It has also been thiolated and tethered to AuNPs for the development of therapeutics[136] and catalytic TEMPO-coated gold apparatuses.[137, 138] It has been applied to NC chemistry previously in order to study the electron transfer capability of Au$_{25}$(SC$_2$H$_4$Ph)$_{18}$ NCs,[139] and the formation of Au-H intermediates during gold Np- and NC-catalyzed alcohol oxidation reactions.[140, 141] We therefore chose to investigate whether TEMPO could be incorporated through the CS-SPAAC reaction as

another proof-of-concept post-synthesis modification. Further, the incorporation of the TEMPO moiety brings potential application of these NCs to memory devices, redox probes and specifically as herein described, electrocatalysis.

To functionalize the p-Au_{144}-N_3 NCs with TEMPO, the hydroxyl group of BCN was converted to a nitrophenoxy carbonate leaving group according to Dommerholt et $al.$,[123] and reacted with 4-amino-TEMPO (Tempamine) to tether BCN to TEMPO via a carbamate group (**Scheme 8**). The resulting BCN-TEMPO substrate was reacted in excess with the p-Au_{144} NCs for 1h before it was dried and washed with methanol to remove excess BCN-TEMPO.
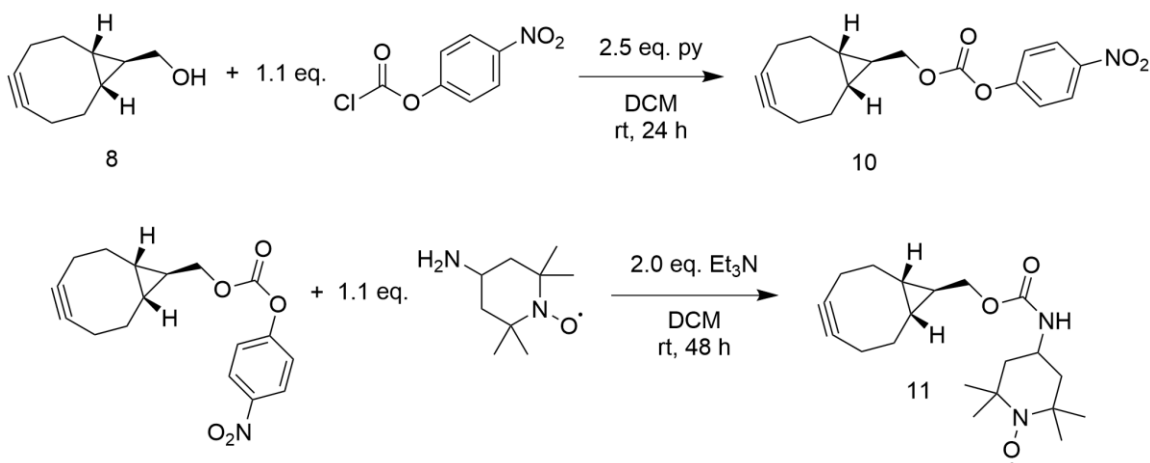
Scheme 8. **Synthesis of BCN-TEMPO (11)**

The complete click reaction of the product was confirmed using infrared spectroscopy (**Figure 11a**), indicated by the complete disappearance of the azide stretch. It was also confirmed by the appearance of an N-H stretch at 3336 cm^{-1} and carbonyl stretch at 1700 cm^{-1}, both attributed to the carbamate group of BCN-TEMPO now tethered to the NC surface. The residual mass within the TGA of the TEMPO-functionalized NCs (47.3 % theoretically, 47.7% experimentally) was consistent with all the surface azides reacting with BCN-TEMPO (**Figure S9).** The presence of the nitroxyl radical on the surface of the cluster was observed with electron paramagnetic resonance (EPR) spectroscopy (**Figure 11b**). Moreover, the CV of 0.15 mM of p-Au_{144}-TEMPO in DCM/0.1 M

TBAPF$_6$ also confirms the presence of TEMPO functionality with redox potential of 0.85 V vs. SCE (**Figure 11c**).
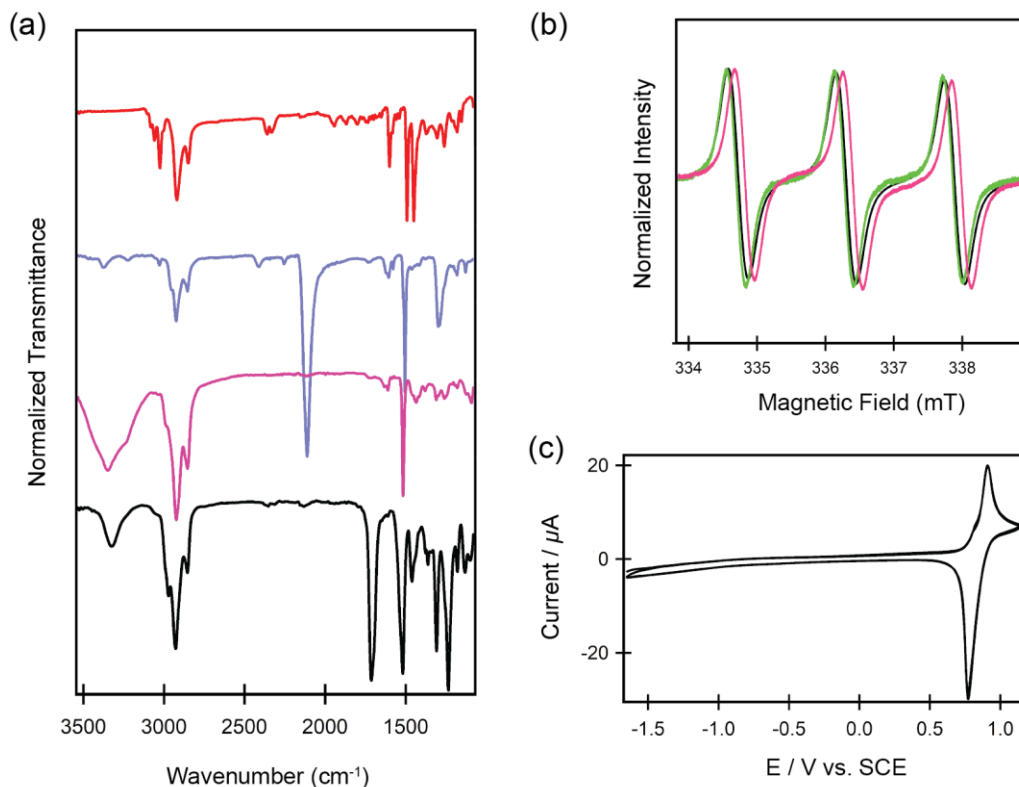
Figure 10. Characterization of *p*-Au$_{144}$-TEMPO. (**a**) Infrared spectra of Au$_{144}$ (red), *p*-Au$_{144}$-N$_3$ (purple), *p*-Au$_{144}$-BCN (pink), and *p*-Au$_{144}$-TEMPO (black). (**b**) EPR spectroscopy of *p*-Au$_{144}$ NCs after click reaction with BCN-TEMPO (black), 4-amino-TEMPO (orange), BCN-TEMPO (green). (**c**) Cyclic voltammogram (CV) of 0.15 mM *p*-Au$_{144}$-TEMPO in DCM/0.1 M TBAPF$_6$ using a 2-mm Pt disk working electrode.

To test its electrocatalytic activity, the *p*-Au$_{144}$-TEMPO was embedded in a sulfonated tetrafluoroethylene-based fluoropolymer-copolymer, Nafion, in order to create a permeable heterogenous catalyst with good ion exchange capacity. The effectiveness of this heterogeneous *p*-Au$_{144}$-TEMPO NC catalyst was then examined by measuring the current response of TEMPO at the working electrode when placed in an electrochemical cell with varying concentrations of an oxidizable substrate, n-butanol (**Scheme 9**).
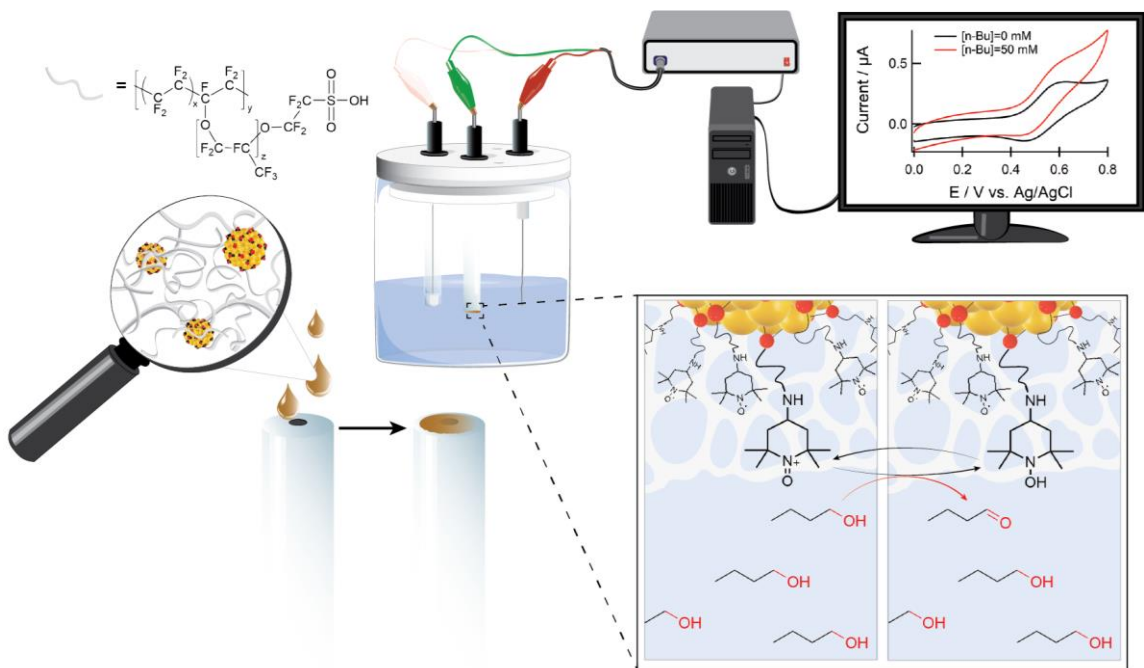
Scheme 9. Drop-casting of *p*-Au$_{144}$-TEMPO in Nafion polymer on to surface of GC electrode and subsequent experimental setup measuring electrocatalytic oxidation of n-butanol to n-butanal at pH of 9.

Nafion and *p*-Au$_{144}$-TEMPO were dissolved in THF, drop casted onto a glassy carbon working electrode and dried overnight. The electrode was then placed in sodium bicarbonate solution at a pH of 9. **Figure 12a** displays typical cyclic voltammogram of *p*-Au$_{144}$-TEMPO modified GC electrode in 0.5 M NaHCO$_3$, pH 9. The capability of the immobilized TEMPO on *p*-Au$_{144}$-TEMPO to electrocatalytically oxidize an alcohol as a model compound was investigated. The alcohol selected was n-butanol according to previous studies showing n-butanol to be the most active in the nitroxyl-mediated electrocatalytic oxidation of alcohols.[142] The electrocatalytic activity of *p*-Au$_{144}$-TEMPO was first investigated using cyclic voltammetry technique. **Figure 12b** displays a series of CVs of the modified GC electrode with *p*-Au$_{144}$-TEMPO in pH 9 in the absence and presence of various concentrations of n-butanol at 10 mV/s scan rate. Moreover, chronoamperograms (CAs) at E$_{app}$=0.6 V vs. Ag/AgCl were generated in which the potential was held constant for 3 minutes and the response in current was measured when 50mM, 100mM, 150mM, and 200mM solutions of n-butanol were added (**Figure 12c**). A plot of current vs. [n-butanol]$^{-1}$ from the extrapolated data indicated the *p*-Au$_{144}$-TEMPO

NCs indeed displayed catalytic behavior (**Figure 12d**). As one may argue that the observed electrocatalytic activity originates from the presence of the gold core, a control experiment was considered. A GC electrode modified with Au_{144} NCs and its reactivity towards the electrocatalytic oxidation of n-butanol was examined in $NaHCO_3$. In fact, the obtained CVs did not show any faradic current. In addition, there was no appreciable change in the CA current in the presence of various n-butanol concentrations (**Figure S12**).
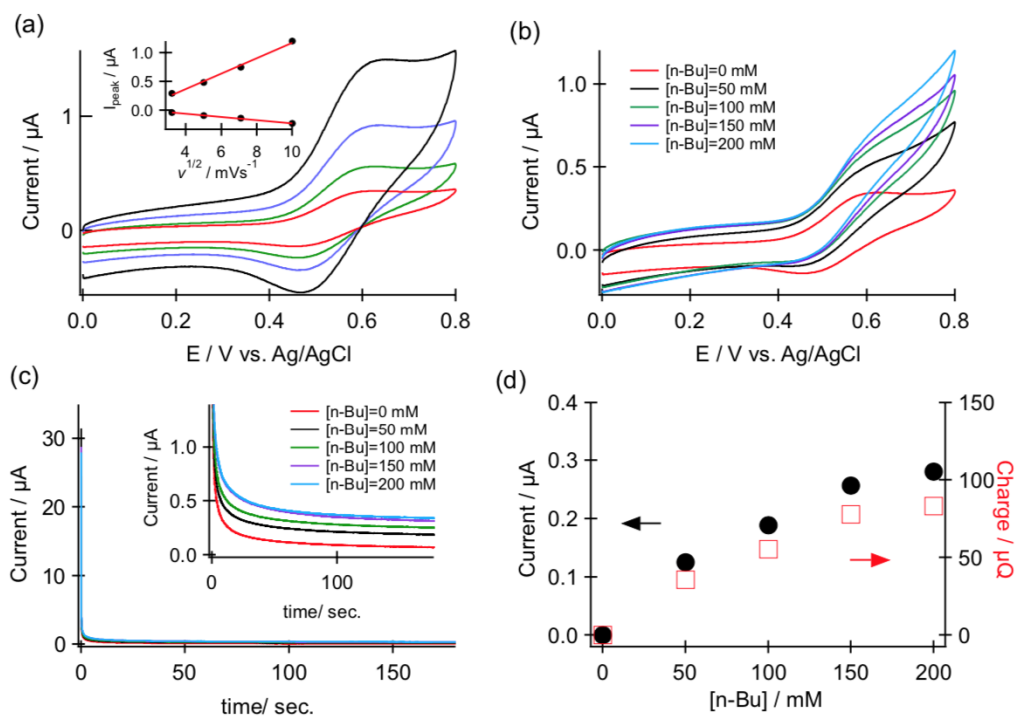
Figure 11. Electrocatalysis of *p*-Au₁₄₄-TEMPO. **(a)** Cyclic voltammograms (CVs) of dropcasted *p*-Au₁₄₄-TEMPO on a 2-mm GC electrode at various scan rates; 10 mV (red), 25 mV (green), 50 mV (purple), and 100 mV/s in 0.5 mM $NaHCO_3$. The inset displays anodic and cathodic peaks versus square root of scan rate. **(b)** CVs of GC-modified *p*-Au₁₄₄-TEMPO in the absence (red) and presence of 50 mM (black), 100 mM (green), 150 mM (purple), and 200 mM (blue) of *n*-butanol in 0.5 mM $NaHCO_3$ at 10 mV/s. **(c)** CA curves of electro-oxidation of *n*-butanol on *p*-Au₁₄₄-TEMPO-modified GC electrode in the absence (red) and presence of 50 mM (black), 100 mM (green), 150 mM (purple), and 200 mM (blue) of *n*-butanol in 0.5 mM $NaHCO_3$ at 0.6 V vs. Ag/AgCl**. (d)** Current and charge vs. n-butanol concentrations. Data are taken from CA curves in panel (c).

3.3   Functionalization of *p*-Au$_{144}$-N$_3$ NCs with Ferrocene

In addition to appending TEMPO to the surface of the *p*-Au$_{144}$-N$_3$ NCs, the click reaction of the NCs with a strained alkyne containing ferrocene was also investigated. Ferrocene (Fc) is a redox-active compound that has been used in nanoparticles for applications such as chemodynamic cancer therapy[143] and chemical sensing[144]. Due to its stability and solubility in common organic solvents, it is a popular proof-of-concept reagent for bestowing function to nanomaterials.[145-149] Dr. Gunawardene previously demonstrated that Fc could be appended to the surface of an azide-functionalized Au$_{25}$(SC$_2$H$_4$-*p*-C$_6$H$_4$-N$_3$)$_{18}$ NC (*p*-Au$_{25}$-N$_3$) via a CS-SPAAC reaction.[150] He observed that all 18 surface azides of *p*-Au$_{25}$-N$_3$ could be functionalized with Fc to produce an Au$_{25}$(SR)$_{18}$ NC with 18 electroactive Fc groups. We therefore sought to compare the reactivity of the *p*-Au$_{144}$-N$_3$ NCs to that of the *p*-Au$_{25}$-N$_3$ NCs using the same Fc click derivative.

To synthesize the Fc click derivative, ferrocene carboxylic acid (Fc-COOH) was coupled to BCN through an esterification reaction using dicyclohexylcarbodiimide (DCC) as a coupling reagent (**Scheme 10**).[150] The BCN-Fc product was purified by column chromatography and confirmed using NMR, IR, and UV-Vis spectroscopic methods, matching the data previously collected and reported by Dr. Gunawardene.
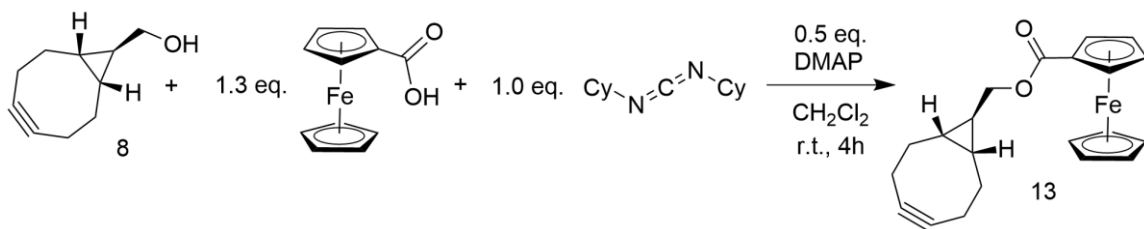
Scheme 10. Synthesis of BCN-Fc (13)

BCN-Fc was then added to the *p*-Au$_{144}$-N$_3$ NCs in an excess of 0.5 equivalents in dichloromethane and stirred for 40 minutes. The reaction mixture was then dried by rotary evaporation and washed with acetonitrile to remove excess Fe-BCN. The IR spectrum of the product still contained a strong azide stretch and so the crude product was redissolved and 1.5 equivalents of Fe-BCN were re-added to the reaction mixture.

The reaction was stirred overnight and washed again, however no further change in the IR spectrum was observed.

The IR spectrum of the starting materials and product (*p*-Au$_{144}$-Fc) can be seen in **Figure 13a**. By comparing the intensity of the azide stretch at 2116 cm^{-1} to the C-C stretching vibration of the *p*-azidophenylethane thiolate ligand at 1506 cm^{-1} in the IR spectrum of the partially clicked product relative to that of the starting material, the percentage of clicked BCN-Fc could be approximated. Prior to the CS-SPAAC reaction, the azide intensity equated to 147.1% of the C-C stretch intensity. Subsequently, the azide stretch equated to 93.2% of the C-C stretch intensity. The change in relative intensity of the two stretches corresponds to 38 ligands clicking on to the surface of the cluster, or in other words, 63.3% of the ligands reacting. The lower reactivity of the *p*-Au$_{144}$-N$_3$ NCs can be largely attributed to the bulk of the Fc groups at the surface of the NCs, likely blocking the residual azides from reacting further. Additionally, a smaller azide stretch overlapping with the azide stretch at 2083 cm^{-1} was observed, indicating a change to the chemical environment of the azides on the surface of the *p*-Au$_{144}$-N$_3$ NCs.
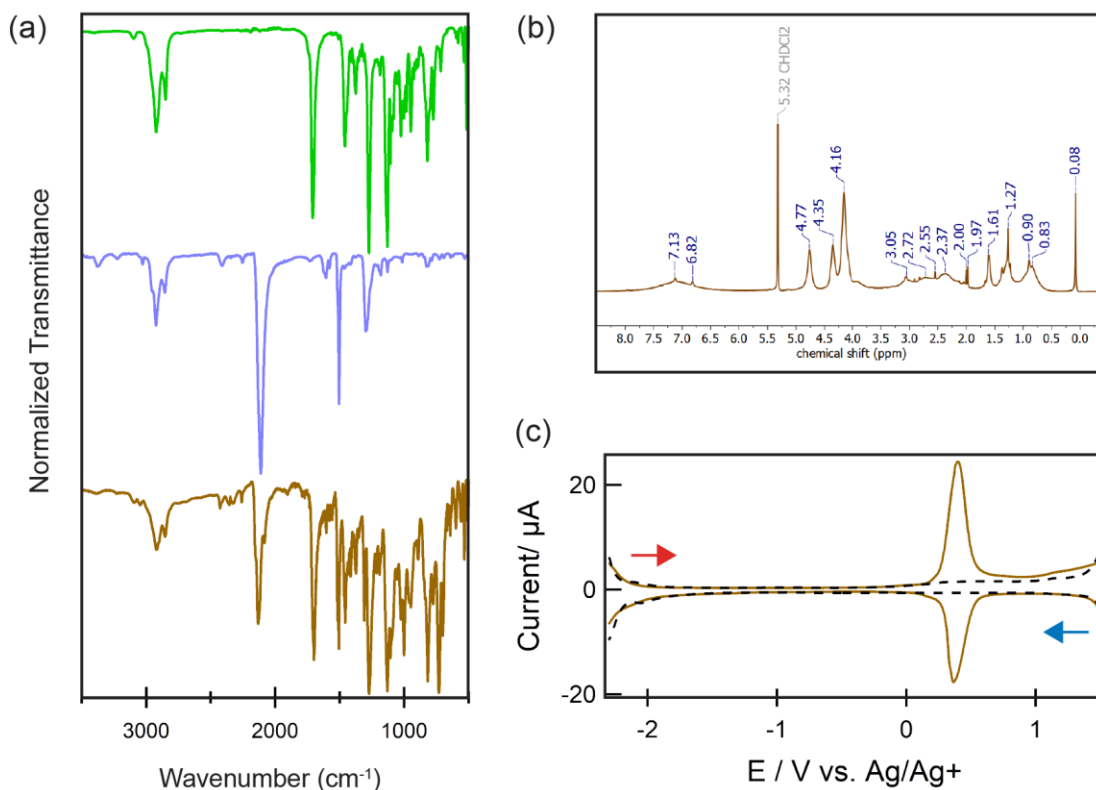
Figure 12. **Characterization of *p*-Au₁₄₄-Fc NCs. (a)** IR spectrum of BCN-Fc (green), *p*-Au₁₄₄-N₃ (purple), and *p*-Au₁₄₄-Fc (brown), **(b)** ^{1}H NMR spectrum of *p*-Au₁₄₄-Fc, **(c)** DPV of 0.13 mM of *p*-Au₁₄₄-Fc in DCM/ 0.1 M TBAPF, with arrows indicating potential scan directions. The dotted line indicates the background scan prior to the addition of the analyte.

Figure 13b shows the ^{1}H NMR spectrum of the click product. Notably, three new broad peaks at 4.77, 4.35 and 4.16 ppm are present in the spectrum that correspond to the protons of the cyclopentadienyl groups of clicked-on BCN-Fc. These peaks are also visible in the proton spectrum of *p*-Au₂₅-N₃ functionalized with surface Fc groups (*p*-Au₂₅-Fc). However, in the *p*-Au₂₅-Fc NC, these peaks are considerably less broadened due to the smaller size regime of the NC and can be identified as two triplets and a singlet, respectively.

Lastly, **Figure 13c** displays the DPV of the *p*-Au₁₄₄-Fc NCs in dichloromethane. A quasi-reversible peak was observed at 0.40 V vs. SCE corresponding to the Fc^0/Fc^{+1} redox activity of the Fc motifs on the surface of the *p*-Au₁₄₄-Fc NCs. Electrochemical

activity attributed to the *p*-Au₁₄₄-Fc NC Au core was not observed in the DPV. Interestingly, the irreversible electroreduction of the surface azide groups at -1.7 V, previously observed in the DPV of the Au_{144}-N_3 NCs, was also not observed in the DPV. The seemingly invisible azide motifs in the electrochemistry of the Fc-decorated NCs emphasize the role that structural arrangement plays in the performance of functional groups within NCs. Unsurprisingly, when scaling up from $Au_{25}(SR)_{18}$ to $Au_{144}(SR)_{60}$, the reactivity of surface ligands towards the CS-SPAAC reaction may therefore vary. While the electrochemical activity of the azide group was masked by the introduction of the BCN-Fc substrate, it has yet to be established whether the reactivity of the residual azides was completely suppressed. In future, these residual azide groups could potentially serve as a handle in order to functionalize the surface of the NCs with multiple surface groups.

3.4   Experimental

3.4.1 Chemicals

Ammonium chloride (≥99.5%, fisher chemical), anhydrous magnesium sulfate (fisher chemical), Hydrogen tetrachloroaurate trihydrate (≥99.9%, Aldrich), zinc dust (≥98%, Aldrich), sodium borohydride (>98%, Acros Organics), 4-nitrophenethyl bromide (98%, Oakwood), potassium thioacetate (98% purity, Oakwood), rhodium(II) acetate dimer (anhydrous, 46% Rh, Acros Organics), cis,cis-1,5-cyclooctadiene (99%, stabilized with 50-200ppm Irganox 1076, Alfa Aesar), lithium aluminium hydride (≥95%, Alfa Aesar), sodium sulfate (≥99%, Acros Organics), potassium tert-butoxide (pure, 1M solution in THF, AcroSeal^tm, Acros Organics), celite 545 filter aid (Fisher Chemical), sodium thiosulfate pentahydrate solution (0.1N, Fisher Chemical), anhydrous sodium sulfate (99%, Acros Organics), tetraoctylammonium bromide (98%, Aldrich), phenylethane thiol(≥99%, Aldrich), sodium nitrite(≥97%, Caledon), sodium azide (≥97%, Aldrich), ethyl diazoacetate (13% wt dichloromethane, Aldrich), bromine (≥99.99, Aldrich), amino-TEMPO (95%, Oakwood), 4-toluenesulfonyl chloride (99%, Oakwood), ferrocene carboxylic acid (98%, oakwood), N,N'-dicyclohexylcarbodiimide (DCC) (99%, Sigma-Aldrich), 4-dimethylaminopyridine (DMAP) (99%, Alfa-Aeasar), dichloromethane-d2 (99.9%, Aldrich), chloroform-d (99.8%, Cambridge Isotope Laboratories), hydrochloric acid(37%, Aldrich), triethylamine (≥99.5%, Millipore), tetra-n-butylammonium

hexafluorophosphate (98%, Aldrich). Solvents were obtained from fisher chemical or Aldrich and used without further purification. Dry solvents were dispensed from an Innovative Technology SPS-400-5 solvent purification system, in which they were dried over alumina and degassed. They were stored over 3Å molecular sieves and used on the day they were obtained.

3.4.2 Instrumentation

Measurements were conducted at room temperature (25 °C) unless otherwise specified.

^{1}H, and ^{13}C$\{^1$H$\}$ spectra were recorded on a Bruker AvIII HD 400 (400MHz). ^{1}H NMR spectra are reported as δ in units of parts per million (ppm) and referenced against residual protonated chloroform (δ 7.26 ppm, s), or dichloromethane (δ 5.32, t), as indicated. Multiplicities are reported as follows: s (singlet), d (doublet), t (triplet), q (quartet), quin (quintuplet), and m (multiplet). Second order splitting patterns, such as the AA'XX' para-substituted aromatic protons in *p*-azidophenylethane thiol, and for the ethyl substituents in the ligands are reported according to the latter multiplicity values based on their appearance. Coupling constants are reported as a J value in Hertz (Hz). The number of protons (n) for a given resonance is indicated as nH, based on spectral integration values. ^{13}C$\{^1$H$\}$ NMR spectra are reported as δ in units of parts per million (ppm) or referenced against residual protonated chloroform (δ 77.0 ppm, t).

Thermogravimetric analysis was performed using a TA Instruments Q50 TGA. Each sample was added as a fine powder to a platinum pan and heated at a rate of 10 °C/min from 25 °C to 1000°C under a flow of nitrogen (100 mL/min).

UV-Visible (UV-Vis) spectra were recorded using an Agilent technologies Cary 5000 UV-Vis-NIR spectrophotometer using standard quartz cells (1 cm path length) with a scan range of 200-1200nm.

Photoluminescence measurements were conducted in dichloromethane using Acton 2300i spectrograph equipped with an iDus BRDD CCD camera. A 532 nm COHERENT laser (model 1037860, VERDI 5W) attached to a cooler (model: T255p) was utilized to excite the NC solutions.

Excitation spectra were measured using a Photon Technology International Quanta Master (QM4) scanning spectrophotometer (PTI, London, Canada) equipped with a Xenon flash lamp, emission monochromator with a grating blazed at 750 nm, and a red sensitive GaAs photomultiplier tube. For emission spectra of the p-Au$_{144}$-N$_3$ and p-Au$_{144}$-BCN NCs, the emission slits were set to 10 nm and the excitation slits were set to 20 nm. For excitation spectra of the p-Au$_{144}$-N$_3$ and p-Au$_{144}$-BCN NCs, the excitation slits were set to 10 nm and the emission slits were opened to 20 nm. For emission spectra of the p-Au$_{144}$-TEMPO, the emission slits were 10 nm, and the excitation slits were 30 nm. For excitation spectra of the Au$_{144}$-TEMPO NCs, the excitation slits were 10 nm and the emission slits were 30 nm. Spectra were smoothed using Fourier Transform smoothing.

Attenuated total reflectance IR (ATR-IR) spectra were recorded using a PerkinElmer Spectrum Two FT-IR spectrometer.

The electrochemistry of the Au$_{144}$ NCs were investigated using a CH instrument (model 760E), and a three-electrode system including a 2 mm Pt disk, Pt coil and Ag/Ag$^+$/TPAPF$_6$ which served as working, counter, and reference electrodes. The solution was purged with Ar prior to the electrochemical studies.

3.4.3 Preparation and Characterization of Compounds

(1R,8S,9R)-Bicyclo[6.1.0]non-4-yn-9-ylmethanol (exo-BCN) (8)
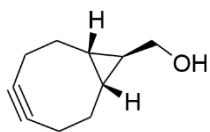
 Prepared according to Dommerholt *et al*[123], with rhodium acetate dimer catalyst loading according to O'Brien *et al.* [124]

Columned 1:1 EtOAc:Hexanes (Rf = 0.4) ^{1}H NMR (CDCl$_3$, 400 MHz): δ (ppm) 3.55 (d, 2H, *J*=6.4 Hz), 2.44-2.40 (m, 2H), 2.33-2.24 (m, 2H), 2.18-2.14 (m, 2H), 1.58 (bs, 1H), 1.45-1.33 (m, 2H), 0.74-0.63 (m, 3H).

(1R,8S,9R)-Bicyclo[6.1.0]non-4-yn-9-ylmethyl (4-nitrophenyl) carbonate (10)
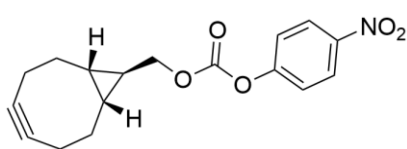
Prepared according to Dommerholt *et al.*[123]

^{1}H NMR (CDCl$_3$, 400 MHz): δ (ppm) 8.29 (d, 2H, *J*=9.2 Hz), 7.39 (d, *J*=8.8 Hz), 4.22 (d, 2H), 2.49-2.15 (m, 6H), 1.48-1.36 (m, 2H), 0.90-0.80 (m, 3H) R$_f$ (1:4 hexanes: ethyl acetate) = 0.5

(1R,8S,9R)-Bicyclo[6.1.0]non-4-yn-9-ylmethyl (2,2,6,6-tetramethylpiperidine-1-oxyl) carbamate (BCN-TEMPO) (13)
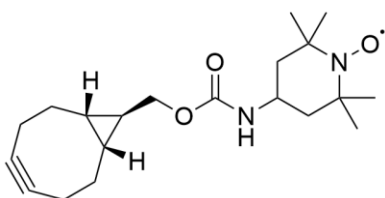
4-Amino-2,2,6,6-tetramethylpiperidine-1-oxyl(Amino-TEMPO) (265 mg, 1.54 mmol, 1.1 eq.) was added to a stirring solution of compound **10** (439 mg, 1.4 mmol, 1.0 eq.) and pyridine (284 mg, 2.8 mmol, 2.0 eq.) in 10 mL of DCM. The reaction was stirred for 24 h and monitored with TLC using 1:4 hexanes: ethyl acetate (R$_f$ = 0). Upon completion, the reaction was concentrated using rotary evaporation to yield a viscous red oil that was purified by column chromatography on neutral alumina (fraction 1, 2% methanol in dichloromethane, Rf=0.89) to obtain a yield of 74% (358 mg, 1.0 mmol) NMR spectra of the radical product could not be obtained but the product was confirmed using ESI-MS, in which it was observed to bind to sodium. C$_{20}$H$_{31}$N$_2$O$_3$•Na$^+$ (M$^+$): 370.2226, found: 370.2229.

(1R,8S,9R)-Bicyclo[6.1.0]non-4-yn-9-ylmethyl Ferrocenoate (BCN-Fc) (12)
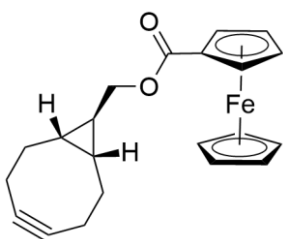
Prepared according to Gunawardene *et al.*[150] Ferrocene carboxylic acid (200 mg, 0.87 mmol, 1.3 eq.) was dissolved in 20 mL of dichloromethane. DCC (138 mg, 0.67 mmol, 1.0 eq.) and DMAP (41 mg, 0.33 mmol, 0.5 eq.) were added to the reaction mixture and stirred with the ferrocene carboxylic acid for 10 minutes. *Exo*-BCN (8) (100 mg, 0.66 mmol, 1.0 eq.) was then added as a solid and the reaction was stirred for 4h before it was concentrated by rotary evaporation and purified by column chromatography (100% dichloromethane, F1, Rf= 0.69). A yield of 163 mg

(68% yield) was obtained. ^{1}H NMR (CDCl$_3$, 400 MHz): δ (ppm) 4.81 (t, 2H, J=2.0 Hz), 4.40 (t, 2H, J=2.0 Hz), 4.21 (s, 5H), 4.15 (d, 2H, J=6.4 Hz), 2.45 (m, 2H), 2.32 (m, 2H), 2.18 (m, 2H), 1.42 (m, 2H), 0.81 (m, 3H).

Click reaction of p-Au$_{144}$-N$_3$ with exo-BCN (9)

p-Au$_{144}$-N$_3$ NCs (23.5 mg, 5.9 x 10^{-4} mmol, 1.0 eq.) were dissolved in 10 mL of dichloromethane in a 25 mL round-bottom flask fitted with a stir bar and BCN (5.9 mg, 3.9 x 10^{-2} mmol, 1.1 eq. per ligand, 66 eq. per cluster) was added as a solid. The reaction was monitored via TLC in 100% EtOAc. After 10 minutes, the BCN spot (BCN R_f = 0.73, Au$_{144}$ R_f = 0) had almost completely faded. The appearance of the reaction had also changed from a reddish-brown solution to a fine black suspension. After 15 minutes, the reaction was concentrated using rotary evaporation and washed repeatedly with 3:1 H$_2$O:EtOH (Note 2:1 H$_2$O:EtOH dissolved the clusters) to obtain the click product in quantitative yield. Prior to the reaction, the azide-functionalized clusters were insoluble in EtOH, but following the reaction, EtOH completely dissolved the clusters. The complete CS-SPAAC conversion of the azide was confirmed via the disappearance of the azide stretch (2116 cm^{-1}) in the infrared spectrum of the product.

Click reaction of p-Au$_{144}$-N$_3$ with BCN-TEMPO (12)

BCN-TEMPO (11) (16.3 mg, 4.7 x 10^{-2} mmol, 90 eq. per NC) was added to a stirring solution of Au$_{144}$(S-C$_2$H$_4$-p-C$_4$H$_4$-N$_3$)$_{60}$ NCs (20.5 mg, 5.2 x 10^{-4} mmol, 1.0 eq.) in 10 mL of DCM. The reaction was stirred for 1 hour, upon which the azide stretch in the FT-IR spectrum of the crude reaction mixture had disappeared. The reaction was concentrated by rotary evaporation and washed with 3 x 10 mL portions of methanol to remove excess strained alkyne.

Click reaction of p-Au$_{144}$-N$_3$ with BCN-Fc (14)

BCN-Fc (12) (21.6 mg, 6.0 x 10^{-2} mmol, 90 eq. per NC) was added to a stirring solution of Au$_{144}$(S-C$_2$H$_4$-p-C$_4$H$_4$-N$_3$)$_{60}$ NCs (26.25 mg, 6.6 x 10^{-4} mmol, 1.0 eq.) in 10 mL of DCM. The reaction was stirred for 40 minutes, dried using rotary evaporation and washed with acetonitrile to remove excess BCN-Fc. An azide stretch was still clearly

visible in the sample's IR spectrum. To progress the reaction further, the same equivalencies of BCN-Fc and solvent were re-added to the sample and the reaction was stirred overnight. Again, the solvent was removed via rotary evaporation and the residual BCN-Fc was washed out with acetonitrile. No further change in the infrared spectrum of the product was observed.

Chapter 3

4   Conclusions and Future Work

4.1   Summary and Conclusions

In this thesis, I synthesized three novel azide-modified $Au_{144}(SR)_{60}$ NCs using a facile one-pot synthetic protocol. The $Au_{144}(SR)_{60}$ NCs were characterized using UV-Visible, ^1H NMR, and IR spectroscopy, each matching the established features in literature of $Au_{144}(SR)_{60}$ NCs. Mass spectrometry and thermogravimetric analysis confirmed the mass of the NCs and highlighted differences in their ionization and fragmentation patterns. While the photoluminescence of the NCs revealed slight shifts in their emission maxima, the electronic influence of the azide moieties greatly impacted the $Au_{144}(SR)_{60}$ NCs' electrochemical features, i.e., reducing the number and intensity of observed redox coupling.

Notably, the utility of the azides on the surface of the $Au_{144}(SR)_{60}$ NCs was demonstrated via the CS-SPAAC reaction. Remarkably, all 60 azide groups of p-Au_{144}-N_3 NCs reacted with BCN under ambient conditions to produce alcohol-soluble NCs. A functional TEMPO derivative was then successfully clicked on to the surface of the NCs and employed in an electrocatalytic application. Lastly, the limitations of the CS-SPAAC reaction were challenged during the reaction of the p-Au_{144}-N_3 NCs with BCN-Fc. This presented an opportunity to observe how the azide groups perform in conjunction with other functional groups on the surface of the NCs. Notably, even in cases where sterically challenging strained-alkyne derivatives were involved, a considerable percentage of ligands still underwent the CS-SPAAC reaction, indicating the robust nature of their reactivity. It can therefore be concluded that the azide moieties served as a reliable handle for introducing functional groups to the NCs without inciting any significant changes to their core features.

Azide-modified Au NCs undoubtedly present an extraordinary opportunity to bestow function to NCs following their synthesis. The $Au_{144}(SR)_{60}$ NC syntheses described here indicate that thermodynamic and kinetic size-directing forces in NC syntheses using

phenylethane thiol can be readily adapted to use azidophenylethane thiol as a vehicle for click chemistry. Based on these findings, interfacial click chemistry has a promising future in the design of functional NCs of all shapes and sizes.

4.2 Future Work

During this thesis, a robust $Au_{144}(SR)_{60}$ platform for click chemistry was developed that could be readily modified via click chemistry without significantly impacting its core features. As described in the first chapter, identical NC size regimes may be accessed using different thiolate ligands, i.e., azidophenylethane thiolate vs. phenylethane thiolate. However, even in the case of small changes to ligand structure, like the incorporation of an azide group, the properties of these identically sized NCs can be distinct from one another. The effects of these small changes are an area of research that has only begun to be investigated. In fact, many aspects of NCs have yet to be fully understood, including the origin of their luminescent features, the extent to which ligand properties can influence their core features, and how changes to their environment, such as temperature and solvent, affect their structure and stability. In future, we can use azide modified NCs not only to introduce function, but also to help address some of these fundamental questions.

For instance, $Au_{144}(SR)_{60}$ NCs are regarded for their electrochemical features, yet during this thesis, azide groups were observed to potentially interfere with the electron transfer (ET) process, subduing the electrochemical features of the NCs. Upon reacting the NCs with large BCN groups, these electrochemical features were not revived. The question of which functional groups/ligand structures $Au_{144}(SR)_{60}$ NCs can tolerate with regards to their electrochemical features therefore arose. Rather than clicking large, and perhaps insulative, groups on to the surface of the NCs via the CS-SPAAC reaction, alternative reactions such as the Staudinger reduction or copper-catalyzed azide–alkyne 1,3-dipolar cycloaddition (CuAAC) could be exploited to establish the relationship between the ligand structure and electrochemical performance of the $Au_{144}(SR)_{60}$ NCs. During the Staudinger reduction, triphenylphosphine would react with the azides to form iminophosphorane intermediates that could be hydrolyzed to produce amine functionalized $Au_{144}(SR)_{60}$ NCs (**Scheme 11a**). If the conversion of the azide groups on

the surface of the NCs to amines restored their electrochemical features, it would confirm the role of the azide in interfering with ET.
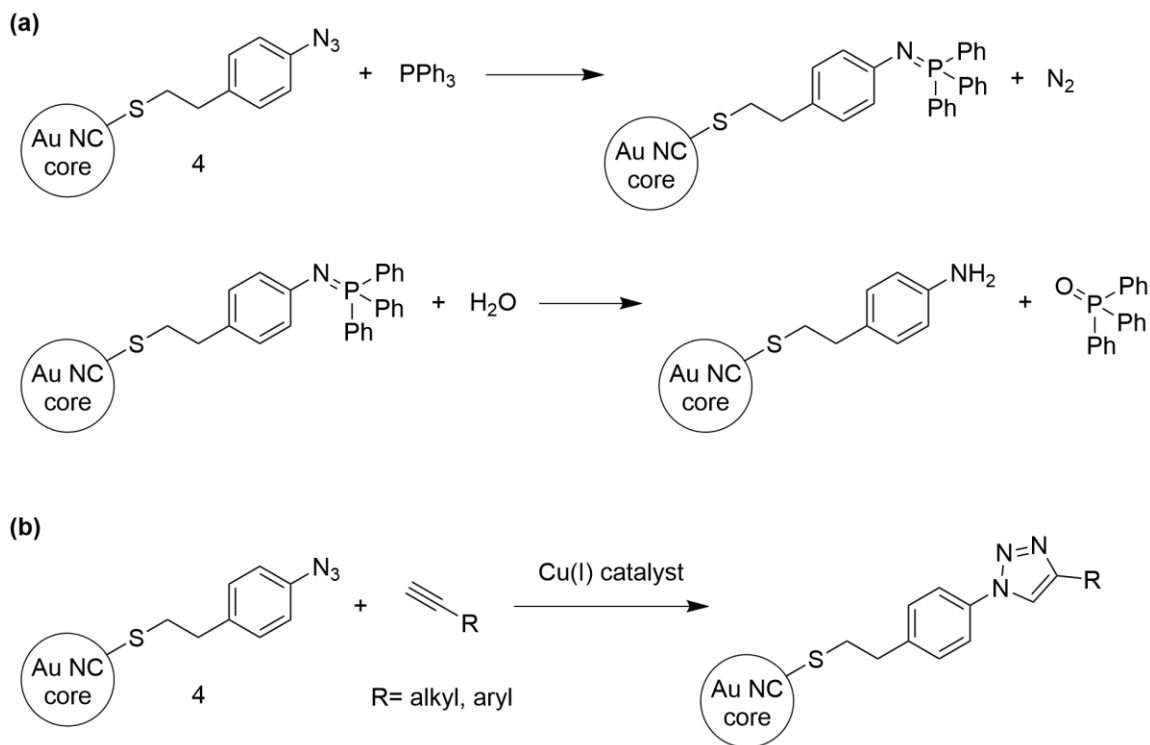
Scheme 11. Alternative post-synthesis modifications of *p*-Au₁₄₄-N₃ NCs. (a) Staudinger reduction reaction, **(b)** CuAAC click reaction.

In addition, if the CuAAC reaction could be successfully conducted on the Au$_{144}$-N$_3$ NCs, it would allow for considerably smaller alkynes to be clicked on to their surface. Using a small alkyne, the zwitterionic nature of the azide group could be quenched without introducing significant steric bulk to the NCs. If the electrochemical features of the Au$_{144}$(SR)$_{60}$ NCs were restored via the CuAAC reaction, it would present an opportunity to take advantage of core electrochemical features and ligand features simultaneously. The ability to conduct CuAAC reactions on the surface of NCs would also greatly improve the breadth and ease by which functionality could be introduced to clusters, as the CuAAC reaction employs conventional linear rather than strained alkynes.

Lastly, despite the click reactions showcased in this thesis, the world of function that could be introduced to Au NCs via the CS-SPAAC reaction remains uncharted. A

component of this research that could be explored is the interaction of the ligands on the surface of the NCs with each other. For instance, aggregation-induced emission (AIE) and p-band intermediate-state- (PBIS) tailored photoluminescence have been examined previously on the surface of NCs but never with the degree of flexibility and versatility that click chemistry affords.[151, 152] Clicking such molecules on to the surface of Au NCs could potentially result in tunable photoluminescence dependent on cluster size and structure. One could take advantage of molecules that are not emissive on their own but become luminescent in specific orientations or concentrations. For example, maleimide and succinimide derivatives have been reported to exhibit clusteroluminescence from n–π* transitions in high concentrations[153]. By simply coupling a strained alkyne with a maleimide derivative, one could click maleimides to the surface of azide functionalized $Au_{25}(SR)_{18}$ and $Au_{144}(SR)_{60}$ NCs and investigate the ability of these types of interligand interactions to generate luminescence (**Scheme 12**).
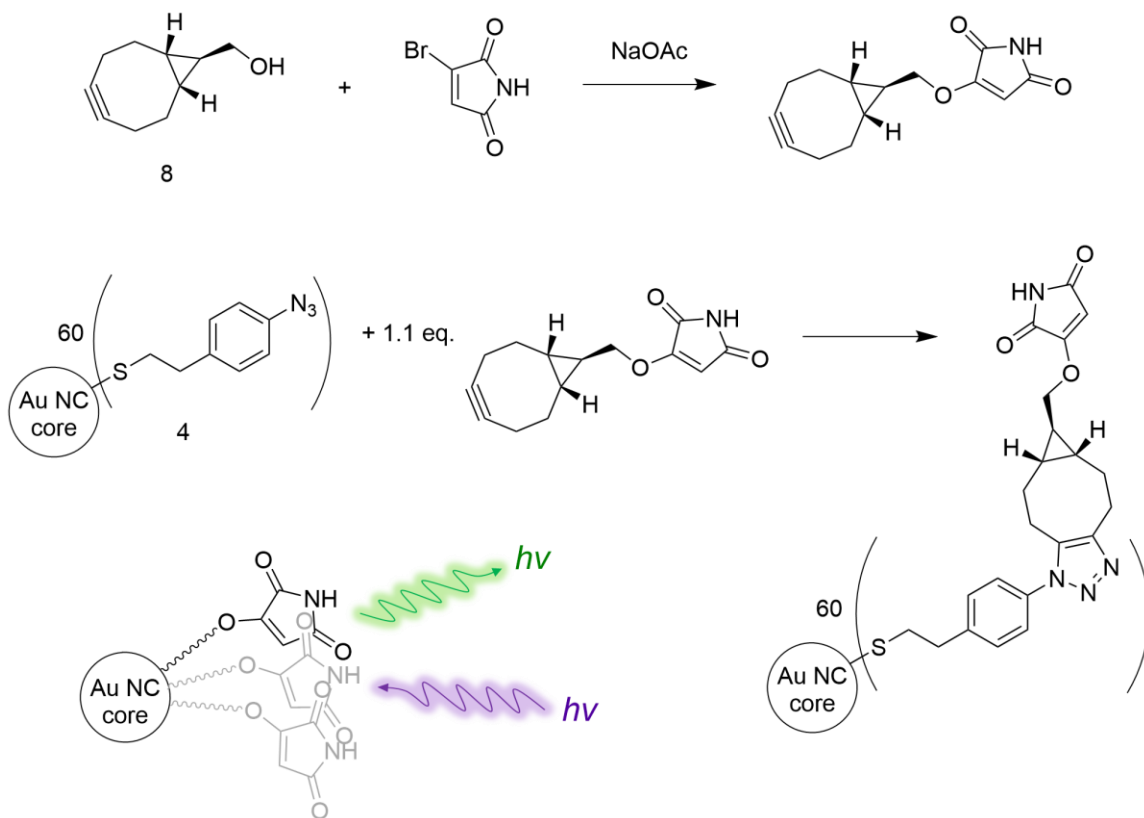
Scheme 12. Synthesis of Maleimide-functionalized $Au_{144}(SR)_{60}$ NCs.

References

(1)   Kauffman, G. B., The role of gold in alchemy. Part I. *Gold Bulletin* **1985,** *18*, 31-44.

(2)   Goswami, N.; Yao, Q.; Chen, T.; Xie, J., Mechanistic exploration and controlled synthesis of precise thiolate-gold nanoclusters. *Coord. Chem. Rev.* **2016,** *329*, 1-15.

(3)   Wu, Z.; MacDonald, M. A.; Chen, J.; Zhang, P.; Jin, R., Kinetic Control and Thermodynamic Selection in the Synthesis of Atomically Precise Gold Nanoclusters. *J. Am. Chem. Soc.* **2011,** *133*, 9670-9673.

(4)   Li, Y.; Zhou, M.; Jin, R., Programmable Metal Nanoclusters with Atomic Precision. *Adv. Mater.* **2021,** *33*, 2006591.

(5)   Liu, C.; Li, G.; Pang, G.; Jin, R., Toward understanding the growth mechanism of $Au_n(SR)_m$ nanoclusters: effect of solvent on cluster size. *RSC Adv.* **2013,** *3*, 9778-9784.

(6)   Yuan, X.; Zhang, B.; Luo, Z.; Yao, Q.; Leong, D. T.; Yan, N.; Xie, J., Balancing the Rate of Cluster Growth and Etching for Gram-Scale Synthesis of Thiolate-Protected Au_{25} Nanoclusters with Atomic Precision. *Angew. Chem., Int. Ed.* **2014,** *53*, 4623-4627.

(7)   Sokołowska, K.; Malola, S.; Lahtinen, M.; Saarnio, V.; Permi, P.; Koskinen, K.; Jalasvuori, M.; Häkkinen, H.; Lehtovaara, L.; Lahtinen, T., Towards Controlled Synthesis of Water-Soluble Gold Nanoclusters: Synthesis and Analysis. *J. Phys. Chem. C* **2019,** *123*, 2602-2612.

(8)   Negishi, Y.; Sakamoto, C.; Ohyama, T.; Tsukuda, T., Synthesis and the Origin of the Stability of Thiolate-Protected Au_{130} and Au_{187} Clusters. *J. Phys. Chem. Lett.* **2012,** *3*, 1624-1628.

(9)   Chen, T.; Yao, Q.; Yuan, X.; Nasaruddin, R. R.; Xie, J., Heating or Cooling: Temperature Effects on the Synthesis of Atomically Precise Gold Nanoclusters. *J. Phys. Chem. C* **2017,** *121*, 10743-10751.

(10)   Wu, Z.; Suhan, J.; Jin, R., One-pot synthesis of atomically monodisperse, thiol-functionalized Au_{25} nanoclusters. *J. Mater. Chem.* **2009,** *19*, 622-626.

(11)   Dreier, T. A.; Compel, W. S.; Wong, O. A.; Ackerson, C. J., Oxygen's role in aqueous gold cluster synthesis. *J. Phys. Chem. C* **2016,** *120*, 28288-28294.

(12)   Zhang, B.; Chen, J.; Cao, Y.; Chai, O. J. H.; Xie, J., Ligand Design in Ligand-Protected Gold Nanoclusters. *Small* **2021,** *17*, e2004381.

(13)   Yang, T.-Q.; Peng, B.; Shan, B.-Q.; Zong, Y.-X.; Jiang, J.-G.; Wu, P.; Zhang, K., Origin of the Photoluminescence of Metal Nanoclusters: From Metal-Centered Emission to Ligand-Centered Emission. *Nanomaterials* **2020,** *10*, 261.

(14)   Kang, X.; Zhu, M., Tailoring the photoluminescence of atomically precise nanoclusters. *Chem. Soc. Rev.* **2019,** *48*, 2422-2457.

(15)   Higaki, T.; Li, Q.; Zhou, M.; Zhao, S.; Li, Y.; Li, S.; Jin, R., Toward the Tailoring Chemistry of Metal Nanoclusters for Enhancing Functionalities. *Acc. Chem. Res.* **2018,** *51*, 2764-2773.

(16)   Pei, Y.; Wang, P.; Ma, Z.; Xiong, L., Growth-Rule-Guided Structural Exploration of Thiolate-Protected Gold Nanoclusters. *Acc. Chem. Res.* **2019,** *52*, 23-33.

(17)   Zhang, P.; Sham, T. K., Tuning the electronic behavior of Au nanoparticles with capping molecules. *Appl. Phys. Lett.* **2002,** *81*, 736-738.

(18)   Chen, Y.; Zeng, C.; Kauffman, D. R.; Jin, R., Tuning the Magic Size of Atomically Precise Gold Nanoclusters via Isomeric Methylbenzenethiols. *Nano Lett.* **2015,** *15*, 3603-9.

(19)   Wang, E.; Xu, W. W.; Zhu, B.; Gao, Y., Understanding the Chemical Insights of Staple Motifs of Thiolate-Protected Gold Nanoclusters. *Small* **2021,** *17*, e2001836.

(20)   Han, W.; Liu, P.; Zheng, M.; Zeng, X. C.; Xu, W. W., Ring Model for Understanding How Interfacial Interaction Dictates the Structures of Protection Motifs and Gold Cores in Thiolate-Protected Gold Nanoclusters. *J. Phys. Chem. Lett.* **2021,** *12*, 3006-3013.

(21)   Lin, D.; Zheng, M.; Xu, W. W., Structural predictions of thiolate-protected gold nanoclusters via the redistribution of Au–S "staple" motifs on known cores. *PCCP* **2020,** *22*, 16624-16629.

(22)   McPartlin, M.; Mason, R.; Malatesta, L., Novel cluster complexes of gold(0)–gold(I). *J. Chem. Soc. D.* **1969**, 334-334.

(23)   Adnan, R. H.; Madridejos, J. M. L.; Alotabi, A. S.; Metha, G. F.; Andersson, G. G., A Review of State of the Art in Phosphine Ligated Gold Clusters and Application in Catalysis. *Adv. Sci.* **2022,** *9*, 2105692.

(24)   Narouz, M. R.; Osten, K. M.; Unsworth, P. J.; Man, R. W. Y.; Salorinne, K.; Takano, S.; Tomihara, R.; Kaappa, S.; Malola, S.; Dinh, C.-T.; Padmos, J. D.; Ayoo, K.; Garrett, P. J.; Nambo, M.; Horton, J. H.; Sargent, E. H.; Häkkinen, H.; Tsukuda, T.; Crudden, C. M., N-heterocyclic carbene-functionalized magic-number gold nanoclusters. *Nat. Chem.* **2019,** *11*, 419-425.

(25)   Lei, Z.; Wan, X. K.; Yuan, S. F.; Guan, Z. J.; Wang, Q. M., Alkynyl Approach toward the Protection of Metal Nanoclusters. *Acc. Chem. Res.* **2018,** *51*, 2465-2474.

(26)   Häkkinen, H., The gold–sulfur interface at the nanoscale. *Nat. Chem.* **2012,** *4*, 443-455.

(27)   Brust, M.; Walker, M.; Bethell, D.; Schiffrin, D. J.; Whyman, R., Synthesis of thiol-derivatised gold nanoparticles in a two-phase Liquid–Liquid system. *J. Chem. Soc., Chem. Commun.* **1994**, 801-802.

(28)   Brust, M.; Fink, J.; Bethell, D.; Schiffrin, D. J.; Kiely, C., Synthesis and reactions of functionalised gold nanoparticles. *J. Chem. Soc., Chem. Commun.* **1995**, 1655-1656.

(29)   Liz-Marzán, L. M., Gold nanoparticle research before and after the Brust–Schiffrin method. *Chem. Commun.* **2013,** *49*, 16-18.

(30)   Perala, S. R. K.; Kumar, S., On the Mechanism of Metal Nanoparticle Synthesis in the Brust–Schiffrin Method. *Langmuir* **2013,** *29*, 9863-9873.

(31)   Luo, Z.; Nachammai, V.; Zhang, B.; Yan, N.; Leong, D. T.; Jiang, D.-e.; Xie, J., Toward Understanding the Growth Mechanism: Tracing All Stable Intermediate Species from Reduction of Au(I)–Thiolate Complexes to Evolution of Au_{25} Nanoclusters. *J. Am. Chem. Soc.* **2014,** *136*, 10577-10580.

(32)   Jin, R.; Qian, H.; Wu, Z.; Zhu, Y.; Zhu, M.; Mohanty, A.; Garg, N., Size Focusing: A Methodology for Synthesizing Atomically Precise Gold Nanoclusters. *J. Phys. Chem. Lett.* **2010,** *1*, 2903-2910.

(33)   Zhu, M.; Qian, H.; Jin, R., Thiolate-Protected $Au_{24}(SC_2H_4Ph)_{20}$ Nanoclusters: Superatoms or Not? *J. Phys. Chem. Lett.* **2010,** *1*, 1003-1007.

(34)   Zhu, M.; Lanni, E.; Garg, N.; Bier, M. E.; Jin, R., Kinetically Controlled, High-Yield Synthesis of Au_{25} Clusters. *J. Am. Chem. Soc.* **2008,** *130*, 1138-1139.

(35)   Qian, H.; Zhu, Y.; Jin, R., Size-Focusing Synthesis, Optical and Electrochemical Properties of Monodisperse $Au_{38}(SC_2H_4Ph)_{24}$ Nanoclusters. *ACS Nano* **2009,** *3*, 3795-3803.

(36)   Qian, H.; Zhu, Y.; Jin, R., Isolation of Ubiquitous $Au_{40}(SR)_{24}$ Clusters from the 8 kDa Gold Clusters. *J. Am. Chem. Soc.* **2010,** *132*, 4583-4585.

(37)   Nimmala, P. R.; Yoon, B.; Whetten, R. L.; Landman, U.; Dass, A., $Au_{67}(SR)_{35}$ Nanomolecules: Characteristic Size-Specific Optical, Electrochemical, Structural Properties and First-Principles Theoretical Analysis. *J. Phys. Chem. A* **2013,** *117*, 504-517.

(38)   Jupally, V. R.; Dharmaratne, A. C.; Crasto, D.; Huckaba, A. J.; Kumara, C.; Nimmala, P. R.; Kothalawala, N.; Delcamp, J. H.; Dass, A., $Au_{137}(SR)_{56}$ nanomolecules: composition, optical spectroscopy, electrochemistry and electrocatalytic reduction of CO_2. *Chem. Commun.* **2014,** *50*, 9895-9898.

(39)   Hesari, M.; Ding, Z.; Workentin, M. S., Electrogenerated Chemiluminescence of Monodisperse $Au_{144}(SC_2H_4Ph)_{60}$ Clusters. *Organometallics* **2014,** *33*, 4888-4892.

(40)   Qian, H.; Jin, R., Ambient Synthesis of $Au_{144}(SR)_{60}$ Nanoclusters in Methanol. *Chem. Mater.* **2011,** *23*, 2209-2217.

(41)   Qian, H.; Jin, R., Controlling Nanoparticles with Atomic Precision: The Case of $Au_{144}(SCH_2CH_2Ph)_{60}$. *Nano Lett.* **2009,** *9*, 4083-4087.

(42)   Qian, H.; Zhu, Y.; Jin, R., Atomically precise gold nanocrystal molecules with surface plasmon resonance. *PNAS* **2012,** *109*, 696-700.

(43)   Tero, T. R.; Malola, S.; Koncz, B.; Pohjolainen, E.; Lautala, S.; Mustalahti, S.; Permi, P.; Groenhof, G.; Pettersson, M.; Häkkinen, H., Dynamic Stabilization of the Ligand-Metal Interface in Atomically Precise Gold Nanoclusters Au_{68} and Au_{144} Protected by meta-Mercaptobenzoic Acid. *ACS Nano* **2017,** *11*, 11872-11879.

(44)   Mammen, N.; Malola, S.; Honkala, K.; Hakkinen, H., Dynamics of weak interactions in the ligand layer of meta-mercaptobenzoic acid protected gold nanoclusters $Au_{68}(m\text{-}MBA)_{32}$ and $Au_{144}(m\text{-}MBA)_{40}$. *Nanoscale* **2020,** *12*, 23859-23868.

(45)   Zhu, L.; Zeng, Y.; Teubner, M.; Grimm-Lebsanft, B.; Ziefuss, A. R.; Rehbock, C.; Ruebhausen, M. A.; Barcikowski, S.; Parak, W. J.; Chakraborty, I., Surface Engineering of Gold Nanoclusters Protected with 11-Mercaptoundecanoic Acid for Photoluminescence Sensing. *ACS Appl. Nano. Mater.* **2021,** *4*, 3197-3203.

(46)   Goswami, N.; Yao, Q.; Luo, Z.; Li, J.; Chen, T.; Xie, J., Luminescent Metal Nanoclusters with Aggregation-Induced Emission. *J. Phys. Chem. Lett.* **2016,** *7*, 962-975.

(47)   Gayen, C.; Basu, S.; Goswami, U.; Paul, A., Visible Light Excitation-Induced Luminescence from Gold Nanoclusters Following Surface Ligand Complexation with Zn^{2+} for Daylight Sensing and Cellular Imaging. *Langmuir* **2019,** *35*, 9037-9043.

(48)   Deng, H.; Huang, K.; Xiu, L.; Sun, W.; Yao, Q.; Fang, X.; Huang, X.; Noreldeen, H. A. A.; Peng, H.; Xie, J.; Chen, W., Bis-Schiff base linkage-triggered highly bright luminescence of gold nanoclusters in aqueous solution at the single-cluster level. *Nat. Commun.* **2022,** *13*, 3381.

(49)   Wu, Z.; Jin, R., On the Ligand's Role in the Fluorescence of Gold Nanoclusters. *Nano Lett.* **2010,** *10*, 2568-2573.

(50)   Zhang, X.-D.; Wu, D.; Shen, X.; Liu, P.-X.; Fan, F.-Y.; Fan, S.-J., In vivo renal clearance, biodistribution, toxicity of gold nanoclusters. *Biomaterials* **2012,** *33*, 4628-4638.

(51)   Chen, Y.-S.; Kamat, P. V., Glutathione-capped gold nanoclusters as photosensitizers. Visible light-induced hydrogen generation in neutral water. *J. Am. Chem. Soc.* **2014,** *136*, 6075-6082.

(52)   Zhang, X.-D.; Luo, Z.; Chen, J.; Song, S.; Yuan, X.; Shen, X.; Wang, H.; Sun, Y.; Gao, K.; Zhang, L.; Fan, S.; Leong, D. T.; Guo, M.; Xie, J., Ultrasmall Glutathione-Protected Gold Nanoclusters as Next Generation Radiotherapy Sensitizers with High Tumor Uptake and High Renal Clearance. *Sci. Rep.* **2015,** *5*, 8669.

(53)   Wu, Z.; Wang, M.; Yang, J.; Zheng, X.; Cai, W.; Meng, G.; Qian, H.; Wang, H.; Jin, R., Well-Defined Nanoclusters as Fluorescent Nanosensors: A Case Study on $Au_{25}(SG)_{18}$. *Small* **2012,** *8*, 2028.

(54)   Pyo, K.; Xu, H.; Han, S. M.; Saxena, S.; Yoon, S. Y.; Wiederrecht, G.; Ramakrishna, G.; Lee, D., Synthesis and Photophysical Properties of Light-Harvesting Gold Nanoclusters Fully Functionalized with Antenna Chromophores. *Small* **2021,** *17*, 2004836.

(55)   Zhang, B.; Wu, Z.; Cao, Y.; Yao, Q.; Xie, J., Ultrastable hydrophilic gold nanoclusters protected by sulfonic thiolate ligands. *J. Phys. Chem. C* **2021,** *125*, 489-497.

(56)   Pigliacelli, C.; Acocella, A.; Diez, I.; Moretti, L.; Dichiarante, V.; Demitri, N.; Jiang, H.; Maiuri, M.; Ras, R. H. A.; Bombelli, F. B.; Cerullo, G.; Zerbetto, F.; Metrangolo, P.; Terraneo, G., High-resolution crystal structure of a 20 kDa superfluorinated gold nanocluster. *Nat. Commun.* **2022,** *13*, 2607.

(57)   Huang, Z.; Ishida, Y.; Yonezawa, T., Basic $[Au_{25}(SCH_2CH_2Py)_{18}]^-\cdot Na^+$ Clusters: Synthesis, Layered Crystallographic Arrangement, and Unique Surface Protonation. *Angew. Chem., Int. Ed.* **2019,** *58*, 13411-13415.

(58)   Wang, Y.; Bürgi, T., Ligand exchange reactions on thiolate-protected gold nanoclusters. *Nanoscale Adv.* **2021,** *3*, 2710-2727.

(59)   Heinecke, C. L.; Ni, T. W.; Malola, S.; Mäkinen, V.; Wong, O. A.; Häkkinen, H.; Ackerson, C. J., Structural and Theoretical Basis for Ligand Exchange on Thiolate Monolayer Protected Gold Nanoclusters. *J. Am. Chem. Soc.* **2012,** *134*, 13316-13322.

(60)   Fernando, A.; Aikens, C. M., Ligand Exchange Mechanism on Thiolate Monolayer Protected $Au_{25}(SR)_{18}$ Nanoclusters. *J. Phys. Chem. C* **2015,** *119*, 20179-20187.

(61)   Zeng, C.; Chen, Y.; Das, A.; Jin, R., Transformation Chemistry of Gold Nanoclusters: From One Stable Size to Another. *J. Phys. Chem. Lett.* **2015,** *6*, 2976-2986.

(62)   Guo, R.; Song, Y.; Wang, G.; Murray, R. W., Does Core Size Matter in the Kinetics of Ligand Exchanges of Monolayer-Protected Au Clusters? *J. Am. Chem. Soc.* **2005,** *127*, 2752-2757.

(63)   Cao, Y.; Fung, V.; Yao, Q.; Chen, T.; Zang, S.; Jiang, D.-e.; Xie, J., Control of single-ligand chemistry on thiolated Au_{25} nanoclusters. *Nat. Commun.* **2020,** *11*, 5498.

(64)   Zhou, S.; Huo, D.; Goines, S.; Yang, T.-H.; Lyu, Z.; Zhao, M.; Gilroy, K. D.; Wu, Y.; Hood, Z. D.; Xie, M.; Xia, Y., Enabling Complete Ligand Exchange on the Surface of Gold Nanocrystals through the Deposition and Then Etching of Silver. *J. Am. Chem. Soc.* **2018,** *140*, 11898-11901.

(65)   Dass, A.; Stevenson, A.; Dubay, G. R.; Tracy, J. B.; Murray, R. W., Nanoparticle MALDI-TOF Mass Spectrometry without Fragmentation: $Au_{25}(SCH_2CH_2Ph)_{18}$ and Mixed Monolayer $Au_{25}(SCH_2CH_2Ph)_{18-x}(L)_x$. *J. Am. Chem. Soc.* **2008,** *130*, 5940-5946.

(66)   Gunawardene, P. N.; Corrigan, J. F.; Workentin, M. S., Golden Opportunity: A Clickable Azide-Functionalized $[Au_{25}(SR)_{18}](-)$ Nanocluster Platform for Interfacial Surface Modifications. *J. Am. Chem. Soc.* **2019,** *141*, 11781-11785.

(67)   Luo, W.; Luo, J.; Popik, V. V.; Workentin, M. S., Dual-Bioorthogonal Molecular Tool: "Click-to-Release" and "Double-Click" Reactivity on Small Molecules and Material Surfaces. *Bioconjugate Chem.* **2019,** *30*, 1140-1149.

(68)   Luo, W.; Gobbo, P.; Gunawardene, P. N.; Workentin, M. S., Fluorogenic Gold Nanoparticle (AuNP) Substrate: A Model for the Controlled Release of Molecules from AuNP Nanocarriers via Interfacial Staudinger–Bertozzi Ligation. *Langmuir* **2017,** *33*, 1908-1913.

(69)   Kolb, H. C.; Finn, M. G.; Sharpless, K. B., Click Chemistry: Diverse Chemical Function from a Few Good Reactions. *Angew. Chem., Int. Ed.* **2001,** *40*, 2004-2021.

(70)   Sletten, E. M.; Bertozzi, C. R., Bioorthogonal Chemistry: Fishing for Selectivity in a Sea of Functionality. *Angew. Chem., Int. Ed.* **2009,** *48*, 6974-6998.

(71)   Agard, N. J.; Prescher, J. A.; Bertozzi, C. R., A Strain-Promoted [3 + 2] Azide−Alkyne Cycloaddition for Covalent Modification of Biomolecules in Living Systems. *J. Am. Chem. Soc.* **2004,** *126*, 15046-15047.

(72)   Kang, X.; Ren, M.; Zhu, M.; Zhang, K., Azide-Functionalized Nanoclusters via a Ligand-Induced Rearrangement. *Chem. Mater.* **2020,** *32*, 6736-6743.

(73)   Gunawardene, P. N.; Martin, J.; Wong, J. M.; Ding, Z.; Corrigan, J. F.; Workentin, M. S., Controlling the Structure, Properties and Surface Reactivity of Clickable Azide-Functionalized $Au_{25}(SR)_{18}$ Nanocluster Platforms Through Regioisomeric Ligand Modifications. *Angew. Chem. Int. Ed.* **2022,** *61*, e202205194.

(74)   Bertorelle, F.; Russier-Antoine, I.; Comby-Zerbino, C.; Chirot, F.; Dugourd, P.; Brevet, P.-F.; Antoine, R., Isomeric Effect of Mercaptobenzoic Acids on the Synthesis, Stability, and Optical Properties of $Au_{25}(MBA)_{18}$ Nanoclusters. *ACS Omega* **2018,** *3*, 15635-15642.

(75)   Chen, Y.; Zeng, C.; Kauffman, D. R.; Jin, R., Tuning the Magic Size of Atomically Precise Gold Nanoclusters via Isomeric Methylbenzenethiols. *Nano Lett.* **2015,** *15*, 3603-3609.

(76)   Zhou, M.; Higaki, T.; Li, Y.; Zeng, C.; Li, Q.; Sfeir, M. Y.; Jin, R., Three-Stage Evolution from Nonscalable to Scalable Optical Properties of Thiolate-Protected Gold Nanoclusters. *J. Am. Chem. Soc.* **2019,** *141*, 19754-19764.

(77)   Schaaff, T. G.; Shafigullin, M. N.; Khoury, J. T.; Vezmar, I.; Whetten, R. L.; Cullen, W. G.; First, P. N.; Gutiérrez-Wing, C.; Ascensio, J.; Jose-Yacamán, M. J., Isolation of Smaller Nanocrystal Au Molecules: Robust Quantum Effects in Optical Spectra. *J. Phys. Chem. B* **1997,** *101*, 7885-7891.

(78)   Schaaff, T. G.; Knight, G.; Shafigullin, M. N.; Borkman, R. F.; Whetten, R. L., Isolation and Selected Properties of a 10.4 kDa Gold:Glutathione Cluster Compound. *J. Phys. Chem. B* **1998,** *102*, 10643-10646.

(79)   Zhu, M.; Aikens, C. M.; Hollander, F. J.; Schatz, G. C.; Jin, R., Correlating the Crystal Structure of A Thiol-Protected Au_{25} Cluster and Optical Properties. *J. Am. Chem. Soc.* **2008,** *130*, 5883-5885.

(80)   Heaven, M. W.; Dass, A.; White, P. S.; Holt, K. M.; Murray, R. W., Crystal Structure of the Gold Nanoparticle $[N(C_8H_{17})_4][Au_{25}(SCH_2CH_2Ph)_{18}]$. *J. Am. Chem. Soc.* **2008,** *130*, 3754-3755.

(81)   Yan, N.; Xia, N.; Liao, L.; Zhu, M.; Jin, F.; Jin, R.; Wu, Z., Unraveling the long-pursued Au_{144} structure by x-ray crystallography. *Sci. Adv.* **2018,** *4*, eaat7259.

(82)   Jadzinsky, P. D.; Calero, G.; Ackerson, C. J.; Bushnell, D. A.; Kornberg, R. D., Structure of a Thiol Monolayer-Protected Gold Nanoparticle at 1.1 Angstrom Resolution. *Science* **2007,** *318*, 430-433.

(83)   Chen, S.; Murray, R. W.; Feldberg, S. W., Quantized Capacitance Charging of Monolayer-Protected Au Clusters. *J. Phys. Chem. B* **1998,** *102*, 9898-9907.

(84)   Schaaff, T. G.; Shafigullin, M. N.; Khoury, J. T.; Vezmar, I.; Whetten, R. L., Properties of a Ubiquitous 29 kDa Au:SR Cluster Compound. *J. Phys. Chem. B* **2001,** *105*, 8785-8796.

(85)   Lopez-Acevedo, O.; Akola, J.; Whetten, R. L.; Grönbeck, H.; Häkkinen, H., Structure and Bonding in the Ubiquitous Icosahedral Metallic Gold Cluster $Au_{144}(SR)_{60}$. *J. Phys. Chem. C* **2009,** *113*, 5035-5038.

(86)   Fields-Zinna, C. A.; Sardar, R.; Beasley, C. A.; Murray, R. W., Electrospray Ionization Mass Spectrometry of Intrinsically Cationized Nanoparticles, $[Au_{144/146}(SC_{11}H_{22}N(CH_2CH_3)^{3+})_x(S(CH_2)_5CH_3)_y]_x{}^+$. *J. Am. Chem. Soc.* **2009,** *131*, 16266-16271.

(87)   Liu, C.; Yan, C.; Lin, J.; Yu, C.; Huang, J.; Li, G., One-pot synthesis of $Au_{144}(SCH_2Ph)_{60}$ nanoclusters and their catalytic application. *J. Mater. Chem. A* **2015,** *3*, 20167-20173.

(88)   Shi, Q.; Qin, Z.; Yu, C.; Liu, S.; Xu, H.; Li, G., Pyridine as a trigger in transformation chemistry from $Au_{144}(SR)_{60}$ to aromatic thiolate-ligated gold clusters. *Nanoscale* **2020,** *12*, 4982-4987.

(89)   Yi, C.; Tofanelli, M. A.; Ackerson, C. J.; Knappenberger, K. L., Optical Properties and Electronic Energy Relaxation of Metallic $Au_{144}(SR)_{60}$ Nanoclusters. *J. Am. Chem. Soc.* **2013,** *135*, 18222-18228.

(90)   Jensen, K. M.; Juhas, P.; Tofanelli, M. A.; Heinecke, C. L.; Vaughan, G.; Ackerson, C. J.; Billinge, S. J., Polymorphism in magic-sized $Au_{144}(SR)_{60}$ clusters. *Nat. Commun.* **2016,** *7*, 11859.

(91)   Ma, X.; Tang, Z.; Qin, L.; Peng, J.; Li, L.; Chen, S., Unravelling the formation mechanism of alkynyl protected gold clusters: A case study of phenylacetylene stabilized Au_{144} molecules. *Nanoscale* **2020,** *12*, 2980-2986.

(92)   Lei, Z.; Li, J.-J.; Wan, X.-K.; Zhang, W.-H.; Wang, Q.-M., Isolation and Total Structure Determination of an All-Alkynyl-Protected Gold Nanocluster Au_{144}. *Angew. Chem. Int. Ed.* **2018,** *57*, 8639-8643.

(93)   Zhou, M.; Zeng, C.; Chen, Y.; Zhao, S.; Sfeir, M. Y.; Zhu, M.; Jin, R., Evolution from the plasmon to exciton state in ligand-protected atomically precise gold nanoparticles. *Nat. Commun.* **2016,** *7*, 13240.

(94)   Ohta, T.; Shibuta, M.; Tsunoyama, H.; Negishi, Y.; Eguchi, T.; Nakajima, A., Size and structure dependence of electronic states in thiolate-protected gold nanoclusters of $Au_{25}(SR)_{18}$, $Au_{38}(SR)_{24}$, and $Au_{144}(SR)_{60}$. *J. Phys. Chem. C* **2013,** *117*, 3674-3679.

(95)   Weissker, H. C.; Escobar, H. B.; Thanthirige, V. D.; Kwak, K.; Lee, D.; Ramakrishna, G.; Whetten, R. L.; Lopez-Lozano, X., Information on quantum states pervades the visible spectrum of the ubiquitous $Au_{144}(SR)_{60}$ gold nanocluster. *Nat. Commun.* **2014,** *5*, 3785.

(96)   Mustalahti, S.; Myllyperkiö, P.; Lahtinen, T.; Salorinne, K.; Malola, S.; Koivisto, J.; Häkkinen, H.; Pettersson, M., Ultrafast electronic relaxation and vibrational cooling dynamics of $Au_{144}(SC_2H_4Ph)_{60}$ nanocluster probed by transient mid-IR spectroscopy. *J. Phys. Chem. C* **2014,** *118*, 18233-18239.

(97)   Wang, D.; Yu, Y.; Sun, T.; Mirkin, M. V., Kinetics of Quantized Charging of Au_{144} Nanoclusters. *Electroanalysis* **2016,** *28*, 2288-2292.

(98)   Chen, S.; Higaki, T.; Ma, H.; Zhu, M.; Jin, R.; Wang, G., Inhomogeneous Quantized Single-Electron Charging and Electrochemical-Optical Insights on Transition-Sized Atomically Precise Gold Nanoclusters. *ACS Nano* **2020,** *14*, 16781-16790.

(99)   Bodappa, N.; Fluch, U.; Fu, Y.; Mayor, M.; Moreno-García, P.; Siegenthaler, H.; Wandlowski, T., Controlled assembly and single electron charging of monolayer protected Au_{144} clusters: An electrochemistry and scanning tunneling spectroscopy study. *Nanoscale* **2014,** *6*, 15117-15126.

(100)   Neidhart, S. M.; Gezelter, J. D., Thermal Conductivity of Gold–Phenylethanethiol ($Au_{144}PET_{60}$) Nanoarrays: A Molecular Dynamics Study. *J. Phys. Chem. C* **2020,** *124*, 3389-3395.

(101)   Chen, S.; Ingram, R. S.; Hostetler, M. J.; Pietron, J. J.; Murray, R. W.; Schaaff, T. G.; Khoury, J. T.; Alvarez, M. M.; Whetten, R. L., Gold nanoelectrodes of varied size: transition to molecule-like charging. *Science* **1998,** *280*, 2098-101.

(102)   Zhou, M.; Wang, D.; Mirkin, M. V., Catalytic Amplification of Au_{144} Nanocluster Collisions by Hydrogen Evolution Reaction. *ChemElectroChem* **2018,** *5*, 2991-2994.

(103)   Seong, H.; Efremov, V.; Park, G.; Kim, H.; Yoo, J. S.; Lee, D., Atomically Precise Gold Nanoclusters as Model Catalysts for Identifying Active Sites for Electroreduction of CO_2. *Angew. Chem. Int. Ed.* **2021,** *60*, 14563-14570.

(104)   Li, C.; Chai, O. J. H.; Yao, Q.; Liu, Z.; Wang, L.; Wang, H.; Xie, J., Electrocatalysis of gold-based nanoparticles and nanoclusters. *Mater. Horiz.* **2021,** *8*, 1657-1682.

(105)   Sood, K.; Shanavas, A., The Role of Gold Nanoclusters as Emerging Theranostic Agents for Cancer Management. *Curr. Pathobiol. Rep.* **2021,** *9*, 33-42.

(106)   Porret, E.; Le Guével, X.; Coll, J. L., Gold nanoclusters for biomedical applications: Toward: In vivo studies. *J. Mater. Chem. B* **2020,** *8*, 2216-2232.

(107)   Zheng, Y.; Wu, J.; Jiang, H.; Wang, X., Gold nanoclusters for theranostic applications. *Coord. Chem. Rev.* **2021,** *431*, 213689.

(108)   Zhu, S.; Wang, X.; Cong, Y.; Li, L., Regulating the optical properties of gold nanoclusters for biological applications. *ACS Omega* **2020,** *5*, 22702-22707.

(109)   Heikkilä, E.; Gurtovenko, A. A.; Martinez-Seara, H.; Häkkinen, H.; Vattulainen, I.; Akola, J., Atomistic Simulations of Functional $Au_{144}(SR)_{60}$ Gold Nanoparticles in Aqueous Environment. *J. Phys. Chem. C* **2012,** *116*, 9805-9815.

(110)   Villarreal, O. D.; Chen, L. Y.; Whetten, R. L.; Yacaman, M. J., Ligand-modulated interactions between charged monolayer-protected $Au_{144}(SR)_{60}$ gold nanoparticles in physiological saline. *PCCP* **2015,** *17*, 3680-3688.

(111)   Mammen, N.; Malola, S.; Honkala, K.; Häkkinen, H., Dynamics of weak interactions in the ligand layer of: Meta-mercaptobenzoic acid protected gold nanoclusters $Au_{68}(m-MBA)_{32}$ and $Au_{144}(m-MBA)_{40}$. *Nanoscale* **2020,** *12*, 23859-23868.

(112)   Nimmala, P. R.; Dass, A., Au$_{99}$(SPh)$_{42}$ Nanomolecules: Aromatic Thiolate Ligand Induced Conversion of Au$_{144}$(SCH$_2$CH$_2$Ph)$_{60}$. *J. Am. Chem. Soc.* **2014,** *136*, 17016-17023.

(113)   Zeng, C.; Chen, Y.; Kirschbaum, K.; Appavoo, K.; Sfeir, M. Y.; Jin, R., Structural patterns at all scales in a nonmetallic chiral Au$_{133}$(SR)$_{52}$ nanoparticle. *Science* **2015,** *1*, e1500045.

(114)   Wijesinghe, K. H.; Sakthivel, N. A.; Sementa, L.; Yoon, B.; Fortunelli, A.; Landman, U.; Dass, A., Nanomolecular Metallurgy: Transformation from Au$_{144}$(SCH$_2$CH$_2$Ph)$_{60}$ to Au$_{279}$(SPh-*t*Bu)$_{84}$. *J. Phys. Chem. C* **2021,** *125*, 20488-20502.

(115)   Debets, M. F.; van der Doelen, C. W. J.; Rutjes, F. P. J. T.; van Delft, F. L., Azide: A Unique Dipole for Metal-Free Bioorthogonal Ligations. *ChemBioChem* **2010,** *11*, 1168-1184.

(116)   Bodappa, N.; Ren, H.; Dong, J. C.; Wu, D. Y.; Tian, Z. Q.; Li, J. F., Solvent-Limited Ion-Coupled Electron Transfer and Monolayer Thiol Stability in Au$_{144}$ Cluster Films. *ChemElectroChem* **2019,** *6*, 101-105.

(117)   Comby-Zerbino, C.; Dagany, X.; Chirot, F.; Dugourd, P.; Antoine, R., The emergence of mass spectrometry for characterizing nanomaterials. Atomically precise nanoclusters and beyond. *Mater. Adv.* **2021,** *2*, 4896-4913.

(118)   Weissker, H. C.; Lopez-Acevedo, O.; Whetten, R. L.; López-Lozano, X., Optical spectra of the special Au$_{144}$ gold-cluster compounds: Sensitivity to structure and symmetry. *J. Phys. Chem. C* **2015,** *119*, 11250-11259.

(119)   Negishi, Y.; Nakazaki, T.; Malola, S.; Takano, S.; Niihori, Y.; Kurashige, W.; Yamazoe, S.; Tsukuda, T.; Häkkinen, H., A Critical Size for Emergence of Nonbulk Electronic and Geometric Structures in Dodecanethiolate-Protected Au Clusters. *J. Am. Chem. Soc.* **2015,** *137*, 1206-1212.

(120)   Qian, H.; Jin, R., Ambient Synthesis of Au$_{144}$(SR)$_{60}$ Nanoclusters in Methanol. *Chem. Mater.* **2011,** *23*, 2209-2217.

(121)   Herbranson, D. E.; Hawley, M. D., Electrochemical reduction of p-nitrophenyl azide: evidence consistent with the formation of p-nitrophenylnitrene anion radical as a short-lived intermediate. *J. Org. Chem.* **1990,** *55*, 4297-4303.

(122)   Dommerholt, J.; van Rooijen, O.; Borrmann, A.; Guerra, C. F.; Bickelhaupt, F. M.; van Delft, F. L., Highly accelerated inverse electron-demand cycloaddition of electron-deficient azides with aliphatic cyclooctynes. *Nat. Commun.* **2014,** *5*, 5378.

(123)   Dommerholt, J.; Schmidt, S.; Temming, R.; Hendriks, L. J.; Rutjes, F. P.; van Hest, J. C.; Lefeber, D. J.; Friedl, P.; van Delft, F. L., Readily accessible bicyclononynes for bioorthogonal labeling and three-dimensional imaging of living cells. *Angew. Chem. Int. Ed.* **2010,** *49*, 9422-5.

(124) O'Brien, J. G. K.; Chintala, S. R.; Fox, J. M., Stereoselective Synthesis of Bicyclo[6.1.0]nonene Precursors of the Bioorthogonal Reagents s-TCO and BCN. *J. Org. Chem* **2018,** *83*, 7500-7503.

(125) Prakash, N.; Rajeev, R.; John, A.; Vijayan, A.; George, L.; Varghese, A., 2,2,6,6-Tetramethylpiperidinyloxyl (TEMPO) Radical Mediated Electro-Oxidation Reactions: A Review. *ChemistrySelect* **2021,** *6*, 7691-7710.

(126) Cao, Q.; Dornan, L. M.; Rogan, L.; Hughes, N. L.; Muldoon, M. J., Aerobic oxidation catalysis with stable radicals. *Chem. Commun.* **2014,** *50*, 4524-43.

(127) Ciriminna, R.; Pagliaro, M., Industrial Oxidations with Organocatalyst TEMPO and Its Derivatives. *Org. Process Res. Dev.* **2010,** *14*, 245-251.

(128) Lamontagne, H. R.; Lessard, B. H., Nitroxide-Mediated Polymerization: A Versatile Tool for the Engineering of Next Generation Materials. *ACS Appl. Polym. Mater.* **2020,** *2*, 5327-5344.

(129) Akakuru, O. U.; Iqbal, M. Z.; Saeed, M.; Liu, C.; Paunesku, T.; Woloschak, G.; Hosmane, N. S.; Wu, A., The Transition from Metal-Based to Metal-Free Contrast Agents for T1 Magnetic Resonance Imaging Enhancement. *Bioconjugate Chem.* **2019,** *30*, 2264-2286.

(130) Biedenbänder, T.; Aladin, V.; Saeidpour, S.; Corzilius, B., Dynamic Nuclear Polarization for Sensitivity Enhancement in Biomolecular Solid-State NMR. *Chem. Rev.* **2022,** *122*, 9738-9794.

(131) Miao, Q.; Nitsche, C.; Orton, H.; Overhand, M.; Otting, G.; Ubbink, M., Paramagnetic Chemical Probes for Studying Biological Macromolecules. *Chem. Rev.* **2022,** *122*, 9571-9642.

(132) Megiel, E., Surface modification using TEMPO and its derivatives. *Adv. Colloid Interface Sci.* **2017,** *250*, 158-184.

(133) Ma, Z.; Mahmudov, K. T.; Aliyeva, V. A.; Gurbanov, A. V.; Pombeiro, A. J. L., TEMPO in metal complex catalysis. *Coord. Chem. Rev.* **2020,** *423*, 213482.

(134) Beejapur, H. A.; Zhang, Q.; Hu, K.; Zhu, L.; Wang, J.; Ye, Z., TEMPO in Chemical Transformations: From Homogeneous to Heterogeneous. *ACS Catalysis* **2019,** *9*, 2777-2830.

(135) Wen, D.; Liu, Q.; Cui, Y.; Yang, H.; Kong, J., TEMPO-Functionalized Nanoporous Au Nanocomposite for the Electrochemical Detection of H_2O_2. *Int. J. Anal. Chem.* **2018,** *2018*.

(136) Li, J.; Zhang, J.; Chen, Y.; Kawazoe, N.; Chen, G., TEMPO-Conjugated Gold Nanoparticles for Reactive Oxygen Species Scavenging and Regulation of Stem Cell Differentiation. *ACS Appl. Mater. Interfaces* **2017,** *9*, 35683-35692.

(137) Swiech, O.; Hrynkiewicz-Sudnik, N.; Palys, B.; Kaim, A.; Bilewicz, R., Gold nanoparticles tethered to gold surfaces using nitroxyl radicals. *J. Phys. Chem. C* **2011,** *115*, 7347-7354.

(138) Swiech, O.; Bilewicz, R.; Megiel, E., TEMPO coated Au nanoparticles: Synthesis and tethering to gold surfaces. *RSC Adv.* **2013,** *3*, 5979-5986.

(139) Liu, Z.; Zhu, M.; Meng, X.; Xu, G.; Jin, R., Electron transfer between $[Au_{25}(SC_2H_4Ph)_{18}]^-TOA^+$ and oxoammonium cations. *J. Phys. Chem. Lett.* **2011,** *2*, 2104-2109.

(140) Conte, M.; Miyamura, H.; Kobayashi, S.; Chechik, V., Spin trapping of Au-H intermediate in the alcohol oxidation by supported and unsupported gold catalysts. *J. Am. Chem. Soc.* **2009,** *131*, 7189-7196.

(141) Chen, H.; Liu, C.; Wang, M.; Zhang, C.; Luo, N.; Wang, Y.; Abroshan, H.; Li, G.; Wang, F., Visible Light Gold Nanocluster Photocatalyst: Selective Aerobic Oxidation of Amines to Imines. *ACS Catal.* **2017,** *7*, 3632-3638.

(142) Rafiee, M.; Miles, K. C.; Stahl, S. S., Electrocatalytic Alcohol Oxidation with TEMPO and Bicyclic Nitroxyl Derivatives: Driving Force Trumps Steric Effects. *J. Am. Chem. Soc.* **2015,** *137*, 14751-14757.

(143) Liu, X.; Jin, Y.; Liu, T.; Yang, S.; Zhou, M.; Wang, W.; Yu, H., Iron-Based Theranostic Nanoplatform for Improving Chemodynamic Therapy of Cancer. *ACS Biomater. Sci. Eng.* **2020,** *6*, 4834-4845.

(144) Al-Madhagi, S.; O'Sullivan, C. K.; Prodromidis, M. I.; Katakis, I., Combination of ferrocene decorated gold nanoparticles and engineered primers for the direct reagentless determination of isothermally amplified DNA. *Microchimica Acta* **2021,** *188*, 117.

(145) Astruc, D., Why is Ferrocene so Exceptional? *Eur. J. Inorg. Chem.* **2017,** *2017*, 6-29.

(146) Collman, J. P.; Devaraj, N. K.; Chidsey, C. E. D., "Clicking" Functionality onto Electrode Surfaces. *Langmuir* **2004,** *20*, 1051-1053.

(147) MacDonald, D. G.; Eichhöfer, A.; Campana, C. F.; Corrigan, J. F., Ferrocene-Based Trimethylsilyl Chalcogenide Reagents for the Assembly of Functionalized Metal–Chalcogen Architectures. *Eur. J. Chem.* **2011,** *17*, 5890-5902.

(148) Stiles, R. L.; Balasubramanian, R.; Feldberg, S. W.; Murray, R. W., Anion-Induced Adsorption of Ferrocenated Nanoparticles. *J. Am. Chem. Soc.* **2008,** *130*, 1856-1865.

(149) Wang, C.; Brudo, A.; Ducrot, L.; Fu, F.; Ruiz, J.; Escobar, A.; Martinez-Villacorta, A.; Moya, S.; Astruc, D., Generation of Catalytically Active Gold

Nanocrystals in Water Induced with Ferrocene Carboxylate. *Eur. J. Inorg. Chem.* **2021,** *2021*, 2471-2479.

(150) Gunawardene, P. N. Nanoorthogonal Surface Modifications of Gold Nanoparticles and Nanoclusters through Strain-Promoted Cycloaddition Chemistry. University of Western Ontario, Electronic Thesis and Dissertation Repository, 2021.

(151) Yang, T.; Shan, B.; Huang, F.; Yang, S.; Peng, B.; Yuan, E.; Wu, P.; Zhang, K., P band intermediate state (PBIS) tailors photoluminescence emission at confined nanoscale interface. *Commun. Chem.* **2019,** *2*, 132.

(152) Bera, D.; Goswami, N., Driving Forces and Routes for Aggregation-Induced Emission-Based Highly Luminescent Metal Nanocluster Assembly. *J. Phys. Chem. Lett.* **2021,** *12*, 9033-9046.

(153) He, B.; Zhang, J.; Zhang, J.; Zhang, H.; Wu, X.; Chen, X.; Kei, K. H. S.; Qin, A.; Sung, H. H. Y.; Lam, J. W. Y.; Tang, B. Z., Clusteroluminescence from Cluster Excitons in Small Heterocyclics Free of Aromatic Rings. *Adv. Sci.* **2021,** *8*, 2004299.

(154) Herbranson, D. E.; Hawley, M. D., Electrochemical reduction of p-nitrophenyl azide: evidence consistent with the formation of p-nitrophenylnitrene anion radical as a short-lived intermediate. *J. Org. Chem* **1990,** *55*, 4297-4303.

Appendices

Appendix A: Supporting Information for Chapter 2

Density Functional Theory (DFT) Calculations of phenylethane thiol versus their azido analogs

Geometry of all the structures at the ground state were optimized using CAM-B3LYP/6-31G basis set. The final orbital energies were calculated using the same basis set for both p and d orbitals.
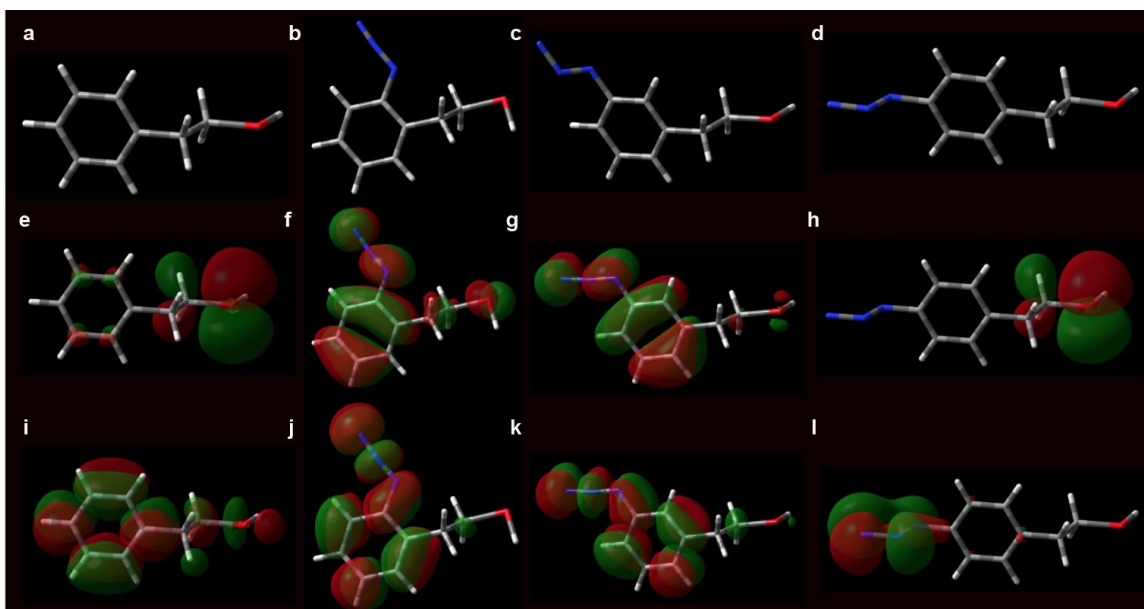

Figure S1. Density functional theory calculation of phenylethanethiol and azido-phenylethenethiol derivatives. Molecular structures of **a**, phenylethanethiol, **b**, *ortho*-azido-phenylethanethiol, **c**, *meta*-azido-phenylethanethiol, and **d**, *para*-azido-phenylethanethiol. (**e–f**) Highest occupied molecular orbital (HOMO) isopotential plots, and (**i–l**) lowest unoccupied molecular orbital (LUMO) isopotential plots of **a-d**. Nitrogen atom; blue, sulphur; red, carbon; gray and hydrogen; white.
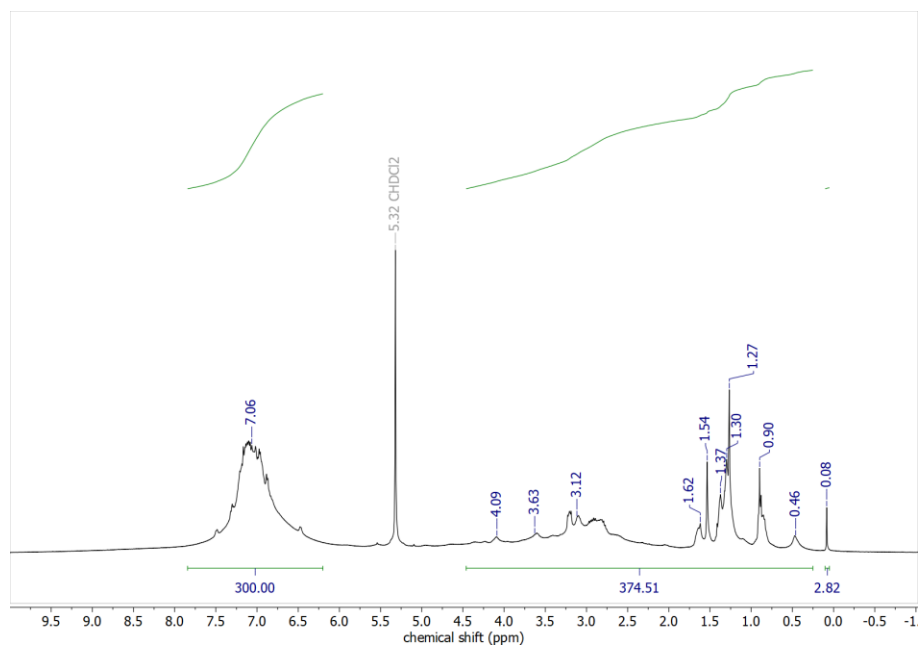
^{1}H NMR spectroscopy of Au$_{144}$(SR)$_{60}$ NCs

Figure S2. ^{1}H NMR spectrum of Au$_{144}$(S-C$_2$H$_4$-Ph)$_{60}$ NCs (Au$_{144}$ NCs) in deuterated dichloromethane.
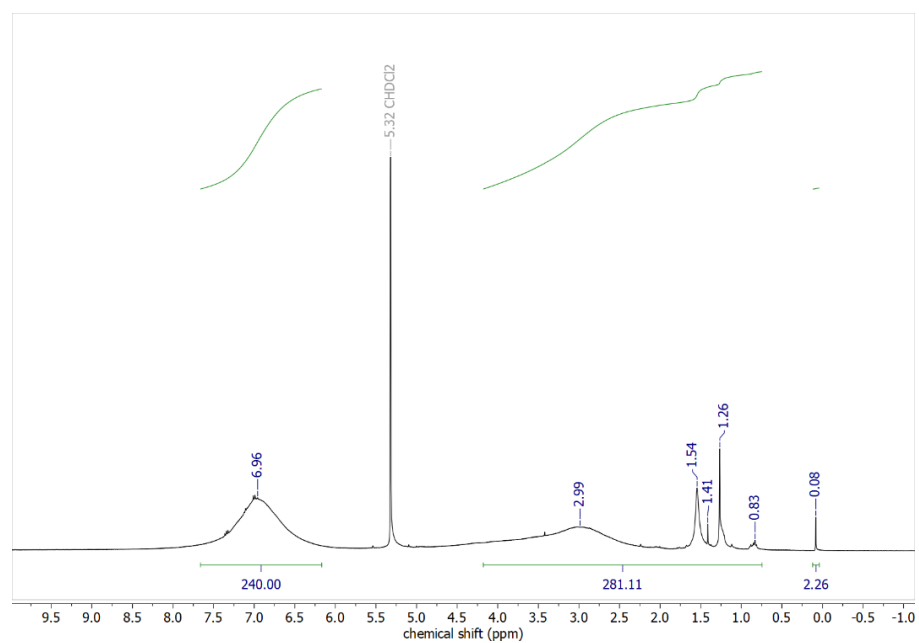
Figure S3. ^{1}H NMR spectrum of Au$_{144}$(SC$_2$H$_4$-o-C$_6$H$_4$-N$_3$)$_{60}$ NCs (o-Au$_{144}$-N$_3$ NCs) in deuterated dichloromethane.

Figure S4. ^1H NMR spectrum of $Au_{144}(SC_2H_4\text{-}m\text{-}C_6H_4\text{-}N_3)_{60}$ NCs ($m\text{-}Au_{144}\text{-}N_3$ NCs) in deuterated dichloromethane.

Figure S5. ^1H NMR spectrum of $Au_{144}(SC_2H_4\text{-}p\text{-}C_6H_4\text{-}N_3)_{60}$ NCs ($p\text{-}Au_{144}\text{-}N_3$ NCs) in deuterated dichloromethane.

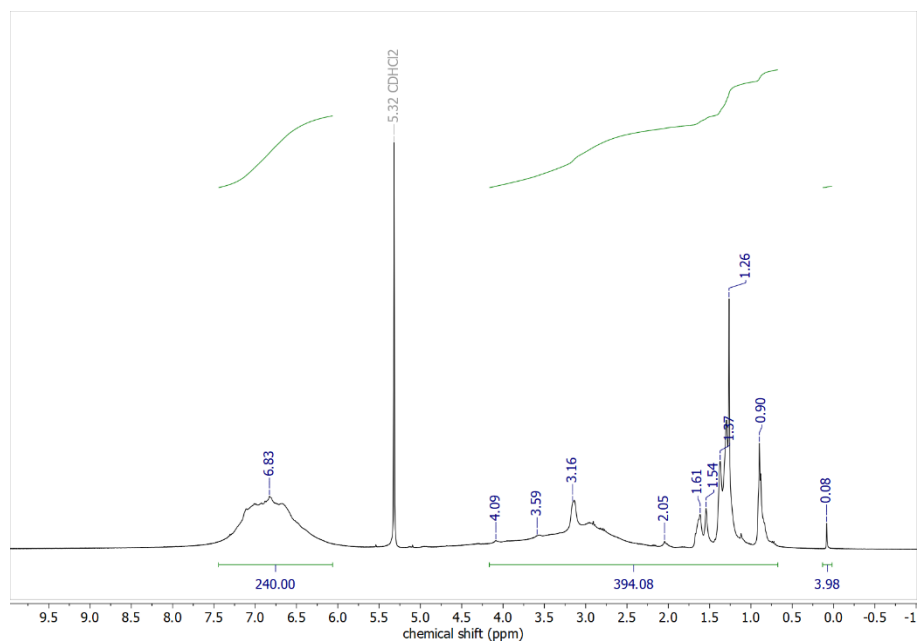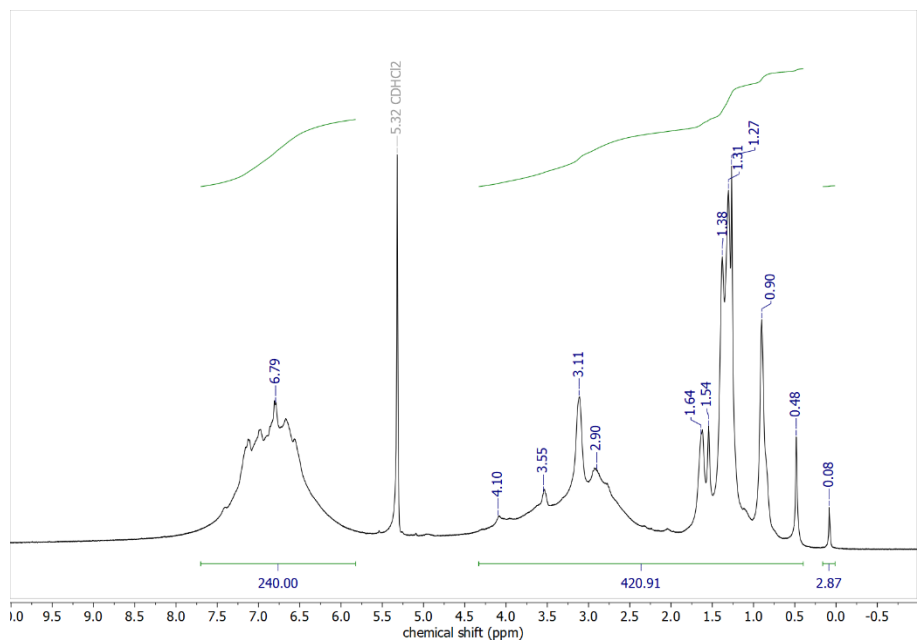# Electrochemistry of *p*-azidophenylethanethioester

To understand the electrochemical properties of *p*-azido-phenylethanethiol, a protected analogue, *p*-azido-phenylethanethioester, was investigated using differential pulse voltammetry (DPV). A solution of azido-phenylethanethioester (5 mM) in dichloromethane with 0.1 M tetra-n-butylammonium hexafluorophosphate ($TBAPF_6$) was prepared and a 2mm-Pt disk served as a working electrode.
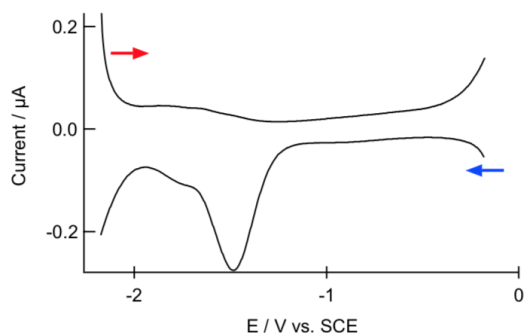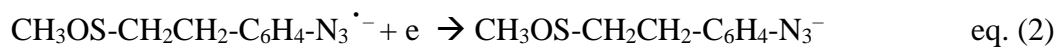

Figure S6. Electrochemistry of *p*-azidophenylethanethioester. DPV of 5 mM *p*-azidophenylethenethioester in dichloromethane containing 0.1 M tetra-n-buthylammonium hexafluorophosphate ($TBAPF_6$) using a 2-mm Pt disk electrode with peak amplitude of 50 mV, a pulse width of 0.05 s, 4 mV increment per cycle, and a pulse period of 0.2 s were applied to obtain DPVs. The arrows indicate potential scan directions.

There is no oxidation peak when WE potential scans towards positive values. Instead, in the reverse scan a peak corresponding to reduction of azide to radical anion ($-PhN_3{}^{\bullet-}$) (eq. 1) at -1.5 V vs. SCE (**Figure S6**) is observed. At more negative potential a small shoulder at -1.8 V is also occurred. The small shoulder could be evidence of second reduction and injection of second electron to the radical anion to generate anionic species (eq. 2).

$$CH_3OS\text{-}CH_2CH_2\text{-}C_6H_4\text{-}N_3 + e \rightarrow CH_3OS\text{-}CH_2CH_2\text{-}C_6H_4\text{-}N_3{}^{\bullet-} \qquad \text{eq. (1)}$$

$$CH_3OS\text{-}CH_2CH_2\text{-}C_6H_4\text{-}N_3{}^{\bullet-} + e \rightarrow CH_3OS\text{-}CH_2CH_2\text{-}C_6H_4\text{-}N_3{}^{-} \qquad \text{eq. (2)}$$

It is worth mentioning that Hawley and co-workers investigated electroreduction of *p*-nitrophenyl azide in various organic solvents.[154] They reported a one-electron reduction of *p*-nitrophenyl azide to anion radical intermediate with a short life-time. They also proposed a mechanism for *p*-$O_2NC_6H_4NH^-$ that further reacts with *p*-$O_2NC_6H_4N_3$ in DMF and forms 4,4'-$O_2NC_6H_4NHNHN{=}NC_6H_4NO_2$, the product of dimerization.
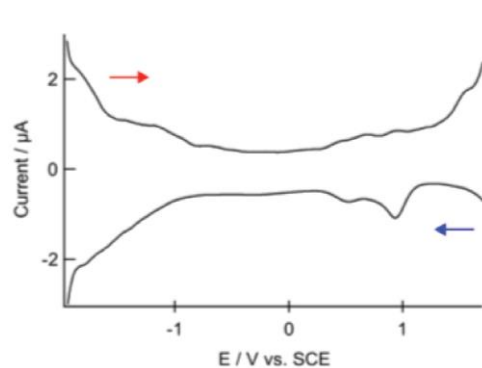
Figure S7. Extended electrochemistry of Au₁₄₄(SR)₆₀ NCs. DPV of 0.25 mM *o*-Au₁₄₄-N₃ in dichloromethane containing 0.1 M tetra-n-butylammonium hexafluorophosphate (TBAPF₆) using a 2-mm Pt disk electrode with peak amplitude of 50 mV, a pulse width of 0.05 s, 4 mV increment per cycle, and a pulse period of 0.2 s were applied to obtain DPVs. The arrows indicate potential scan directions.

Appendix B: Supporting Information for Chapter 3

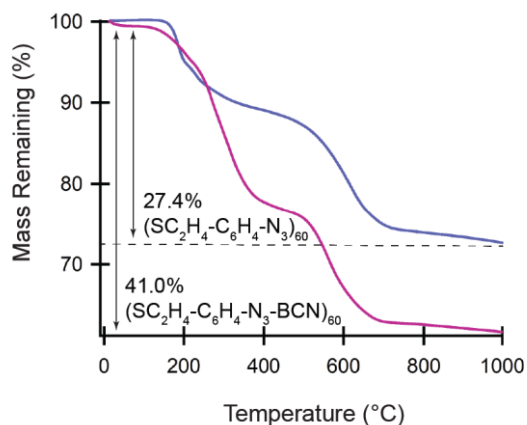## Thermogravimetric Analysis (TGA) of $Au_{144}(SR)_{60}$ NCs

Figure S8. TGA of p-Au_{144}-N_3 NCs (purple) and p-Au_{144}-BCN NCs (pink).
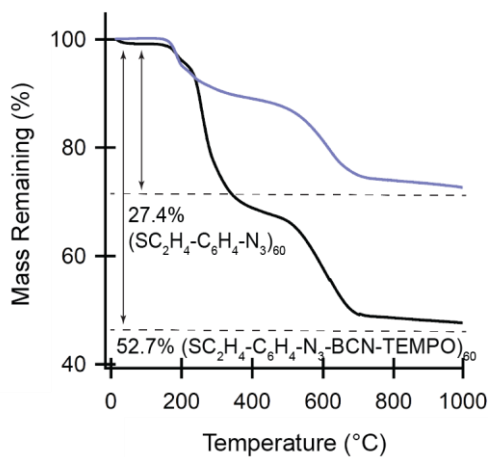
Figure S9. TGA of p-Au_{144}-N_3 NCs (purple) and p-Au_{144}-TEMPO NCs (black).

Table S1. Theoretical and Experimental TGA Mass Percentages.

Sample	Ligand Molecular Weight (g/mol)	Theoretical Residual Mass Percentage for $Au_{144}(SR)_{60}^{0}$ NC	Theoretical Residual Mass Percentage for $[Au_{144}(SR)_{60}^{-1}][TOA^{+}]$ NC	Experimental Residual Mass Percentage
p-Au_{144}-N_3	178.23	72.62	71.76	72.68
p-Au_{144}-BCN	328.45	59.00	58.44	61.67
p-Au_{144}-N_3-TEMPO	527.71	47.25	46.89	47.65

Electrochemistry of Click Products
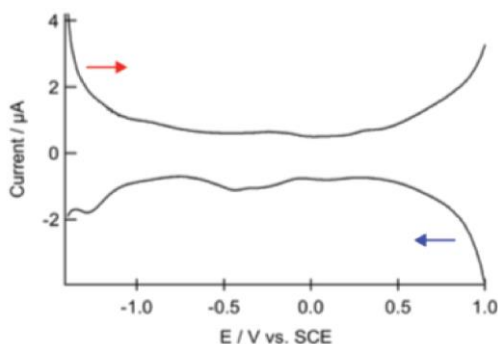
Figure S10. Electrochemistry of p-Au$_{144}$-BCN NCs. DPV of 0.25 mM p-Au$_{144}$-BCN$_{60}$ in dichloromethane containing 0.1 M tetra-n-butylammonium hexafluorophosphate (TBAPF$_6$) using a 2-mm Pt disk electrode with peak amplitude of 50 mV, a pulse width of 0.05 s, 4 mV increment per cycle, and a pulse period of 0.2 s were applied to obtain DPVs. The arrows indicate the direction of potential scans.
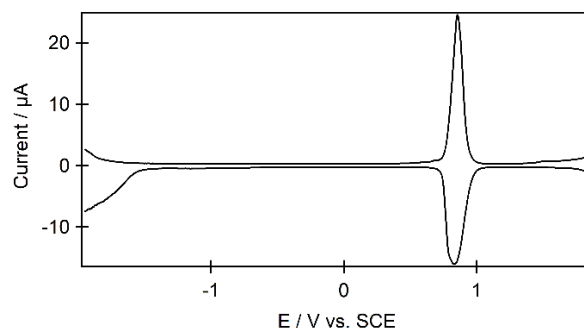
Figure S11. DPV of *p*-Au₁₄₄-TEMPO NCs. 0.15 mM *p*-Au$_{144}$-TEMPO in DCM/0.1 M TBAPF$_6$ using a 2-mm Pt disk working electrode
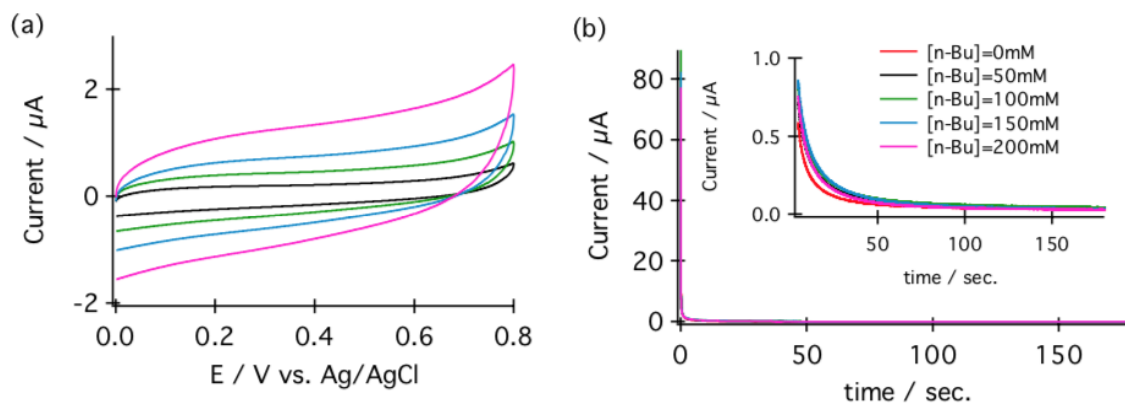
Figure S12. **Extended electrocatalysis of Au$_{144}$ NC**. Cyclic voltammograms (CVs) of Au$_{144}$-modified glassy carbon electrode in 0.5 M bicarbonate solution at 10 (black), 25 (green), 50 (blue) and 100 (pink) mV/s. (**b**) Chronoamprograms of (**a**) in the same solution in the absence (red) and presence of 50, 100, 150, and 200 mM of n-butanol at E$_{app}$=0.6 V vs. Ag/AgCl.
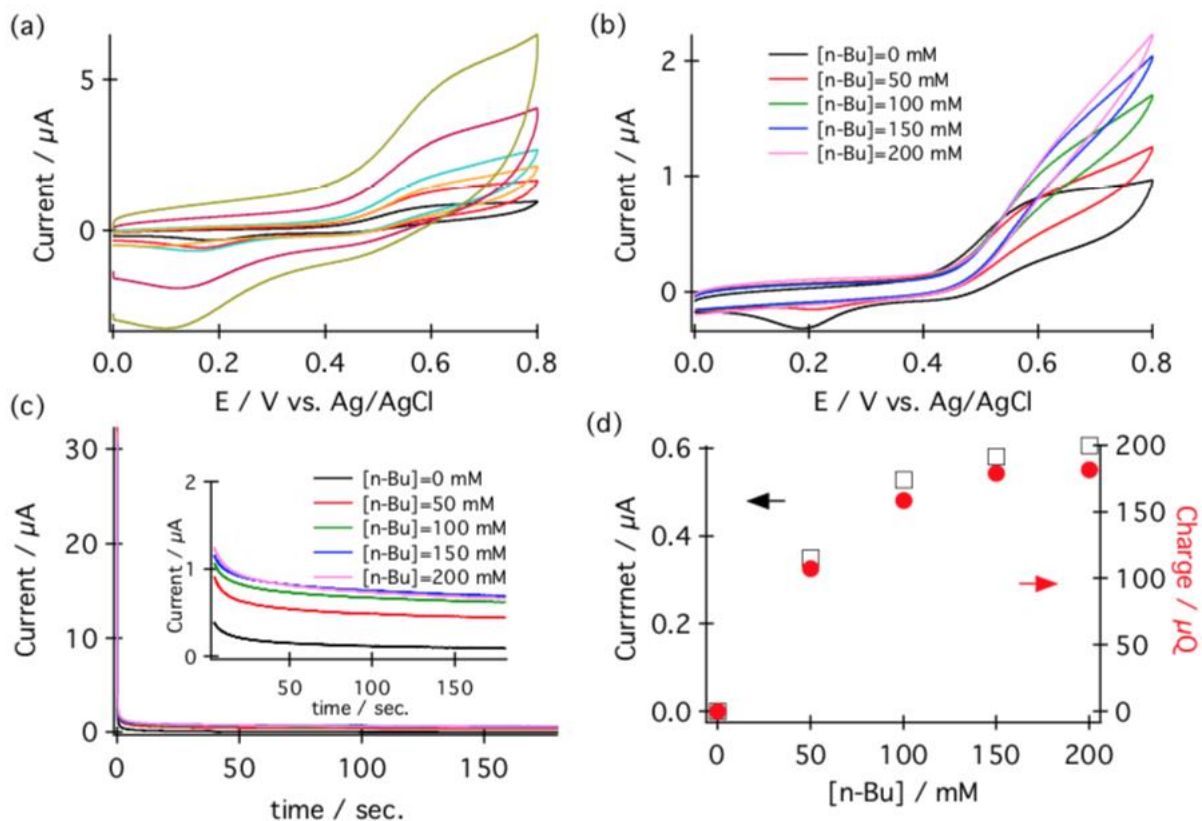
Figure S13. **Extended electrocatalysis of *p*-Au₁₄₄-TEMPO**. (**a**) Cyclic voltammograms (CVs) of dropcasted *p*-Au₁₄₄ -TEMPO on a 2-mm GC electrode at various scan rates; 10 mV (red), 25 mV (green), 50 mV (purple), and 100 mV/s in 0.13 M Na₂CO₃/0.02 M NaHCO₃, pH 11. (**b**) CVs of GC-modified *p*-Au₁₄₄ -TEMPO in the absence (black) and presence of 50 mM (red), 100 mM (green), 150 mM (blue), and 200 mM (pink) of *n*-butanol in 0.13 M Na₂CO₃/0.02 M NaHCO₃, pH 11 at scan rate of 10 mV/s. (**c**) Chronoamperometry (CA) curves of electro-oxidation of *n*-butanol on *p*-Au₁₄₄ -TEMPO-modified GC electrode in the absence (black) and presence of 50 mM (red), 100 mM (green), 150 mM (blue), and 200 mM (pink) of *n*-buthanol in 0.13 M Na₂CO₃/0.02 M NaHCO₃, pH 11 at E꜀ₐₚₚ=0.6 V vs. Ag/AgCl. (**d**) Current and charge vs. n-butanol concentrations. Data are taken from CA curves in panel (**c**).

Curriculum Vitae

EDUCATION

MSc Organic Chemistry Candidate, Workentin Group   **September 2020 – 2022**

University of Western Ontario, London, ON

Grade Report:

CHEM 9507Q	ADVANCED CHEM COMMUNICATIONS	0.25	089
CHEM 9603R	ADV NMR SPEC II	0.25	088
CHEM 9555T	ORGANIC PHOTOCHEMISTRY	0.25	090
CHEM 9663S	ADVANCED POLYMER CHEMISTRY II	0.25	090

- TA Experience:

    o Resource room and forum for Chem 2213A

    o Filmed, edited, and voiced over Chem 2213A laboratory videos

    o Resource room and forum for Chem 2223B

BSc Honors Specialization in Chemistry   **September 2016 – April 2020**

University of Western Ontario, London, ON

- Clubs and Organizations: Western Chem Club (2018 -2020), Medway-Sydenham Hall Residence Council (2017), Girls' Novice Rowing Team (2017)

PUBLICATIONS

Wu, J.; Winiarz, P.; Patel, D.; de Jong, J.; Tong, D.; Chidley, T.; Vemula, N.; Pagenkopf, B. L., Synthesis of Hexahydropyridazines by [4 + 2] Cycloaddition of Donor–Acceptor Cyclobutanes and cis-Diazenes. *Org. Lett.* **2020,** *22* (8), 3140-3144.

RESEARCH AND WORK EXPERIENCE

NSERC USRA, Workentin Group   **May 2020 – September 2020**

4491 (Thesis) Student, Workentin and Corrigan Groups   **September 2019 – April 2020**

Synthesized and characterized silver thiolate nanoclusters, a joint project between the Workentin Group and the Corrigan Group

NSERC USRA, Pagenkopf Group   **May 2019 – September 2019**

Synthesized range of organic compounds, specifically 4-phenyl-1,2,4-triazole-3,5-dione, aryl- and methoxy- activated cyclobutanes, and hexahydropyridizene derivatives

NSERC USRA, Noel Group   **May 2018 –August 2018**

Trained in radiation safety and conducted electrochemical experiments

Field Crop Research Assistant   **May 2017 – September 2018**

University of Guelph and the Ontario Ministry of Agriculture, Food and Rural Affairs, Guelph, ON

Gathered soil samples and measured their nitrate content throughout the growing season

Assistant Naturalist and Interpreter   **June 2016-September 2016**

Murphy's Point Provincial Park, Tay Valley, ON

Hosted Visitors' Center and educated campers on various native species, ran the Discovery Program within the park, conducted snake monitoring and odonate surveys

Stewardship Youth Ranger   **June 2015 – September 2015**

Ministry of Natural Resources and Forestry, Guelph, ON

Conducted plant identification surveys, aided in fish identification, water quality assessment, and stream restoration

Lifeguard and Water Safety Instructor   **2013-2016**

City of Guelph, ON

CONFERENCE PARTICIPATION

CCCE Calgary 2022 Presenter   **June 2022**

Title: The Pursuit of Functionality: Equipping Au_{144} Nanoclusters with Click Chemistry

CCCE 2021 Virtual Presenter   **June 2021**

Title: Customizable Nanoclusters: Tuning the Properties of Noble Metal Nanoclusters via Interfacial Click Chemistry

CCCE Quebec 2019 Volunteer and Poster Presenter   **June 2019**

Created and presented a poster about the formation of hexahydroxypyridizine derivatives from the [4+2] cycloaddition reaction of donor-acceptor cyclobutanes with cis-diazenes

VOLUNTEER ACTIVITIES

Let's Talk Science Volunteer   **September 2020-2022**

Ran workshops for elementary school classes to educate and spark their interest in science

SCHOLARSHIP AND ACADEMIC HONOURS

Lipson-Baines Award   **2021-2022**

NSERC CGSM   **2021-2022**

Dean's Honour List   **2016-2020**

Western Continuing Admission Scholarship   **2016-2020**

CERTIFICATION AND TRAINING

Liquid Nitrogen Dispensary and NMR training   **2019**

Workplace Hazardous Material Information System (WHMIS)   **2019**

Laboratory Safety & Hazardous Waste Management   **2018**

Safe Campus Community   **2018**

Nuclear Safety and Radiation Training   **2018**

Standard First Aid with CPR-C with AED   **2016**

Lifesaving Society Swimming Instructor   **2015**

Water Safety Instructor   **2015**